HIGH-PRESSURE NUCLEAR MAGNETIC RESONANCE STUDIES OF FUEL CELL MEMBRANES

By

EUGENE STEPHANE MANANGA

A dissertation submitted to the Graduate Faculty in Physics in partial fulfillment of the requirements for the degree of Doctor of Philosophy

The City University of New York

2005

UMI Number: 3187396

UMI Microform 3187396

ProQuest Information and Learning Company
300 North Zeeb Road
P.O. Box 1346
Ann Arbor, MI 48106-1346

This manuscript has been read and accepted for the Graduate Faculty in Physics in satisfaction of the dissertation requirement for the degree of Doctor of Philosophy.

06/29/2005 Professor Steve G. Greenbaum
Date Chair of Examining Committee

06/29/2005 Professor Suttan Catto
Date Executive Officer

Professor Chen Ying-Chih

Professor Marten L. denBoer

Professor Joel Gersten

Professor Ruth E. Stark

Supervisory Committee

The City University of New York

ABSTRACT

HIGH-PRESSURE NUCLEAR MAGNETIC RESONANCE STUDIES OF FUEL CELL MEMBRANES

By

EUGENE STEPHANE MANANGA

Advisor: Professor Steve G. Greenbaum

This thesis focuses on the use of high pressure NMR to study transport properties in electrolyte membranes used for fuel cells. The main concern is in studying the self-diffusion coefficients of ions and molecules in membranes and solutions, which can be used to characterize electrolytes in fuel cells. For this purpose, a high-pressure fringe field NMR method to study transport properties in material systems useful for fuel cell and battery electrolytes, was designed, developed, and implemented.

In this investigation, pressure is the thermodynamic variable to obtain additional information about the ionic transport process, which could yield the crucial parameter, activation volume. Most of the work involves proton NMR, with additional investigations of others nuclei, such as fluorine, phosphorus and lithium.

Using the FFG method, two fuel cell membrane types (NAFION-117, SPTES), and different dilutions of phosphoric acid were investigated, as was LiTf salt in Diglyme solution, which is used as a lithium battery electrolyte.

In addition to high-pressure NMR diffusion measurements carried out in the fringe field gradient for the investigation of SPTES, pulse field gradient spin echo NMR was also used to characterize the water diffusion, in addition to measuring diffusion rates as a function of temperature. This second method allows us to measure distinct diffusion coefficients in cases where the different nuclear (proton) environments can be resolved in the NMR spectrum.

Polymer electrolyte systems, in which the mobility of both cations and anions is probed by NMR self-diffusion measurements using standard pulsed field gradient methods and static gradient measurements as a function of applied hydrostatic pressure, were also investigated. The material investigated is the low molecular weight liquid diglyme / $LiCF_3SO_3$ (LiTf) complexes which can be used as electrolytes in lithium batteries.

Finally, high-pressure diffusion coefficient measurements of phosphoric acid in water at different concentrations: proton (^1H) and phosphorus (^{31}P) nuclei have been performed using the static field gradient spin-echo nuclear magnetic resonance. This study is expected to be helpful in improving the understanding of phosphoric acid fuel cell technology.

DEDICATION

In the memory of:

***My sister*, NGO MANANGA SUZANNE CLAIRE**

***My father*, MANANGA MAURICE EMMANUEL**

***My Uncle,* NYOBE ADALBERT**

***My grandma*, NGO NYOBE SAPHERIE**

***My Ant*, NGO NJOCK ANNE**

To:

***My mother*, NGO LISSOUCK MONIQUE**

***My brothers,* MANANGA MICHEL, RENE, MAURICE, DIEUDONNE**

***My sisters,* MANANGA DELPHINE, JEANNETTE**

***My children,* MANANGA NDJOCK MAURICE, JOB EMMANUEL, MANANGA BETINA SUZANNE…**

ACKNOWLEDGEMENTS

I was very fortunate to have Professor Steve Greenbaum as my thesis advisor. He was always available to provide me valuable advice, both scientific and professional. Therefore, I am taking this opportunity to give grateful and sincere thanks to him for the support he provided to me during difficult times. The way he guided, taught, and supported me was something that only he could do. Words are not enough to be able to explain his high level of generosity. God bless him.

Looking back five years ago, after being admitted to the Doctoral Program in Mechanics at the University of Paris XII, France, I had meetings and discussions with Professor Joel Gersten about the Ph. D program in Physics at the City University of New York. It was then that I decided to pursue my dream of obtaining my doctorate in the USA system. After a short interview he gave to me, Professor Joel Gersten enthuastically recommended me to the Ph. D program. Then, he encouraged, prepared and guided me to pass the hard CUNY Ph. D Physics qualifying exam. Next, he advised me to complete my thesis with Professor Greenbaum. In addition to the previous elements, he attended my second exam as a committee member and accomplished his goal in the supervision of my final defense exam. I am infinitely grateful to him. God bless him.

I also take this opportunity of expressing my deep appreciation to other members of my committee: Professor Ruth Stark, Professor Marten denBoer, and Professor Ying-Chih

Chen for taking time out from their busy schedules to participate in the examination committee, read my thesis, made important remarks and suggested corrections to it.

Special thanks go out to Dr. Jay Jayakody and Dr. Phil Stallworth, for their help in teaching me the techniques of NMR, performing experiments and discussing the measurements.

I would like also to thank Dr. Phil and Mr. Rich Krumm for their technical assistance, include designing and building the high-pressure probe, and the copper beryllium (CuBe) bomb.

I would like to thank Dr. Eric Sigmund for sending me his thesis, which helped me improve my understanding of FFG technique.

I would like to thank Lawyer Nicole Thompson, Esq. for the numerous help she provided to me including translations from French to English, and English to French.

I would also like to thank all the other members of the NMR lab at Hunter College who helped me during this work: A. Khalfan, G. Bennett, N. Leifer and J. Zapata-Farrington.

I am also very grateful to Dr. Michele Vittadello and his wife Julianne McConnell for their love, and their spiritual support. I am very happy to be a member of their family, and feel secure near them.

Thanks also to the holy trinity church of New York and the group prayers of the cathedral Saint Patrick of New York to keep my spirituality positive.

I remember my sister Ngo Mananga Suzanne saying to me “imagination is more important than knowledge, I will always pray that you will reach the highest education level in this world….” Thank you Suzanne and your soul lay to rest in peace.

I also remember my brother, Mananga Michel, offering me two Astronomy encyclopedias on my 12th birthday. I also remember him explaining the fundamentals of Astronomy, Technology and monitoring my high school grades in Mathematics, Physics, Chemistry and Technology. Thank you so much, Michel, and God bless you.

I extend special thanks to the Honorable Judge Aminatou Alioum, the Honorable Judge Hayatou Zakiatou, Professor Owono Ateba, Professor Abdouli Belgacem, Mr. Atanga Cosmas, Dr. Nguini Effa’a Jean Baptiste, Dr. Nguenang Jean Pierre, Mr. Tiwang Fokoua Raymond and Journalist, Benoit Bitchoka who brought me help, love and moral support when I was leaving Africa to the USA.

Sincere thanks go to my teenager’s good friends: Mr. Bell Ndjock Eloge, Mr. Mpessa Mouyenga Andre and Mr. Sieodji David. I was very lucky to be surrounded by such friendship and good will.

It is also and occasion to remember the souls of those quite to close me, are absent today: my dad, Mananga Maurice Emmanuel; my sister, Ngo Mananga Suzanne Clair; my nephew, Goueth Raoul Maurice; my grandma, Ngo Nyobe Zapherie; my grandfather, Lissouck Thomas; my uncle, Nyobe Adalbert; my ant, Ngo Ndjock Anne; my cousins, Nyemb Albert, Ngo Nyobe Christiane; my friends, Bessala Mballa Roger Marin, Fotso Celestin; and a good family friend, Nguedi Banana Alfred.

Finally, I will like to thank my family for all their love and support, which has kept me going more than once: Tamara Faith Hinton, Ngo Lissouck Monique, Lissouck Phillips, Ngo Mananga Delphine, Ngo Mananga Jeannette, Mananga Michel, Mananga Rene Thomas, Mananga Ndjock Maurice Emmanuel, Mananga Dieudonne Bienvenu, Mrs. Mananga Burns Lisa, Mrs. Kodock Martine, Mrs. Ngango Eleanor and especially my deceased sister, **Ngo Mananga Suzanne Claire** and father, **Mananga Maurice Emmanuel** to whom I dedicated this thesis.

This work was supported by the U.S. Air Force Office of Scientific Research, the U.S. Office of Naval Research and the National Institutes of Health, through the MBRS-RISE Program.

Last but not least, I'd like to thank Dr. Gail Smith for offering me the prestigious Postdoctoral Fellowship under the National Science Foundation (NSF)/ MAGNET-STEM Program at The Graduate Center of the City University of New York.

TABLE OF CONTENTS

LIST OF TABLES

LIST OF FIGURES

PART 1:

GENERAL INTRODUCTION

Chapter1:

Nuclear Magnetic Resonance (NMR)

1.1 Introduction

Nuclear Magnetic Resonance is a branch of spectroscopy, which encompasses all studies of the nature of the nuclear spin energy levels of material systems and of the transitions induced between them through the absorption or emission of electromagnetic radiation. More specifically, nuclear magnetic resonance is a branch of radio-frequency spectroscopy with a domain of frequencies extending at present from a thousand MHz to the frequency of the separation between two Zeeman levels of a proton spin in the Earth's magnetic field, which is 2 kHz[1]. The radio-frequency spectroscopy methods used to investigate the very small interaction energies to which nuclear magnetic moments give rise are also used to increase the understanding of nuclear electric quadrupole effects. Early spectroscopy showed that a nucleus might possess a magnetic moment as well as an electric quadrupole moment, the latter having its origin in a nonspherically symmetric nuclear charge distribution. The significant difference between both moments is that the

magnetic dipole moment interacts with a magnetic field while the nuclear electric quadrupole moment interacts with an electrostatic field gradient. In addition to these effects, the expansion of the nuclear electric quadrupole Hamiltonian had shown the hexadecapole terms[2], which are very small compared to the quadrupole term, and ordinarily outside the range of experimental detectability. In this thesis, priority has been given to nuclei with dipole magnetic moment spin I = 1/2 (^{1}H, ^{19}F, ^{31}P).

1.2 Historical overview: The first observations of NMR

Normally, credit for NMR first observation should go to Rabi and co-workers in 1939[3, 4] who used a beam of silver atoms. The noticeable change in the fluxes of beams representing the different energy states of the nuclear magnetic moments was the detection of transitions.

However, the term NMR has come to be used as a convention for experiments, which differ from those of Rabi. The experiments set by the convention in respect of NMR are those through the detection of the transitions with the energy absorbed from the RF field rather than through changes in the particle flux reaching a detector as in the beam experiments. Next, the term NMR is commonly reserved for phenomena occurring in bulk matter rather than in a beam of essentially non-interacting atoms. As a result of these two important conventions, the first observations of NMR are attributed to two independent groups: Purcell, Torrey and Pound, working on the east coast of America

and Bloch, Hansen and Packard working on the west coast. They published their discoveries almost simultaneously in the same volume of Physical Review in 1946 [5, 6].

1.3 Principle

The principle is such that an a r.f. generator supplies the electromagnetic energy which is absorbed by the nuclear spin system polarized by an external magnetic field. So, the electromagnetic detection of resonance plays an important role in the NMR technique. The presence of nuclear moments in large numbers is crucial to enhance the sensitivity of the electromagnetic means of detection since the energies involved are precisely those of the transitions induced, not amplified by any trigger effect. Therefore, bulk matter samples are necessary: solids, liquids, or gases under appreciable pressure. Two important methods of detection are used in NMR: the pulsed NMR technique, and the continuous wave (CW) method. The CW method is the technique traditionally used in most branches of spectroscopy and consists of looking at the system's response to a small sinusoidal disturbance of varying frequency at resonance. The pulse NMR spectrometer method that is used as one of the techniques of investigation in this thesis consists of looking at the time response to a transient excitation. In both methods, an NMR signal is produced by a precessing magnetization in the specimen under investigation. Results of the two methods have been shown to be equivalent, one response being the Fourier transform of the other. However, nowadays pulsed NMR has eclipsed CW NMR because

relaxation times (T_1, T_2) are easily measurable, and the signal-to-noise ratio is more favorable using pulse methods.

1.4 Magnets

Most magnetic resonance experiments need magnets. The desired magnetic field B_0 produced by the magnet must be intense, time-independent and homogeneous. Working at a higher field increases the energy splitting and therefore has the effect to improve the signal sensitivity through increasing the Boltzmann factor and to improve the resolution by chemical shift expansion. Since frequency stability is directly related to magnetic field stability, the magnet must produce a steady field in order to avoid the fluctuations in the Larmor frequency. Also, the magnet must produce a field, which is constant in space, because any variation in field over the sample volume will show up by a shortening of the free induction decay (FID) or broadening of the resonance. Homogeneity is therefore a precondition for resolution. There are three kinds of magnets to consider for use in magnetic resonance: electromagnets, permanent magnets, and superconducting magnets. A superconducting magnet ($\left|\overrightarrow{H_0}\right|$ = 7.1 T, i.e. ^{1}H resonance frequency = 300 MHz) has been used in all investigations in this thesis. The superconducting magnets offer an unbeatable combination of stability and field strength at lower costs compared to the traditional electromagnets.

Superconducting solenoids for NMR spectrometers are presently manufactured by at least five companies: Bruker Spectrospin, JEOL, Japan Magnet Systems Oxford Instruments, and Varian[7].

1.5 Relaxation processes

The literature of continuous wave NMR discussed less the NMR relaxation processes compared to the situation in pulse experiments. From an experimental point of view, the relaxation phenomenon can be observed only indirectly in CW measurements. But, the situation is totally different in pulse experiments, which are concerned with the time recovery of the magnetization after excitation for a very short period. Therefore, the relaxation processes become a priority when processing a pulse experiment.

By considering spin ½ nuclei which have two energy states in a static magnetic field $\vec{H}_0$, a Boltzmann distribution of spin occurs between the energy levels, which gives rise to a small excess of nuclei in the lower energy state. This small excess of nuclei or difference of the population gives rise to the magnetization, which can be calculated according to Curie's law. If the resonance condition is produced in the sample after equilibrium is reached, the nuclei absorb energy from the $\vec{H}_1$ field and the populations of the two spin states tend to equalize. When $\vec{H}_1$ is removed, the system returns to the former equilibrium distribution appropriate to $\vec{H}_0$. The population difference is then restored again and the energy previously acquired by the spin system is transferred to the surroundings. Such energy changes between the spin systems and the lattice is called

spin-lattice relaxation or longitudinal relaxation (T_1). However, additional relaxation processes called spin-spin relaxation or transverse relaxation (T_2), which involves interaction between the spins without any exchange with the lattice, is given much consideration. In addition, for the static field gradient method mostly used in our investigation, T_2 processes can complicate the self-diffusion measurements. Therefore, it is important to report that nuclear relaxation parameters are one of the most important sources of information about structure and molecular dynamics.

T_2* is the time constant which describes the decay of the magnetization in the x-y plane and T_2 (spin-spin relaxation) an intrinsic relaxation time which is characteristic of the magnetization decay in one of the spin isochromats without any field inhomogeneity effects. The T_2 relaxation time and the NMR linewidth, $\delta\omega$ (angular frequency) are related as shown in the following equation [8,19]:

$$\delta\omega = 1/T_2^* = 1/T_2 + \gamma\Delta H_o \qquad [1.1.1]$$

In this thesis, all T_2 measurements are performed by using pulsed spin echo (PSE) NMR in a homogeneous $\vec{H}_0$. This technique is advantageous over the fringe field gradient (FFG) method, because T_2 can be measured independently of the diffusion coefficient D. In FFG method, the parameters T_2 and D affect the overall echo decay as described in chapter 2 of part 2.

Measurements of the T_1 relaxation time are typically performed by two-pulse sequences: inversion (also called the 180-90) and saturation recovery (also called the 90-90). In each of these two-pulse sequences, the first pulse prepares the spins and the second pulse measures the magnetization after the waiting period.

In the inversion recovery sequence, the first pulse π inverts the magnetization of the spin system and after the waiting period τ, the second pulse π/2 measures the magnetization recovery from $-M_o$ to M_o. M_o is the thermal equilibrium magnetization which can be reach only after waiting for a time much longer than T_1. Specifically, the magnetization after waiting for a time τ is given by:

$$M(\tau) = Mo\,(1-2\exp(-\tau/T_1)). \qquad [1.1.2]$$

In the saturation recovery sequence, the range of magnetization is Mo, and the magnetization is given by:

$$M(\tau) = Mo\,(1-\exp(-\tau/T_1)). \qquad [1.1.3]$$

In our investigation, T_1 measurements using NMR in the homogeneous Bo were necessary and very helpful to estimate some acquisition parameters (Recycle delay or Rd) used in the fringe field gradient method. A delay time of at least $5T_1$ must be inserted in each cycle before repeating a pulse sequence to avoid saturation effects [7,8]. It is also important to report that dipolar and quadrupolar interactions, chemical shift anisotropy, spin rotation and scalar coupling generate the fluctuations in local magnetic field that facilitate relaxation. Nevertheless, dipolar and (or) quadrupolar mechanisms dominate relaxation in most materials.

1.6 Diffusion Mechanism

The main purpose of this thesis is to investigate ionic and molecular motion through various polymeric electrolytes and the characterization of ionic motion is of great importance in fully understanding and advancing fuel cell technology.

Hahn's observation [21] that the bulk diffusion of nuclei in an inhomogeneous static field caused the spin echo to decay is an example of a general circumstance of great utility in applications of magnetic resonance in Physics, Chemistry, and Biology. When a nucleus diffuses, it moves from a place where its precession frequency has one value to another place experiencing a different magnetic field strength with a different precession frequency. Therefore, it is obvious that a frequency modulation is associated with the motion of nuclei. Such effects will be treated mathematically using the Bloch equations in the derivation of important formulas in part 2. This problem was first solved by Slichter [11] and independently by Hahn and Maxwell [12]. Using different means, Van Vleck [13], McConnell [14], Archer [15] and Anderson [16] discovered the same result.

Self-diffusion is the random translational motion of molecules (or ions) driven by internal kinetic energy [17]. As a consequence, the diffusion also provides information on the interactions and shape of the diffusing molecule. In this thesis, we have studied only the translational diffusion, which is the most fundamental form of transport in chemical and biochemical systems. We have developed an NMR instrumentation (static field gradient) to determine molecular self-diffusion coefficients as a function of applied hydrostatic pressure. The measurement of the diffusion coefficient as a function of pressure has yielded additional information about the ion transport process, and vital parameters such as the activation volume are obtained.

Our first application of high-pressure diffusion measurements was in NAFION, a sulfonated fluoropolymer currently used as the electrolyte in Polymer Electrolyte Membrane (PEM) fuel cells. NAFION membrane had showed superior performance in fuel cells operating at moderate temperatures (‹ 90^{o} C) and high relative humidity with pure hydrogen as a fuel[18]. Earlier work in our lab produced results for variable pressure spin-lattice relaxation (T_1), which probes very local scale motions, and our collaborators at the US Naval Academy (J.J. Fontanella et al.) measured electrical conductivity as a function of pressure in NAFION [19,20,21].

Next, we investigated diglyme/LiTf solution relevant to Lithium battery research, phosphoric acid, and highly sulfonated Polyarylenethioethersulfones for fuel cells applications using both Pulse Gradient Spin-Echo (PFG) and Fringe field techniques (FFG).

Nowadays, the PFG method is preferred to the steady-gradient experiment because it affords better definition and control over the time during which diffusion is observed. But the FFG (fringe-field gradient) method is mainly used in this thesis because we are mainly concerned about measuring diffusion as a function of pressure, which is difficult to do via PFG methods. This aspect will be clearly explained in the Research methods part.

1.7. High Pressure NMR

Pressure is one of the most important thermodynamic parameters, which determine the state of a system. The measurement of the diffusion coefficient is usually performed as a function of temperature to obtain activation energies. In our investigation, we have measured the self-diffusion coefficient at elevated pressure to obtain a wealth of additional information about the ion transport process, such as activation volume.

As Benedek and Purcell [22] had pointed out, high pressure is known also to cause relatively large changes in viscosity and hence diffusion coefficient. This can be seen easily from the Stokes-Einstein equation:

$$D = \kappa_B T / f, \qquad [1.1.4]$$

where κ_B is the Boltzmann constant, T is absolute temperature, and f is the friction coefficient. The friction factor for the simple case of a spherical particle with an effective hydrodynamic or Stokes radius r in a solution of viscosity η is given by:

$$f = 4\pi\eta r . \qquad [1.1.5]$$

The technique of high pressure NMR in FFG involves positioning the non-magnetic vessel pressure (bomb) in an inhomogeneous magnetic field, and applying a hydrostatic pressure on the sample within the bomb. Bridgman had suggested for the first time the use of copper beryllium (CuBe) as a nonmagnetic high-pressure bomb. The set of measurements on relaxation, diffusion and viscosity under high pressure done by Benedek and Purcell had led to the discovery that CuBe, a heat treatable alloy, makes a very satisfactory high pressure, non-magnetic bomb which might well be used for other magnetic investigations under high pressure.

In our investigation, we have used a bomb made of copper beryllium (CuBe), which will be described in detail later in the experimental part.

Chapter 2:

Fuel Cells and Lithium-Ion Batteries

2.1 Introduction

Fuel cells are old technology, and their first invention is widely attributed to Sir William Grove in 1839. They operate like batteries that also convert energy that is stored in chemical form into electricity. But, in contrast to batteries, they don't store the chemical reactants but rather they oxidize externally supplied fuel and hence do not need to be recharged. Fuel cells as electrochemical devises converting chemical energy to electricity are in principle more efficient than classical heat engines because they avoid the Carnot's theorem limitation.

The electrolyte material generally characterizes fuel cell types. In the past a few decades, significant progress has been made particularly in Polymer Electrolyte Membrane Fuel Cells, sometimes referred to as Proton Exchange Membrane (both terms abbreviated PEM). This thesis focuses mainly on progress in PEM materials used for Fuel Cells, with Nafion and similar materials used as membranes. We also investigated phosphoric acid

solutions because of their relevance to Phosphoric Acid Fuel Cells (PAFC). Currently there are five major most promising types of fuel cell: Proton Exchange Membrane Fuel Cell (PEMFC), Phosphoric Acid Fuel Cell (PAFC), Alkaline Fuel Cell (AFC), Molten Carbonate Fuel Cell (MCFC), and Solid Oxide Fuel Cell (SOFC). Only the PEMFC with additional study of phosphoric acid solutions will be discussed in this thesis. Since the overall cell's efficiency is largely governed by the rate of ion transport through the electrolyte, the main goal of my investigation is the study of ionic and molecular motion through various polymeric electrolytes. Using NMR techniques with both pulse field gradient (PFG) and fringe field gradient (FFG), important transport properties such as translational diffusion and relaxation process have been investigated. The application of pressure and temperature as independent thermodynamic parameters has yielded respectively the vital parameters of activation volume and activation energy. In addition to the fuel cell studies, I also investigated diglyme/LiTf solutions, relevant to lithium battery electrolytes.

2.2 Polymer Electrolyte Membrane Fuel Cells (PEMFC)

A polymer is a long, repeating chain of atoms, formed through the linkage of many molecules called monomers. Currently, the most important class of polymer electrolytes membrane used in PEMFC is the perfluorosulfonic acid (PFSA) membranes, which are a type of ion-exchange membranes. One of these membranes is NAFION, which shows superior performance in fuel cells operating at moderate temperature ($< 90^0$C) and high

relative humidity with pure hydrogen as a fuel [18]. Also, PFSA has been shown to have high H^+ transport and exhibits great thermal stability and high chemical stability to most reagents. Therefore, fuel cells using them exhibit many advantages such as high performance, no free corrosive liquid in the cell and minimal material corrosion problems, and demonstrated long life [23,24,25]. This thesis will focus mostly on the understanding of the transport properties of the membranes used as the electrolytes for PEMFC. The PEMFC basically requires hydrogen and oxygen as its inputs, though the oxidant may also be ambient air, and the hydrogen must be humidified. Their operating temperatures are around 90^0 C. The membrane-electrode assembly is the electrochemical heart of system. The dissociation of hydrogen gas by catalyst is observed on the anode according to the reaction:

$$H_2 \rightarrow 2H^+ + 2e^- \qquad [1.2.1]$$

The hydrogen ions diffuse through the membrane of the cell to reach the cathode where they combine catalytically with oxygen and electrons coming from the anode to form water, according to the reaction:

$$4H^+ + O_2 + 4e^- \rightarrow 2H_2O \qquad [1.2.2]$$

The state of hydration of membrane electrolyte is a crucial parameter, which can be controlled to optimize the PEMFC performance. If the membrane is too dry, its ionic diffusion and its conductivity fall resulting to the reduction of the fuel cell' performance. An excess of water in the fuel cell can lead to cathode flooding problems, also resulting in less than optimal performance [26,27,28]. Several studies have examined the water percentage behavior in the membranes, which will be discussed later. Figure 1.1 shows the schematic of PEMFC.

Nafion is the membrane electrolyte most often studied for this type of fuel cell. Nafion is a perfluorosulfonate polymer, which naturally combines, in one macromolecule, the high hydrophobicity of the perfluorinated backbone with the extremely high hydrophilicity of the sulfonic acid functional groups. In the presence of water, this gives rise to some hydrophobic/hydrophilic nano-separation. The sulfonic acid functional groups aggregate to form a hydrophilic domain. When this is hydrated, protonic charge carriers form within inner space charge layers by dissociation of the acidic functional groups, and proton conductance assisted by water dynamics occurs. While the well-connected hydrophilic domain is responsible for the transport of protons and water, the hydrophobic domain provides the polymer with the morphological stability and prevents the polymer from dissolving in water [18]. The schematic representation of the microstructures of Nafion-117 is given in Figure 1.2.

A general formula of Nafion in either the acid form or the salt form is [23,29]:

$$\sim (CF_2CF_2)_n\text{-}CF_2CF\sim$$

$$\mathbf{I}$$

$$O\,(CF_2CF\text{-}O)_m CF_2CF_2SO_2X$$

$$\mathbf{I}$$

$$CF_3$$

Where X = F denotes NAFION-F, the precursor; X = O-K+ denotes NAFION-K; X = OH, denotes NAFION-H. For commercial materials, m is usually equal to one and n varies from about 5 to 11. In this thesis, we investigated the NAFION-117, named NAFION-H, the acid form of the material. The number n is 7, m = 1, and its equivalent weight (EW) is 1100. Its thickness is about 0.18 mm. Structurally, Nafion consists of a

backbone of tetrafluoroethylene with pendent side chains of perfluorinated vinyl ethers, which terminate in sulfonic acid groups.

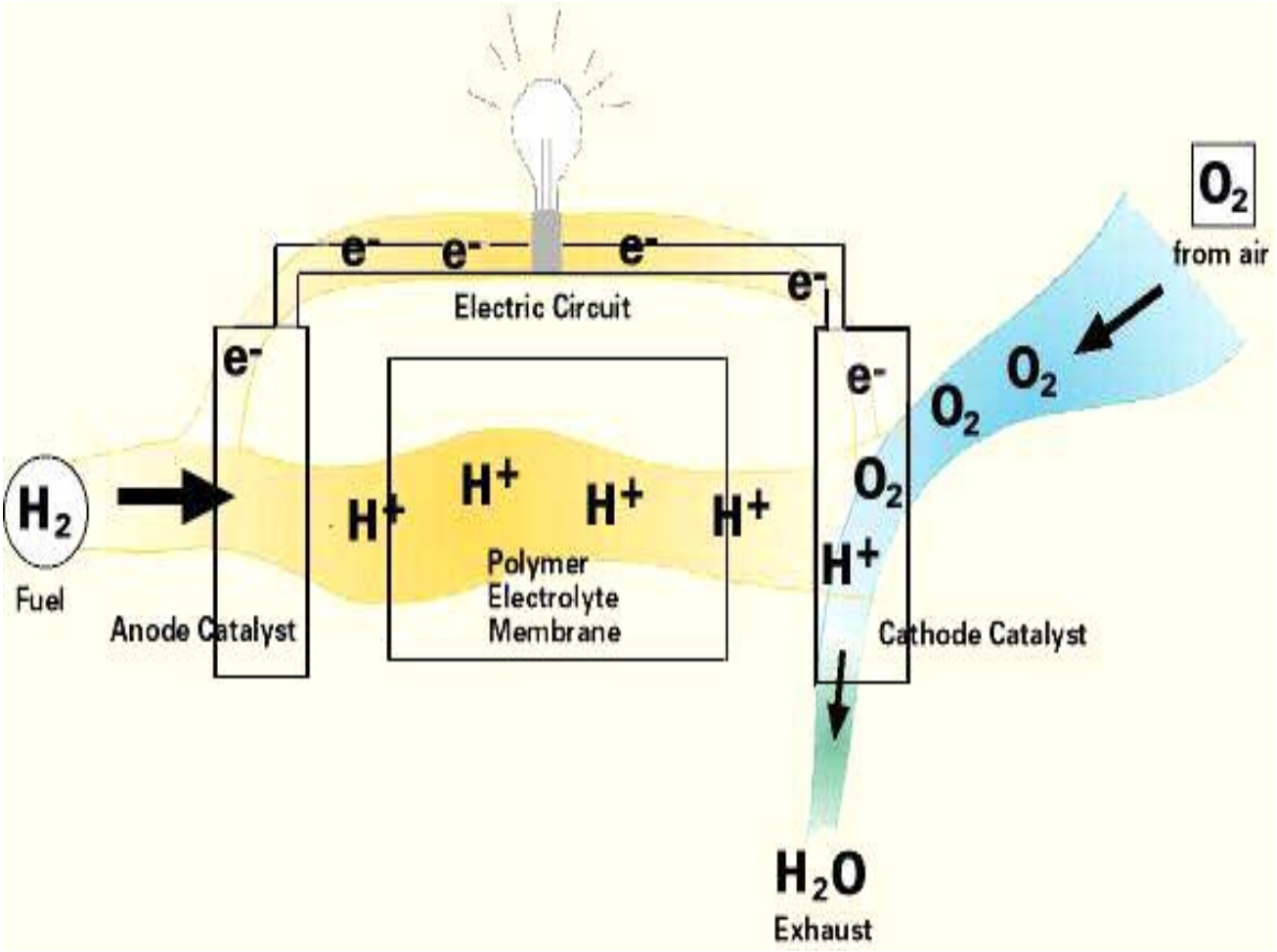

Figure 1.1: Scheme of PEM fuel cell

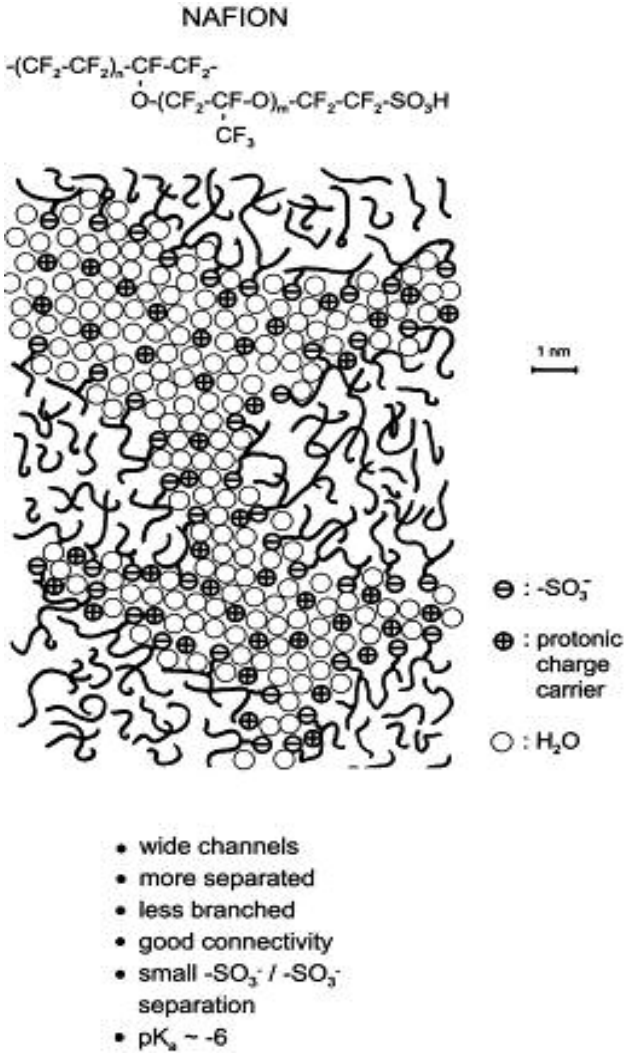

Figure 1.2: Schematic representation of the microstructures of Nafion.

The second membrane electrolyte studied in this thesis is the sulfonated polyareylenethioethersulfones (SPTES). This membrane is potentially superior candidate for fuel cells for 120^{o} C operation. SPTES is a copolymer membrane and its general formula is:

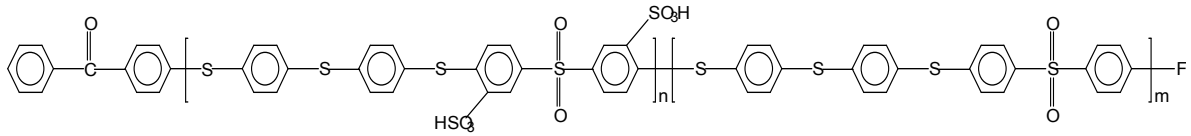

n = 0 ~1, m = 1-n

Several investigations examining both the water and the methanol behavior in the membrane SPTES will be discussed later.

2.3. Direct Methanol Fuel Cell

The direct-methanol fuel cell (DMFC) is similar to the PEM fuel cell in that it uses a solid polymer membrane as an electrolyte. Unlike the hydrogen PEMFC, the DMFC uses methanol directly as a fuel. While potentially a very attractive solution to the issues of hydrogen storage and transportation, the principal problem facing the commercial application of the DMFC today stems from its relatively low performance in comparison to hydrogen fueled PEMFCs. The principal problem is the lower electrochemical activity of the methanol as compared to hydrogen, giving rise to lower cell voltages and hence, efficiencies. Also, methanol is miscible in water, so some of its liability is to cross the water-saturated membrane and oxidize on the cathode side, further lowering the cell efficiency. However, direct methanol fuel cells (DMFCs) are attractive because methanol

is relatively cheap and easily transported and converted into energy. Methanol is an ideal fuel for the application of fuel cells in electric vehicles since it is the simplest organic liquid fuel. The potential advantages of the methanol liquid-feed fuel cell over cells designed for gas-feed may be summarized as follows: elimination of fuel vaporizer and its associated heat source and controls, elimination of complex humidification and thermal management systems, dual-purpose use of the liquid methanol/water as fuel and as an efficient stack coolant, significantly lower system size, weight and temperature than existing fuel cell systems [23,24,25,26]. Figure 1.3 represents the schematic of a direct methanol fuel cell. On the anode, the liquid methanol/water mixture (typically 1M methanol concentration) is fed according to the reaction:

$$CH_3OH + H_2O \rightarrow CO_2 + 6H^+ + 6e^- \qquad [1.2.3]$$

On cathode, fed with oxygen gas or air, the reaction is:

$$O_2 + 4H^+ + 4e^- \rightarrow 2H_2O \qquad [1.2.4]$$

The overall cell reaction is:

$$2CH_3OH + 3O_2 \rightarrow 2CO_2 + 4H2O \qquad [1.2.4]$$

In this thesis, we report an investigation of methanol transport in polymer electrolyte membrane based on highly sulfonated polyarelenethioethersulfones (SPTES) for direct methanol fuel cell (DMFC) applications. Comparison with previous studies on methanol transport in Nafion membrane will be made. This will extend the understanding of the behaviors of methanol crossover through the SPTES and Nafion membranes under various conditions.

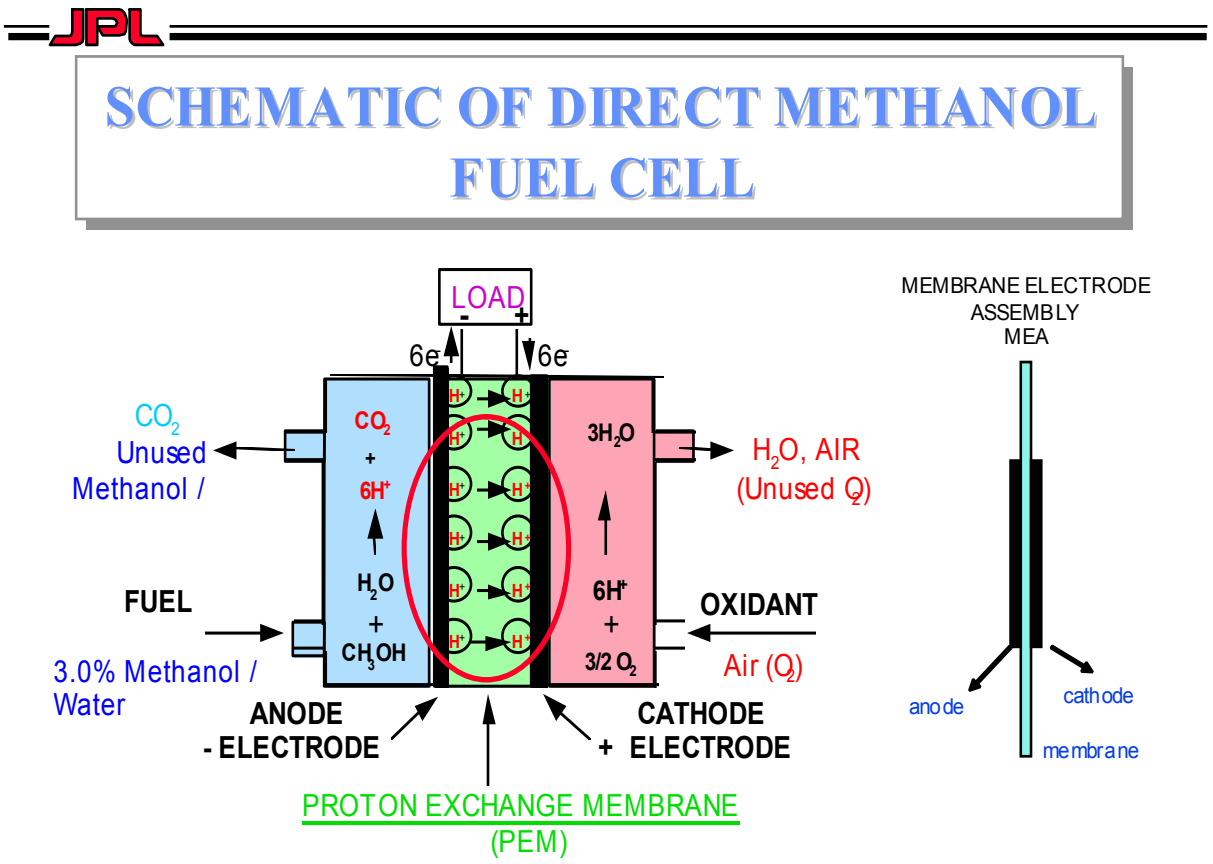

Figure 1.3: Direct Methanol Fuel Cell

2.4. Phosphoric Acid Fuel Cell (PAFC)

Phosphoric acid fuel cells use liquid phosphoric acid as an electrolyte. They are the most mature fuel cell technology in terms of system development and commercialization activities. These fuel cells present some disadvantages making them less used in many applications. They are typically large and heavy. As a result, they are less powerful than other fuel cells, given the same weight and volume. They are 85 percent efficient when used for the co-generation of electricity and heat, but less efficient at generating electricity alone (37 to 42 percent). This is only slightly more efficient than combustion-based power plants, which typically operate at 33 to 35 percent efficiency. PAFCs are expensive and require an expensive platinum catalyst, which raises the cost of the fuel cell.

In this thesis, we have studied ionic transport of phosphoric acid in water as a function of concentration using high pressure NMR technique as tool of investigation. These studies reported later will be helpful to improve the understanding of phosphoric acid fuel cell.

2.5 Lithium-Ion Batteries

A battery is an electrochemical device that converts the chemical energy contained in its active materials directly into electric energy by means of oxidation-reduction reactions. The batteries are not subject to the limitations of the Carnot cycle dictated by the second law of thermodynamics, as are heat engines. Batteries, therefore, are capable of having

higher energy conversion efficiencies. A battery consists of one or more cells connected in series or parallel, or both, depending on the desired output voltage and capacity. Depending on their capability of being electrically recharged, batteries are identified as primary and secondary. Primary batteries are non rechargeable and usually inexpensive, lightweight source of packaged power for portable electronic and electric devices, lighting, photographic equipment, toys, memory backup, and a host of other applications, giving freedom from utility power. Unlike primary batteries, secondary batteries are rechargeable. Their energy densities are generally lower than those of primary batteries. In addition to these two types of batteries, there are also the reserve batteries, which can be classified by the type of activating medium or mechanism that is involved in the activation. In this thesis, we studied ionic transport properties for diglyme/Lithium triflate solutions, which can be used for the electrolyte in lithium batteries. Moreover, the diglyme LiTf system is a liquid analogue of poly (ethylene oxide) solid polymer electrolytes. High-pressure NMR measurements of the solutions will be presented in the fourth part of this thesis. Figure 1.4 illustrates the Lithium-Ion batteries scheme.

Lithium-ion (Li-ion) batteries are comprised of cells that employ lithium intercalation compounds as the positive and negative electrode materials. As a battery is cycled, lithium ions (Li^+) exchange between the positive and negative electrodes. Typically, the positive electrode material is a metal oxide with a layered structure, such as lithium cobalt oxide ($LiCoO_2$), which are the first batteries to be marketed, or a material with a tunneled structure, such as lithium manganese oxide ($LiMn_2O_4$), on a current collector of aluminum foil. The negative electrode material made of layered material is typically a graphitic carbon. The Lithium-Ion Batteries present major advantages over other types of

batteries: sealed cells; no maintenance required, long cycle life, broad temperature range of operation, long shelf life, low self-discharge rate, rapid charge capability, high rate and high power discharge capability, high coulombic and energy efficiency, high specific energy and energy density, no memory effect. The major disadvantages they present are: high initial cost, degrades at high temperature, need for protective circuitry, capacity loss or thermal runaway when overcharged, venting and possible thermal runaway when crushed, cylindrical designs typically offer lower power density than NiCd or NiMH [30].

Lithium-Ion Batteries are now applicable to consumer electronics, such as cell phones, laptop computers, and personal data assistants, as well as military electronics, including radios, mine detectors and thermal weapons sights. Other applications include aircraft, spacecraft, satellites, and eventually electric or hybrid electric vehicles.

The following equation shows the chemical reaction in one kind of lithium cell.

$$Li_xC + Li_{1-x}CoO_2 \rightarrow LiCoO_2 + C \qquad [1.2.5]$$

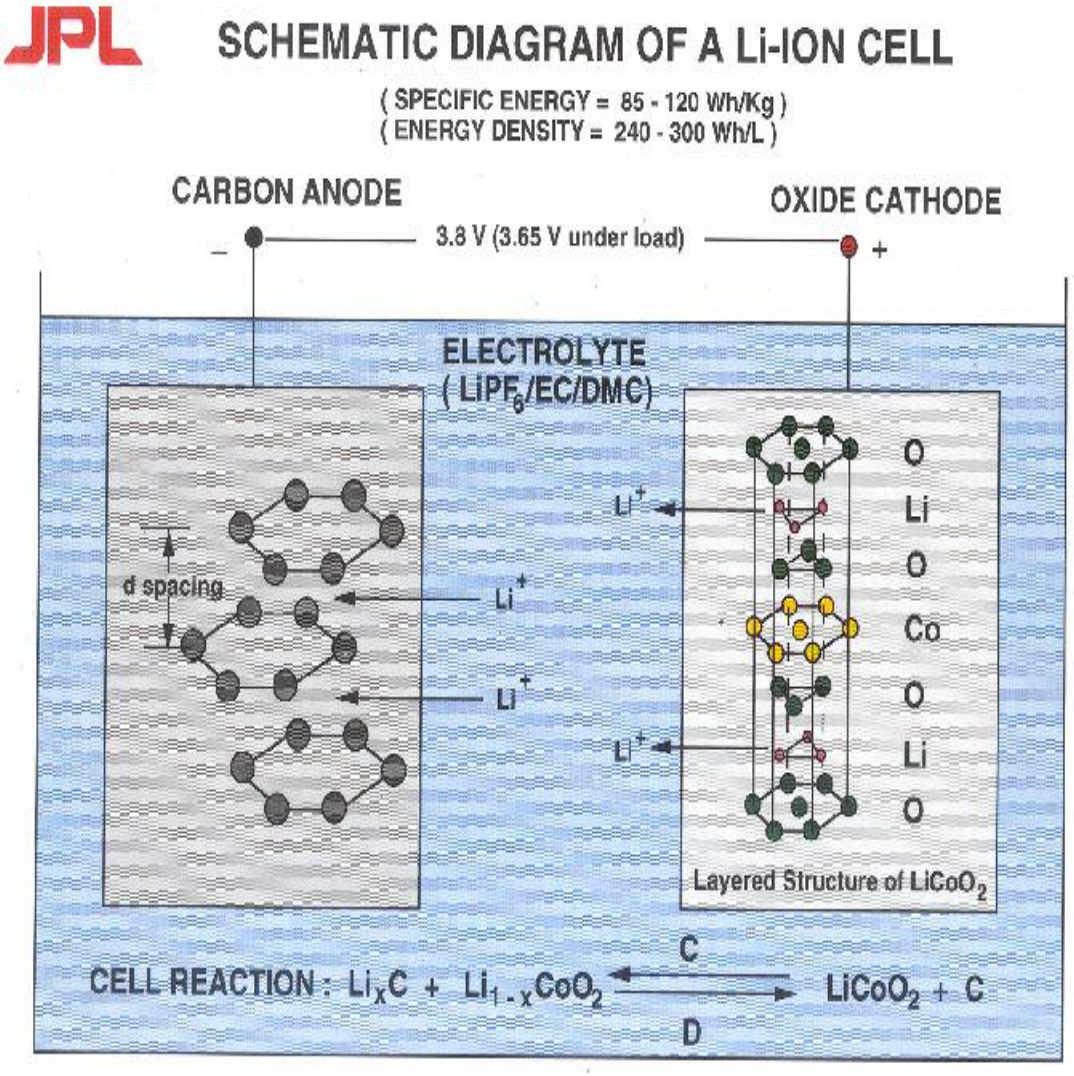

Figure: 1.4: Lithium-Ion Battery

PART 2:

THEORETICAL BACKGROUND

Chapter1:

Basic Theory of Nuclear Magnetic Resonance (NMR)

1.1 Simple Quantum Mechanical Treatment

A spin is a fundamental property of matter responsible for NMR. Therefore, all nuclei experiencing the magnetic resonance phenomena possess a spin.

Consider a nuclear spin possessing an angular momentum $\hbar\vec{I}$ and a magnetic moment $\vec{\mu}$. The two quantities are proportional to each other according to a fundamental symmetry theorem or the Wigner-Eckart theorem of quantum mechanics:

$$\vec{\mu} = \gamma\hbar\vec{I} \qquad [2.1.1]$$

where γ is the gyromagnetic ratio of the nucleus. ħ is Planck's constant h divided by 2π.

The application of a magnetic field $\vec{H}$ produces interaction energy of the nucleus of amount $-\vec{\mu}.\vec{H}$. Therefore, we have the Hamiltonian of the Zeeman interaction given by

$$H_{zeeman} = -\vec{\mu}.\vec{H} \qquad [2.1.2]$$

With the field $\vec{H}$ along the z direction of the laboratory frame, the Hamiltonian can be rewritten as:

$$H_{zeeman} = -\gamma\hbar\left|\vec{H}\right|I_z, \qquad [2.1.3]$$

Where I_z is the z-component of I quantized into $2I + 1$ levels whose energies, **E**, the eigenvalues for the Hamiltonian H_{zeeman} are given by

$$E = -\gamma\hbar\left|\vec{H}\right|m, \qquad [2.1.4]$$

Where m is the magnetic quantum number which may have the values

$$I,\ I-1\ ,\ I-2,\ \ldots,\ -I+2,\ -I+1\ ,\ -I. \qquad [2.1.5]$$

Hence there is a constant separation, ΔE, between adjacent energy levels, where

$$\Delta E = \gamma\hbar\left|\vec{H}\right|. \qquad [2.1.6]$$

The selection rule governing magnetic dipole transitions is

$$\Delta m = \pm 1; \qquad [2.1.7]$$

Thus NMR occurs when an oscillating external magnetic field, $\vec{H}_1$ is applied with the correct polarization and which satisfies the frequency condition

$$\hbar\omega_0 = \Delta E = \gamma\hbar\left|\vec{\mathrm{H}}\right|. \qquad [2.1.8]$$

Hence

$$\omega_0 = \gamma\left|\vec{\mathrm{H}}\right| \qquad [2.1.9]$$

Equation [2.1.9] gives the resonance condition where ω_o is the angular frequency of the radiation from $\vec{\mathrm{H}}_1$ which is absorbed by the resonating nuclei. This equation can be also viewed as satisfying the conservation of energy. Note that Planck's constant has disappeared from the resonance condition. This fact suggests that the result is closely related to a classical picture.

The transition between two nuclear spin levels can be induced by applying a small sinusoidal radio-frequency (rf) magnetic field $\vec{\mathrm{H}}_1$ ($\left|\vec{\mathrm{H}}_1\right| << \left|\vec{\mathrm{H}}\right|$) perpendicular to the applied static field $\vec{\mathrm{H}}$. The Hamiltonian for this interaction is:

$$\mathrm{H'}_{zeeman} = -\vec{\mu}.\vec{\mathrm{H}}_1 \qquad [2.1.10]$$

If $\vec{\mathrm{H}}_1$ is so small that time dependent perturbation theory applies, then the transition probability per unit time is given by the Golden rule:

$$P_{mm'} = \gamma^2 \vec{\mathrm{H}_1}^2 \left| < m\left|\mathrm{I}_x\right|m' > \right|^2 \delta\left(\nu_{mm'} - \nu\right) \qquad [2.1.11]$$

Where

$$\nu_{mm'} = \frac{\Delta E_{mm'}}{h} = \frac{\gamma\left|\vec{\mathrm{H}}\right|m = m'|}{2\pi} \qquad [2.1.12]$$

The following figure illustrates the schematic diagram of Zeeman energy levels of spin-1/2 and spin-3/2.

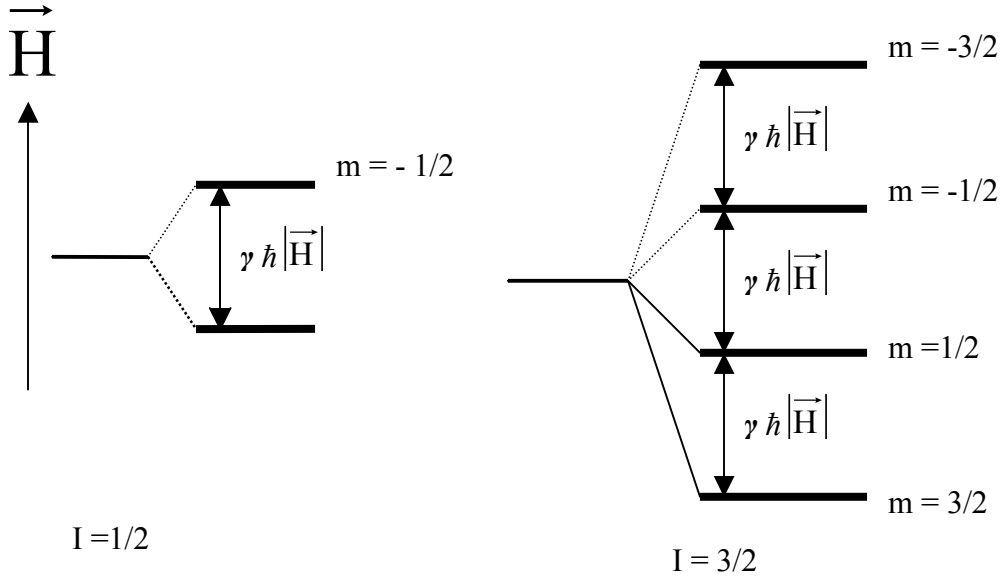

Figure 2.1: Zeeman energy levels for spin -1/2 and spin -3/2 cases.

1.2 Classical Macroscopic Treatment

Classical description of the motion of a spin system in an external magnetic field $\vec{H}$ is more helpful to visualize NMR by giving an open physical picture.

For a system with many molecular magnetic moments, a vector called the macroscopic magnetization $\vec{M}$ is defined as

$$\vec{M} = \sum_i \vec{\mu}_i \qquad [2.1.13]$$

It is the sum of all the individual nuclear magnetic moments per unit volume. When a static magnetic field $\vec{H}$ is applied, $\vec{M}$ undergoes precession about the direction of $\vec{H}$. The motion of $\vec{M}$ in the external field $\vec{H}$ is described by

$$\frac{d\vec{M}}{dt} = \gamma \vec{M} \times \vec{H} \qquad [2.1.14]$$

Instead of the fixed laboratory frame (x, y, z), it is easier to examine the spin system in the rotating frame (x', y', z') of frequency ω. The transformed equation is

$$\left(\frac{d\vec{M}}{dt}\right)_{rot} = \left(\frac{d\vec{M}}{dt}\right)_{lab} - \vec{\omega} \times \vec{M} = \gamma \cdot \vec{M} \times \vec{H} - \vec{\omega} \times \vec{M} = \gamma \vec{M} \times \left(\vec{H} + \vec{\omega}/\gamma\right) \qquad [2.1.15]$$

We see that the time derivative of $\vec{M}$ viewed from the reference frame rotating at $\vec{\omega}$ is the same as that in the stationary reference frame except for a substitution of a new field

$$\vec{H}_e = \vec{H} + \vec{\omega}/\gamma \qquad [2.1.16]$$

$\overrightarrow{H_e}$ is the effective field and the term $\vec{\omega}/\gamma$ represents a fictitious magnetic field component in the rotating frame. If we remember that $\vec{H}$ consists of a static field $\vec{H}_0$ in the z-direction and an rf field $\vec{H}_1$ in the x-direction, the transformed effective field becomes:

$$\overrightarrow{H_e} = \left(\left|\vec{H}_0\right| + \omega/\gamma\right)e_{z'} + \left|\vec{H}_1\right|e_{x'}. \qquad [2.1.17]$$

More details and advanced description about the classical treatment are described in reference [8,29,84].

1.3 Pulse NMR and Pulse Sequences: FID and Spin Echo

1.3.1 Pulse NMR: FID[86]

The free induction decay (FID) signal is the signal seen immediately after the 90^o pulse, due to the small voltage induced in the rf coil by the dephasing spins. This induced voltage is a measure of the component of a magnetization $\vec{M}$ in the horizontal plane after the rf pulse. The magnetization $\vec{M}$ decays due to spin-spin interaction and inhomogeneity of the static field $\vec{H}$. As seen in the classical treatment, the total magnetization vector is the sum of smaller magnetization vectors each arising from a small volume experiencing a homogeneous applied field. Such a small segment is called a spin isochromat [8,75]. According to the classical description and to the Larmor Theorem, $\vec{M}$ will precess about

the x'-axis with frequency $\gamma\left|\vec{H}_1\right|$ when an oscillating field $\vec{H}_1$ is applied along x**.** This makes $\vec{M}$ tip in longitudinal direction. The tipping angle θ of $\vec{M}$ is given by:

$$\theta = \gamma\left|\vec{H}_1\right| t_p \,, \qquad [2.1.18]$$

where t_p is the duration of $\vec{H}_1$, which can be such that it makes the magnetization $\vec{M}$ tip by an angle 90°, as illustrated in Figure 2.3.

a) initially**,** $\vec{M}$ is aligned along $\vec{H}$;

b) at the end of 90° pulse applied on x'-axis**,** $\vec{M}$ lies in y'-axis**;**

c) after the pulse, $\vec{M}$ dephases in x-y plane.

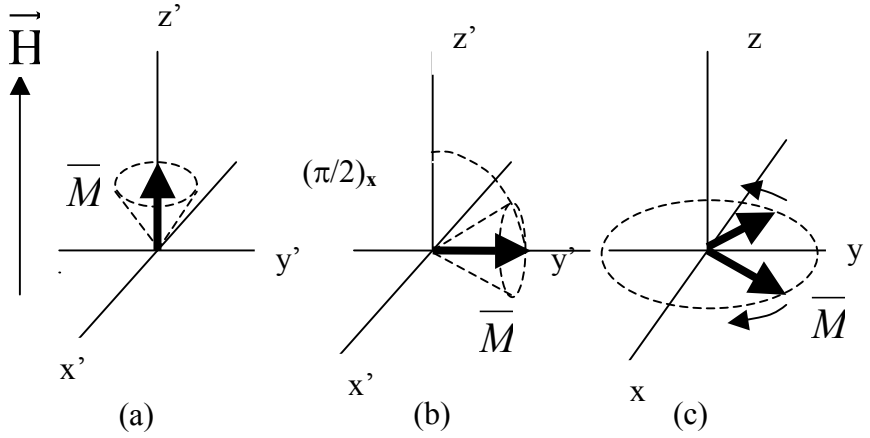

Figure 2.2: Effect of rf Pulse

By the end of the so-called 90° pulse, $\vec{M}$ has rotated down to the xy-plane.

The motion of a nuclear magnetization vector $\vec{M}$ in a constant magnetic field $\vec{H}$ and an oscillating magnetic field (rf field) $\vec{H}_1$ perpendicular to $\vec{H}$ and rotating around it with an angular velocity ω, is described by the equations of Bloch [10]:

$$\frac{d\overrightarrow{M}}{dt} = \gamma \overrightarrow{M} \times \left[\left(\left| \overrightarrow{\mathrm{H}} \right| + \frac{\omega}{\gamma} \right) e_z + \left| \overrightarrow{\mathrm{H}_1} \right| e_x \right] - \frac{\mathrm{M}_z - \mathrm{M}_0}{\mathrm{T}_1} e_z - \frac{\mathrm{M}_x e_x + \mathrm{M}_y e_y}{\mathrm{T}_2} \qquad [2.1.19]$$

Where

γ	is the gyromagnetic ratio,
e_x, e_y, e_z	are the unit vectors along the rotating frame,
$\mathrm{M_o}$	is the equilibrium magnetization at t = 0,
$\mathrm{T_1}$	is the longitudinal relaxation time
$\mathrm{T_2}$	is the transverse relaxation time.

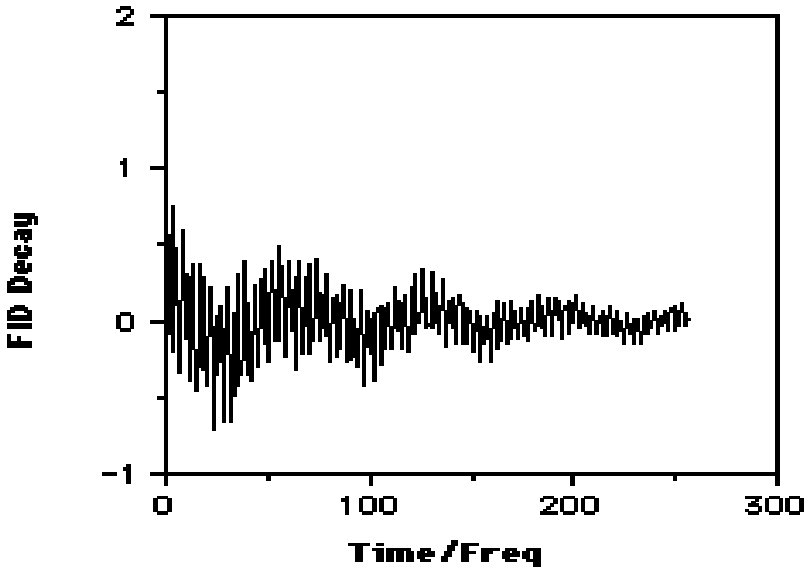

Figure 2.3: The Free Induction Decay

1.3.2 Pulse sequences: Hahn Spin Echo[85]

Just after finishing graduate studies, Erwin Hahn burst on the world of science with his remarkable discovery, Spin Echoes. His discovery provided the key impetus to the development of pulse methods in NMR, and must therefore be ranked among the most significant contributions to magnetic resonance.

In our method, we have used 90^o radio frequency pulses to excite the magnetization and 180^o pulses to refocus the spins to generate signal echoes.

The measurement of self-diffusion in its simplest form consists of carrying out a spin echo experiment. The experiment starts with a 90^o pulse, following which the magnetic vector $\vec{M}$ precesses in the plane perpendicular to the direction of $\vec{H}$, and an FID occurs. After the interval τ, an 180^o RF pulse is introduced. Following another interval τ, the magnetic spins recluster and a spin echo voltage signal is observed.

Figure 2.5 illustrates the 90^o-180^o pulse sequences.

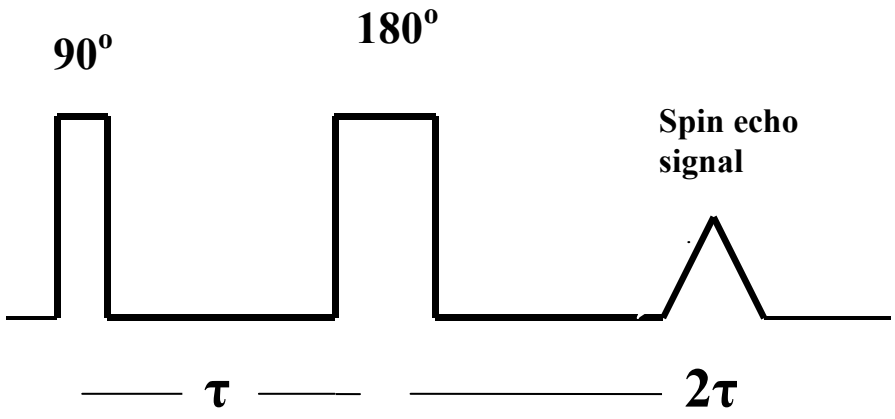

Figure 2.4: 90^o-180^o pulse sequences

Chapter 2:

Some Important Formulas in Nuclear Magnetic Resonance

2.1 Dipolar and Quadrupolar Relaxation

As indicated in the first part of this thesis, dipolar and quadrupolar mechanisms are predominant factors, which cause relaxation in most materials.

It is important to report that efficient relaxation occurs where there are many local magnetic fields fluctuating at or near the Larmor frequency, ω_L, for the observed nuclei. In the following equation, the spectral density ($J(\omega_L)$) represents the local magnetic fields present.

$$J(\omega_L) = \frac{\tau_c}{1 + \omega_L^2 \tau_c^2} \qquad [2.2.1]$$

In this equation, the spectral density at a given Larmor frequency, ω_L, is dependent upon the correlation time, τ_c.

2.1.1 Dipolar Relaxation

A nucleus experiencing the local magnetic fields of neighboring nuclei is subject to dipolar interactions. The strength of the interaction is dependent of the nature of the interacting nuclei which is given by their gyromagnetic ratios, γ, the distance separating them, r, and their relative orientation. A small perturbation of the system will modify these factors and then produce the change of the strength of the dipolar interaction, thereby giving rise to relaxation. The theory of Bloembergen, Purcell and Pound (BPP theory) established the derivation of the relaxation times (T_1, T_2, $T_{1\rho}$) for nuclei experiencing homonuclear dipolar interactions, where $T_{1\rho}$ is called spin-lattice relaxation in the rotating frame [8,31,32,33]. The formulas are the following:

$$\left(\frac{1}{T_1}\right)_{\text{hom}} = \left(\frac{\mu_0}{4\pi}\right)^2 \frac{2\gamma^4\hbar^2 I(I+I)}{5r^6}\left\{J(\omega_L) + 4J(2\omega_L)\right\} \quad [2.2.2]$$

$$\left(\frac{1}{T_2}\right)_{\text{hom}} = \left(\frac{\mu_0}{4\pi}\right)^2 \frac{\gamma^4\hbar^2 I(I+I)}{5r^6}\left\{3J(0) + 5J(\omega_L) + 2J(2\omega_L)\right\} \quad [2.2.3]$$

$$\left(\frac{1}{T_{1\rho}}\right)_{\text{hom}} = \left(\frac{\mu_0}{4\pi}\right)^2 \frac{\gamma^4\hbar^2 I(I+I)}{5r^6}\left\{3J(\omega_1) + 5J(\omega_L) + 2J(2\omega_L)\right\} \quad [2.2.4]$$

Where μ_0 is the permeability of a vacuum, $\hbar$ and I, previously defined.

As we can see in these equations, all three relaxation processes are dependent on local magnetic field fluctuations given by the spectral densities, J (ω_L). In addition, T_2 is sensitive to static fields given by the spectral density, $J(0)$, and $T_{1\rho}$ is also dependent on motions occurring at the rotational frequency, ω_1, in the $\vec{H}_1$ field. However, in the limit ω_1 tends to zero, $T_{1\rho}$ will approach T_2.

However, for relaxation processes due to heteronuclear interactions, we have the following group of equations:

$$\left(\frac{1}{T_1}\right)_{het} = \left(\frac{\mu_0}{4\pi}\right)^2 \frac{2\gamma_I{}^2\gamma_S{}^2\hbar^2 S(S+1)}{15r^6}\left\{J(\omega_1-\omega_S)+3J(\omega_1)+6J(\omega_1+\omega_S)\right\} \quad [2.2.5]$$

$$\left(\frac{1}{T_2}\right)_{het} = \left(\frac{\mu_0}{4\pi}\right)^2 \frac{\gamma_I{}^2\gamma_S{}^2\hbar^2 S(S+1)}{15r^6}\left\{4J(0)+J(\omega_1-\omega_S)+3J(\omega_1)+6J(\omega_s)+6J(\omega_1+\omega_S)\right\} \quad [2.2.6]$$

Where S and I refer the observed nuclei and the relaxing nuclei respectively, and r is the separation distance between the interacting nuclei.

2.1.2 Quadrupolar Relaxation

Nuclei with a quadrupolar moment are non-spherical (I>½) and can interact with fluctuating electric field gradients, thereby undergoing relaxation. The following equation describes the T_1 behavior for quadrupolar relaxation [31]:

$$\left(\frac{1}{T_1}\right)_{quad} = \frac{3}{40}\frac{2I+3)}{I^2(2I-1)}\left(1+\frac{\eta^2}{3}\right)\left(\frac{eQ}{\hbar}\frac{\partial^2 V}{\partial z'^2}\right)^2\left\{J(\omega_L)+4J(2\omega_L)\right\} \quad [2.2.7]$$

The parameters η, Q, $\frac{\partial^2 V}{\partial z'^2}$ represent respectively, an asymmetry factor, the quadrupole moment and the principal component of the electric field gradient tensor.

2.2 Diffusion in an Inhomogeneous Magnetic Field (FFG).

Diffusion in an inhomogeneous static magnetic field (g = ∂H/∂z) causes a spin echo to decay rapidly as the time between pulses is increased (T_2 also causes decay). The voltage amplitude of the spin echo is proportional to the magnetization M according to the equation:

$$M(\tau) = M_0 \exp\{-2/3[3\tau/T_2 + (\gamma g)^2 D \tau^3]\} \quad , \qquad [2.2.8]$$

Where M_0 is the magnetization at t = 0. Intuitively, the cause of the decay is the change in the nuclear precession frequency by diffusing to a different point in the sample at which the static field is different owing to the inhomogeneity in the magnetic field.

The next step is to describe the formal theory behind the diffusion in an inhomogeneous magnetic field.

Using the definition of the complex magnetization

$$M \equiv M_x + iM_y, \qquad [2.2.9]$$

the Bloch equations can be written in the form

$$\partial M(x,y,z,t)/\partial t = -i\gamma h(x,y,z)M(x,y,z,t) - M(x,y,z,t)/T_2 \qquad [2.2.10]$$

where

$$h(x, y, z) \equiv H(x, y, z) - H_o \qquad [2.2.11]$$

and H_o is the spatial average field over the sample. Since M describes a two-dimensional effect, the longitudinal relaxation time T_1 does not apply in this plane (x, y).

We proceed that, when the static field is inhomogeneous, we must include the effect of the spread in precession frequency. We therefore add the precession driving terms giving

$$\partial M(x,y,z,t)/\partial t = -i\gamma h(x,y,z)M(x,y,z,t) - M(x,y,z,t)/T_2 + D\nabla^2 M(x,y,z,t) \qquad [2.2.12]$$

where D is the diffusion coefficient.

For simplicity, we assume the inhomogeneous magnetic field has axial symmetry so that

$$H(x, y, z) = H_o + z\,(\partial H/\partial z) \qquad [2.2.13]$$

Substituting [2.2.13] for h (x, y, z), we obtain an equation describing free precession in a static magnetic field, which has a gradient along the z-direction:

$$\partial M/\partial t = -i\gamma z(\partial H/\partial z)M - M/T_2 + D\nabla^2 M. \qquad [2.2.14]$$

We try a solution

$$M(r,t) = M_o \exp(-t/T_2)\exp[-i\gamma z(\partial H/\partial z)t]A(t). \qquad [2.2.15]$$

When this solution is substituted in [2.2.14], we get a differential equation for A (t)

$$(1/A)dA/dt = -D(\gamma\partial H/\partial z)^2 t^2 \qquad [2.2.16]$$

or $$A = A(0)\exp[-D(\gamma\partial H/\partial z)^2 t^3/3]. \qquad [2.2.17]$$

The constant A *(0)* we incorporate into M_o giving

$$M(r,t) = M_o \exp(-t/T_2)\exp[-i\gamma z(\partial H/\partial z)t]\exp[-D(\gamma\partial H/\partial z)^2 t^3/3] \qquad [2.2.18]$$

for the magnetization following an initial π/2 pulse. This equation describes the development of magnetization with time from its initial value M_o at t = 0.

We now need to consider what happens if we apply a π pulse at time τ producing a rotation about the y-axis. The magnetization density just prior to the pulse is

$$M(r,\tau^-) = M_o \exp(-\tau/T_2)\exp[-i\gamma z(\partial H/\partial z)\tau]\exp[-D(\gamma\partial H/\partial z)^2\tau^3/3]. \qquad [2.2.19]$$

The π pulse leaves M_y unchanged, and changes M_x into $-M_x$**.** This is equivalent to changing

$-\gamma\, z(\partial H/\partial Z)\tau$ into $\pi + \gamma\, z(\partial H/\partial Z)\tau$. [2.2.20]

Thus at $t = \tau^+$

$$M(r,\tau^+) = M_o \exp(-\tau/T_2)\exp[i\gamma z(\partial H/\partial z)\tau]\exp(i\pi)\exp[-D(\gamma\partial H/\partial z)^2\tau^3/3]. \quad [2.2.21]$$

We now use [2.2.18] to describe the development of M^+ in time following τ**:**

$$M(r,t-\tau) = M(r,\tau)\exp[-(t-\tau)/T_2]\exp[-i\gamma z(\partial H/\partial z)(t-\tau)]\exp[-D(\gamma\partial H/\partial z)^2(t-\tau)^3/3]. \quad [2.2.22]$$

Substituting [2.2.19] we see that at $t - \tau = \tau$ (or $t = 2\tau$), the complex phase factors cancel, giving

$$M(r,2\tau) = M_o \exp(-2\tau/T_2)\exp[-D(\gamma\partial H/\partial z)^2 2\tau^3/3]. \quad [2.2.23]$$

This is **Erwin Hahn's** famous result of diffusion in the presence of a magnetic field gradient (1950) [1,10]. This equation shows that the transverse relaxation time T_2 and the diffusion coefficient D both give contributions to echo decay. To solve the equation for D, the values of the gradient $(\partial H/\partial z)$ and the relaxation time T_2 must be known, as well as the gyromagnetic ratio γ of the specific nuclei under study. The first term of the equation [2.2.23] represents the attenuation due to spin-spin relaxation and the second term is the attenuation due to diffusion.

Carr and Purcell (1954), and Torrey (1956) obtained the same expression by using a less intuitive but a more rigorous derivation. Singer and Abragam also obtained the same equation more intuitively [1,34,35,36,37].

However, nowadays most of the diffusion studies are carried out in homogeneous field with the pulsed-gradient, spin-echo technique. This method allows for keeping the T_2 contribution constant. There are three possible variables with this experiment: the time between the gradient pulses, Δ, the gradient strength, g, and the gradient pulse length, δ. By varying either the strength or duration of the gradient pulse, the effect of T_2 relaxation is kept constant throughout the entire experiment and the echo signal is solely due to diffusion. If diffusion occurs in the time interval Δ, then the echo amplitude can be modeled with the following equation (Stejskal and Tanner 1965) [8,37,51]:

$$A(2\tau) = A(0) \exp[-\gamma^2 g^2 D\delta^2 (\Delta - \delta/3)] \qquad [2.2.24]$$

2.3 Diffusion in presence of Pulse Field Gradient: The Stejskal and Tanner Pulse Sequence

The macroscopic aspect will be used in this approach. Let us start with Bloch equations including the effects of diffusion.

The Bloch equations for the macroscopic nuclear magnetization,

$$\vec{M}(\vec{r},t) = M_x \vec{i} + M_y \vec{j} + M_z \vec{k} \qquad [2.2.25]$$

including the diffusion of magnetization, are given by [1,10]:

$$\frac{\partial \vec{M}(\vec{r},t)}{\partial t} = \gamma \vec{M} \times \vec{H}(\vec{r},t) - \frac{M_x \vec{i} + M_y \vec{j}}{T_2} - \frac{(M_z - M_o)\vec{k}}{T_1} + D\vec{\nabla}^2 \vec{M} \,. \qquad [2.2.26]$$

In the case of anisotropic diffusion, the last term in equation [2.2.26] would be replaced by:

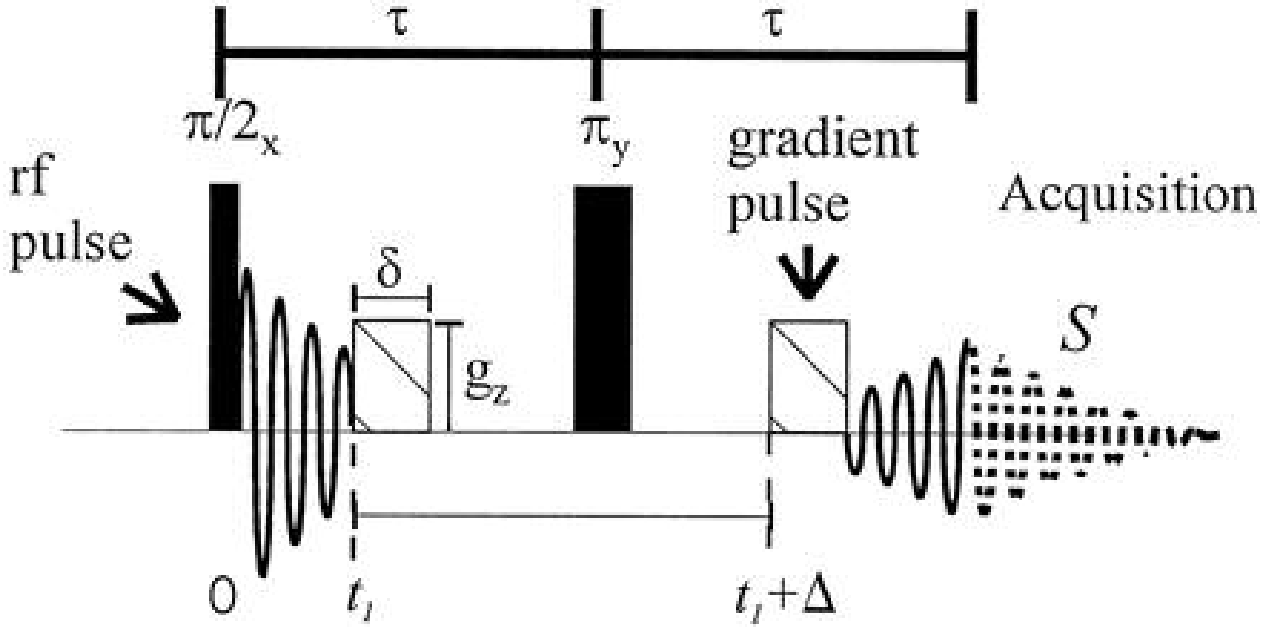

Figure 2.5: The Pulse Field Gradient, The Stejskal and Tanner Pulse Sequence

$$\vec{\nabla}(\vec{D}.\vec{\nabla}M) \qquad [2.2.27]$$

Let $H_x = H_y = 0$, [2.2.28]

and assuming that the inhomogeneities caused by g are much smaller than B_o, we can write to a first approximation that

$$H_z = H_0 + (\vec{g}.\vec{r}) \qquad [2.2.29]$$

Where the vector g may be assumed constant through the sample.

Note that:

$$\vec{M} \times \vec{H} = (M_y H_z - M_z H_y)\vec{i} + (M_z H_x - M_x H_z)\vec{j} + (M_x H_y - M_y H_x)\vec{k} \qquad [2.2.30]$$

With these assumptions and in the absence of r.f. field, the equation of motion for the complex transverse precessing magnetization $M = M_x + iM_y$ follows from equation [2.2.26]:

$$\frac{\partial M}{\partial t} = i\omega_0 M - i\gamma(\vec{g} \times \vec{r})M - \frac{M}{T_2} + D\vec{\nabla}^2 M \qquad [2.2.31]$$

where

$$\omega_0 = \gamma H_0 \qquad [2.2.32]$$

is the Larmor frequency.

In the absence of diffusion (i.e. $D = 0$), the transverse magnetization relaxes exponentially with a time constant T_2 according to the form

$$M = \psi e^{-i\omega_0 t - t/T_2} \qquad [2.2.33]$$

where ψ represents the amplitude of the precessing magnetization unaffected by the relaxation. If we substitute equation [2.2.33] into [2.2.31], we obtain

$$\frac{\partial \psi}{\partial t} = -i\gamma(g.r)\psi + D\nabla^2\psi \qquad [2.2.34]$$

In the absence of diffusion, equation [2.2.34] is a first-order ordinary differential equation with solution

$$\psi(r,t) = S\exp(-i\gamma r.F) \qquad [2.2.35]$$

where S is a constant and

$$F(t) = \int_0^t g(t')dt'. \qquad [2.2.36]$$

Now, if we consider the case of the PFG pulse sequence, then during the period from the $\pi / 2$ pulse to the π pulse, we have:

$$\psi(r,t) = S\exp(-i\gamma r.F), \qquad [2.2.37]$$

and S corresponds to the value of ψ immediately after the $\pi / 2$ pulse.

After the π pulse, we have

$$\psi(r,t) = S\exp(-i\gamma r.(F - 2f)), \qquad [2.2.38]$$

where

$$f = F(\tau). \qquad [2.2.39]$$

Combining equations [2.2.37] and [2.2.38], we have

$$\psi(r,t) = S\exp(-i\gamma r.(F - 2H(t-\tau)f)), \qquad [2.2.40]$$

where H (t) is the Heaviside step function. We note here that equation [2.2.40] is valid for the Hahn spin-echo pulse sequence.

Now, we discuss the Stejskal and Tanner Pulse Sequence in the presence of diffusion. Assuming a solution of equation [2.2.34] including the effects of diffusion to be of the

form of equation [2.2.40], but allowing the amplitude S to be a function of t (i.e., S (t)), we obtain the following equation after substitution of [2.2.40] into [2.2.34]:

$$\frac{dS(t)}{dt} = -\gamma^2 D[F - 2H(t-\tau)f]^2 S(t) \qquad [2.2.41]$$

Integrating equation (2.3.13) from t = 0 to t = 2τ, we obtain

$$\begin{aligned} \ln\left[\frac{S(2\tau)}{S(0)}\right] &= \int_0^{\tau} -\gamma^2 D F^2 dt + \int_{\tau}^{2\tau} -\gamma^2 D\left[F - 2f\right]^2 dt \\ &= -\gamma^2 D\left\{\int_0^{2\tau} F^2 dt - 4f\int_{\tau}^{2\tau} F dt + 4f^2\tau\right\} \end{aligned} \qquad [2.2.42]$$

If we apply the gradient pulses as shown in the pulse sequences in Figure 2.5 and neglect the effects of any background gradients, then we can define g (t) as in the following table 2.1:

Subinterval of Pulse Sequence	g(t)
$0 < t < t1$	0
$T_1 < t \leq t_1 + \delta$	g
$T_1 + \delta < t \leq t_1 + \Delta$	0
$T_1 + \Delta < t \leq t_1 + \Delta + \delta$	g
$T_1 + \Delta + \delta < t \leq 2\tau$	0

Table 2.1: Field gradient g (t) for the Stejskal and Tanner Pulse Sequence

Using the above definition of g (t), F (t) is calculated as follows:

$$F(t) = \int_0^{t_1} 0\,dt + \int_{t_1}^{t_1+\delta} g\,dt + \int_{t_1+\delta}^{t_1+\Delta} 0\,dt + \int_{t_1+\Delta}^{t} g\,dt \qquad [2.2.43]$$
$$= g(t + \delta - t_1 - \Delta).$$

Using the symbolic algebra package Maple [17,83], we obtain the result

$$\ln\left[\frac{S(2\tau)}{S(0)}\right] = -\gamma^2 g^2 D \delta^2 (\Delta - \frac{\delta}{3}). \qquad [2.2.44]$$

The equation [2.2.44] is not a function of t_1, and thus the placement of the gradient pulses in the sequence is of no consequence; for example, there is no requirement that the gradient pulses be symmetrically placed around the π pulse.

2.4 Activation Volume

The ionic transport related to mechanical motions must produce volume fluctuations that can be probed by changing the pressure. The parameters are generally expressed in an Arrhenius equation:

$$A = A_o e^{\frac{-G}{RT}}, \qquad [2.2.45]$$

are related to diverse motional processes. These parameters could be a relaxation rate ($1/T_1$ or $1/T_2$), conductivity σ, or diffusion D.

In the Arrhenius equation, G is the Gibbs free energy and R is the gas constant.

The Gibbs free energy G is defined as [39]:

$$G = F + PV, \qquad [2.2.46]$$

where the Helmholtz free energy, F, is related to the internal energy E through a Legendre transformation:

$$F = E - TS. \quad [2.2.47]$$

With the relations

$$S = -\left(\frac{\delta G}{\delta T}\right)_p \text{ , and} \quad [2.2.48]$$

$$V = \left(\frac{\delta G}{\delta p}\right)_T \quad [2.2.49]$$

The Gibbs free energy can be extracted from the Arrhenius equation [2.2.45]:

$$G = -RT \ln\left(\frac{A}{A_0}\right) \text{ or} \quad [2.2.50]$$

$$G = -RT \ln A + RT \ln A_0 . \quad [2.2.51]$$

Using the diffusion as parameter of motional process, we have:

$$G = -RT \ln D + RT \ln D_0 . \quad [2.2.52]$$

D_0 is the diffusion coefficient at zero Gibbs free energy. Using the relation (2.4.5)

$$V = \left(\frac{\delta G}{\delta p}\right)_T = -RT\left(\frac{\delta \ln D}{\delta p}\right)_T \quad [2.2.53]$$

In the variable pressure experiment, we identify V in the previous equation with the activation volume ΔV. Therefore, ΔV is the activation volume for diffusion mechanism.

$$\Delta V = V = -RT\left(\frac{\delta(\ln D)}{\delta p}\right)_T \quad [2.2.54]$$

Similarly, in the case of relaxation and conductivity mechanism, the activation volume is respectively written as [40,42]:

$$\Delta V = V = -RT\left(\frac{\delta\left(\ln T_1\right)}{\delta p}\right)_T \qquad [2.2.55]$$

$$\Delta V = V = -RT\left(\frac{\delta\left(\ln \sigma\right)}{\delta p}\right)_T \qquad [2.2.56]$$

PART 3:

EXPERIMENTS

Chapter 1:

Research Methods

1.1 Introduction

Measurement of slow diffusion in electrolytes as a function of pressure requires techniques employing Static-Fringe Field Gradients [43,44,49]. Typically, self-diffusion measurements are made by Pulsed-Field Gradient methods [8,45,50]. The Static-Fringe Field Gradient is used for this investigation since it is much larger in magnitude than that obtained with NMR probe gradient coils. Furthermore, it is advantageous because of the relative ease of incorporating a pressure cell into the experiment.

There are other less direct methods for determining self-diffusion by NMR, such as measuring longitudinal and transverse spin relaxation.

1.2 Static-Fringe Field Gradient

The fringe field gradient (FFG) diffusion technique takes advantage of the large static gradient associated with an NMR superconducting magnet away from the center of the solenoid where the field is highly homogeneous. This large gradient in the fringe field of superconductive magnets allows the measurement of root-mean square molecular displacements as small as 200 A and self-diffusion coefficients, D, as small as about 10^{-12} cm^2/s. This idea was first published by Kimmich and co-workers [43,47].

In order to measure lower diffusion coefficients, the magnetic field gradient must be increased. The difficulties connected with the mechanical, electrical, and thermal requirements for increasing the field gradient strength limit the applicability of the pulsed field gradient (PFG) spin-echo technique to materials with diffusion coefficients exceeding $\sim 10^{-9}\,cm^2/s$.

Callaghan proposed a special pulse sequence MASSEY to overcome the difficulties of mismatch of the pulses and of possible mechanical shocks when using large field gradient pulses [45,48].

The ultimate step toward higher gradient stabilities is, however, to avoid any electronic control and, hence, any finite harmonics of the gradient. We therefore considered the constant gradients that occur in the fringe field of superconducting magnets with a very high strength and extreme stability. The measurement of the self-diffusion coefficient consists of carrying out a spin echo experiment.

Another advantage of the static-fringe-gradient method is that only minimal changes in the spectrometer configuration are required because the superconducting magnets

produce the field gradient naturally. Furthermore, problems related to mismatch of the gradient pulses, eddy currents, and mechanical shocks when using large field-gradient pulses are avoided.

The smallest diffusion coefficient measured in our series of experiments was $D_{min} = 1.6 \times 10^{-8}$ cm^2/s. This order of magnitude of the diffusion coefficient still remains accessible by pulsed field-gradient techniques available in our lab.

However, fringe-field gradient methods also have several disadvantages that make them rarely used today compared with the PFG techniques. One of the inherent problems of the FFG technique derives from the fact that the central value of the fringe field of a magnet is considerably lower than the field at the center of the magnet; the lower field will then result in a lower NMR frequency and reduced signal intensity. The sensitivity is even more reduced by the fact that a radiofrequency pulse of width $t_{w,}$ applied in the presence of a field gradient, will excite only a small slice of thickness Δz determined by the relation [49,31]:

$$\Delta z = 2\pi / (\gamma g t_w), \qquad [3.1.1]$$

where g is the field gradient strength oriented in the z direction of the main magnetic field. For example, the pulse width of duration $t_w = 2.6$ μs, in a gradient g = 0.253 T/cm, excites a slice of thickness $\Delta z = 0.4$ mm, assuming that the resonant nuclei are protons. The small number of irradiated nuclei thus results in a generally poor nuclear induction signal. In addition, precise positioning of the sample in the fringe field becomes very important. In our experiment, we have improved the sensitivity further by using flat RF coil geometries, which are more adapted to the thin slice. Another disadvantage of the

fringe-field gradient is that it is not possible to separate the effects of diffusion from spin-spin relaxation in a single experiment.

Demco, Johansson and Tegenfeldt [46] had pointed out another obvious disadvantage of the fringe-field gradient method. The gradient causes severe line broadening, masking possible chemical-shift differences between individual components in complex multicomponent systems, and further lowering the signal strength.

Jeglic et al.[51] had reported an analytical evaluation of the fringe magnetic field gradient and the resonance frequency in space inside and outside the coil of a typical superconducting magnet by a simple model that takes into account the actual geometry of the superconducting coil and the shim system.

Hall and Norwood [44] had demonstrated a technique for studying diffusion that can readily be implemented on a conventional NMR spectrometer. Unlike other techniques, this technique allows easy separation of transverse relaxation and diffusion, and in addition permits the individual components of a system to be studied. The major drawback of the technique is that it is relatively time consuming since it requires the acquisition of two-dimensional data sets with very high resolution and a good signal-to-noise ratio.

1.3 Pulsed field gradient

Experimental determination of D:
Pulsed Gradient Spin-Echo NMR

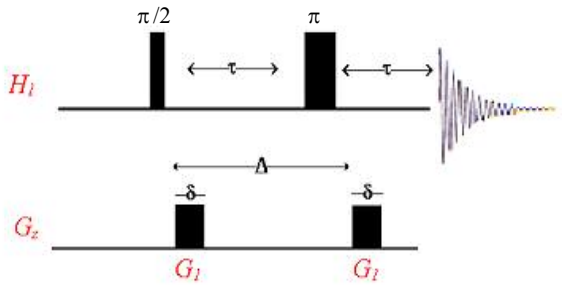

Echo decay profile in typical proton NMR diffusion experiment

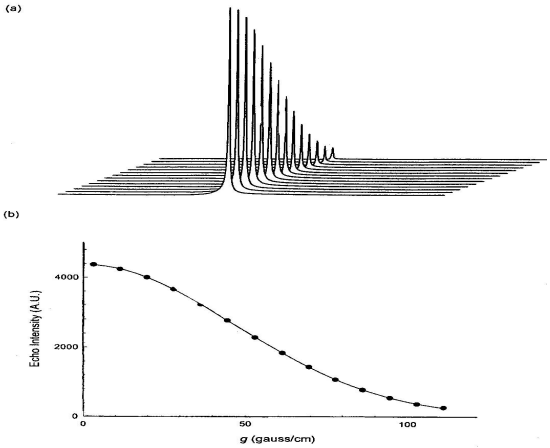

Echo attenuation fit to gaussian:

γ= nuclear gyromagnetic ratio
G = gradient strength
δ= gradient duration
Δ= gradient-refocusing pulse delay
D = self diffusion coefficient

$$A(G) = \exp[-\gamma^2 G^2 D \delta^2(\Delta-(\delta/3))]$$

Figure 3.1: Pulse Gradient Spin-Echo NMR

The static-fringe field gradient spin echo experiment was significantly improved by Stejskal and Tanner (1965), in the form of the pulsed-gradient spin-echo technique. Here the basic magnetic field is homogeneous throughout the experiment. The effective dispersion and refocussing of the spins occurs in two identical field gradient pulses [37] almost always rectangular of the same sign, separated in time so as to fit into the chosen rf pulse sequence interval.

According to a dimensional scale, we can range the pulsed field gradient (PFG) NMR in the gap between neutron scattering which is sensitive to nuclear position correlations over a few Angstroms and tracer measurements which require macroscopic displacements on the scale of millimeters and are therefore applicable only to molecules undergoing rapid diffusion. This PFG dimensional scale might be regarded as the organizational domain of molecules and includes features of macromolecular solutions, mesophase structure of liquid crystals, emulsions and highly disperse biological assemblies [45]. To that end, we point out PFG techniques are more commonly used as a probe of liquid state molecular organization.

Applying the magnetic field gradient in pulses instead of continuously (i.e., steady gradient experiment) circumvents a number of experimental limitations[51]: Since the gradient is off during acquisition, the line width is not broadened by the gradient, and thus the method is suitable for measuring the diffusion coefficient of more than one species simultaneously. The time over which diffusion is measured is well defined because the gradient is applied in pulses; this is of particular importance to studies of restricted diffusion. As the gradient is applied in pulses it is normally possible to separate the effects of diffusion from spin-spin relaxation[17].

However, potential problems with pulsed gradient methods exist and have been underlined previously.

There are many pulsed field gradient spin-echo methods namely the basic 90^{o}-180^{o} experiment (Stejskal and Tanner sequence), three-pulse sequences (stimulated echo method), Carr-Purcell echo train PGSE techniques, PGSE sequences using alternating or non-rectangular field-gradient pulses. Gross and Kosfeld have discussed the practical aspects of these latter two field-gradient pulses in some detail[52].

1.4 High Pressure in FFG

In our investigation, we have used a bomb made of copper beryllium, which will be described later in more detail.

This presentation includes high pressure NMR study of water self-diffusion in Nafion-117 membrane, and of proton (^{1}H) and fluorine (^{19}F) self-diffusion in diglyme/LiTf solution. The spin-lattice relaxation time T_1 was also measured as a function of hydrostatic pressure over a range of 1 bar-2.5 kbar.

Activation volumes were extracted from the diffusion coefficient pressure dependence.

1.5 Gradient Calibration

1.5.1 First step: the measured gradient

We used an axial Hall probe gauss meter to measure the magnetic field as a function of the z-position inside the bore of the superconducting magnet. Moving the Hall probe downward in the z-axis in increments of 5mm, the magnetic field for each new z-position is measured with the gauss meter. The results are reported in the Figure 3.2.

From the field values measured previously, we calculate the gradient as a function of the z-position as plotted in the Figure 3.3.

1.5.2 Second step: the calculated gradient

We have run four nuclei (^{1}H, ^{19}F, ^{7}Li, ^{11}B) in saturated aqueous solution of $LiBF_4$, at different resonance frequencies. The self-diffusion coefficients have been measured in the fringe-field probe. Using the diffusion in a steady field gradient relation:

$$g^2D=\text{Constant}, \qquad [3.1.4]$$

We calculate the gradient g_{cal} from the relation

$$g^2_{exp}D_{exp} = g^2_{cal}D_{cal} \qquad [3.1.5]$$

and

$$g_{cal} = g_{exp}\,(D_{exp} / D_{cal})^{1/2} \qquad [3.1.6]$$

Where D_{cal} is the diffusion-coefficient measured in the PFG method, D_{exp}, the experimental diffusion coefficient measured in the fringe field technique, and g_{exp}, the measured gradient deduced from the figure 3.3.

The linear interpolation method has assisted us to obtain a better calibration of the measured gradient. The results of the calculated gradient versus the z-position are reported in the Figure 3.4.

To fill in the gap in the calculated gradient values obtained by the above procedure, we have run only distilled water at 20^{o} C to measure the self-diffusion coefficients of proton nucleus ^{1}H at many different frequencies. Processing as previously, we have obtained the calculated gradient calibration showed in Figure 3.5.

The behavior of the graph of the measured gradient in the first step is very similar to the behavior of the graph of the calculated gradient measured in the second step. This suggests that the calculated gradient is a good estimation of the gradient that can be used in our fringe-field gradient method.

1.5.3 Third step

Here, we have set the self-diffusion coefficient of proton (^{1}H, in distilled water) from the value found in the standard table [54] (and also verified by the PFG method). Running the distilled water at 73.3 MHz resonance frequency in the high-pressure bomb probe in the fringe-field and using the fringe-field gradient equation, we have deduced the value of the

gradient g = 0.253 T/cm which is obviously more accurate and used for subsequent proton diffusion measurements (see Figures 3.6 and 3.7).

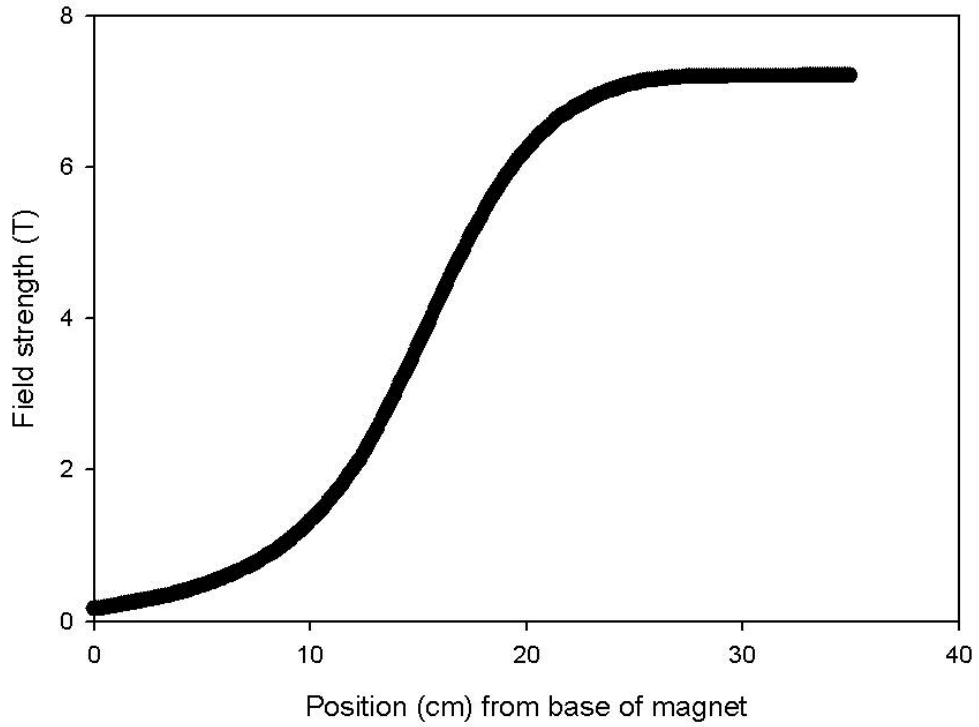

Figure 3.2: Field Strength versus Position

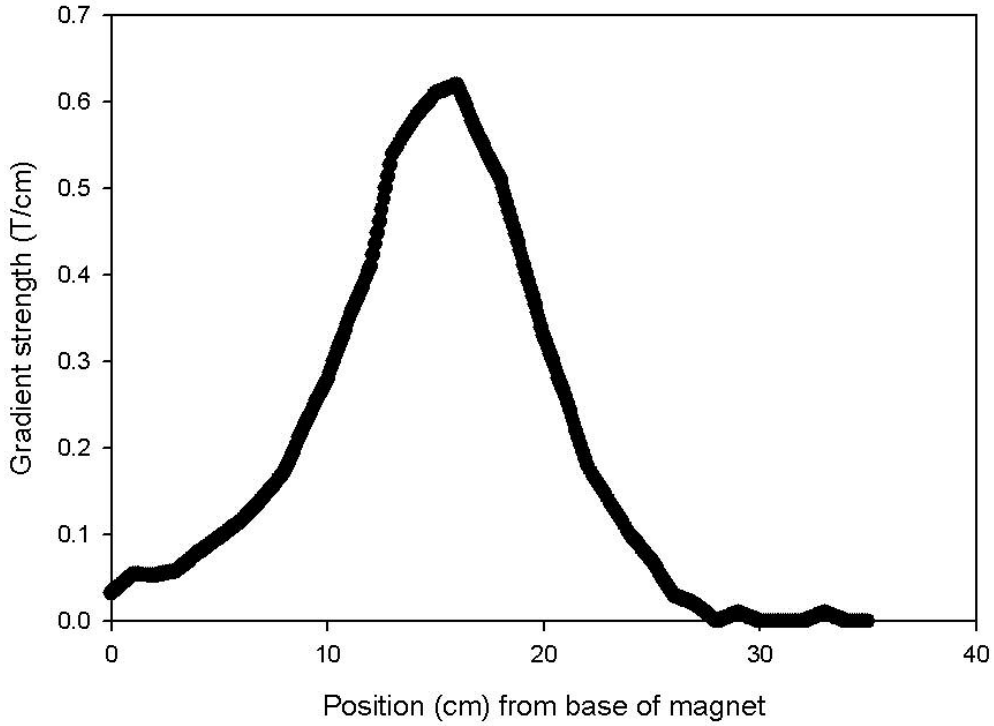

Figure 3.3: Gradient Strength versus Position

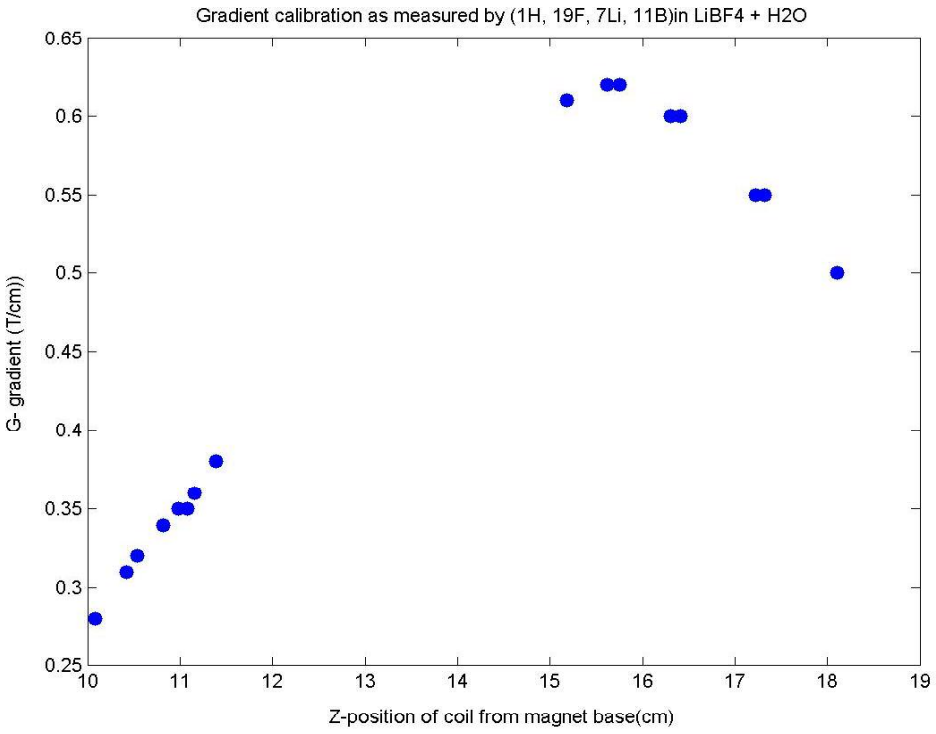

Figure 3.4: Field Gradient versus z- Position

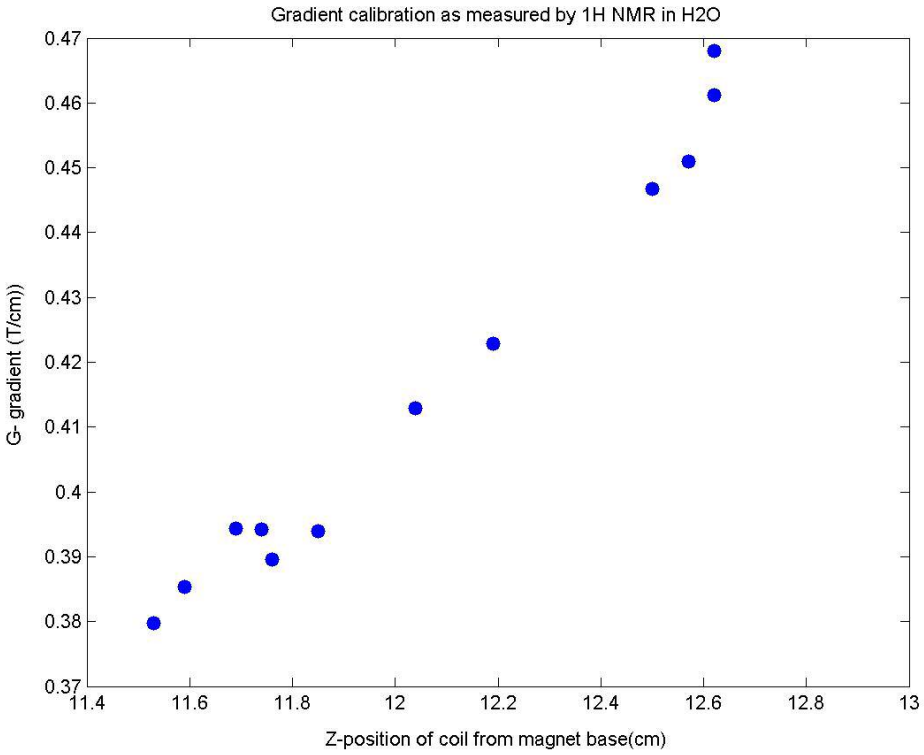

Figure 3.5: Field Gradient versus z-Position

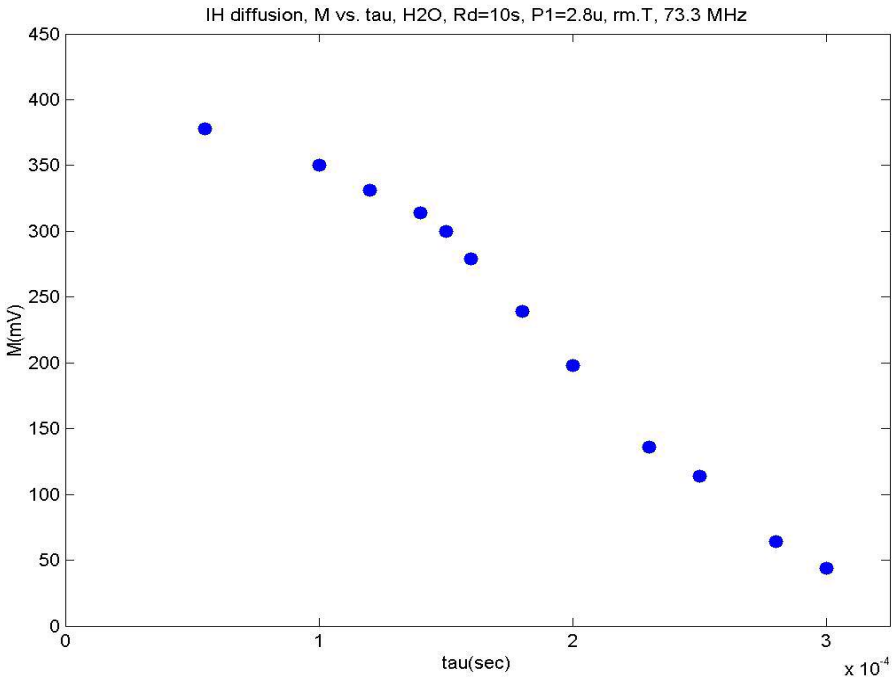

Figure 3.6: A typical plot of NMR spin-echo intensity, which is directly proportional to the nuclear magnetization, vs. the pulse separation for a static magnetic gradient.

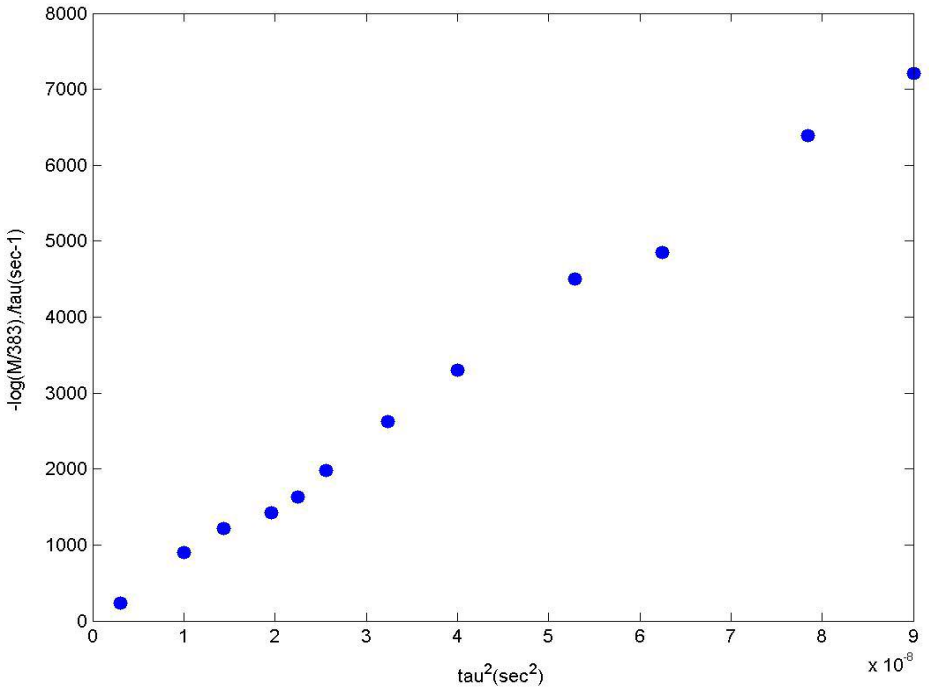

Figure 3.7: Graph of the nuclear magnetization vs. the square of the pulse separation. The graph shows a decrease in magnetization with an increase in pulse separation.

Chapter 2:

Experimental Equipment

2.1 Description of Hardware: Spectrometer and Probe

2.1.1 NMR Spectrometer

All the diffusion measurements were conducted with a Novex^{TM} NMR spectrometer interfaced to a microcomputer and a Lecroy 9400 digital oscilloscope, in conjunction with a Cryomagnet System superconductor magnet of central field strength of 7.3 T. A block diagram of Novex^{TM} NMR spectrometer and its accessories is shown in Figure 3.8. The function of each accessory is explained explicitly in reference [8,53]. The radiofrequency synthesizer produces an oscillating electrical signal with a very well defined frequency. The pulse gate is a fast switch, which is opened at defined moments in order to allow the radiofrequency reference wave to pass through. The effect is to chop a 'time-slice' out of the sinusoidal r.f. waveform. The duration of an r.f. pulse is referred as

the pulse width. The r.f. amplifier scales up the gated waveform so as to produce a large-amplitude r.f. pulse for transmission to the probe.

The preamplifier is a low noise radiofrequency amplifier which scales up the tiny NMR signal to a more convenient voltage level.

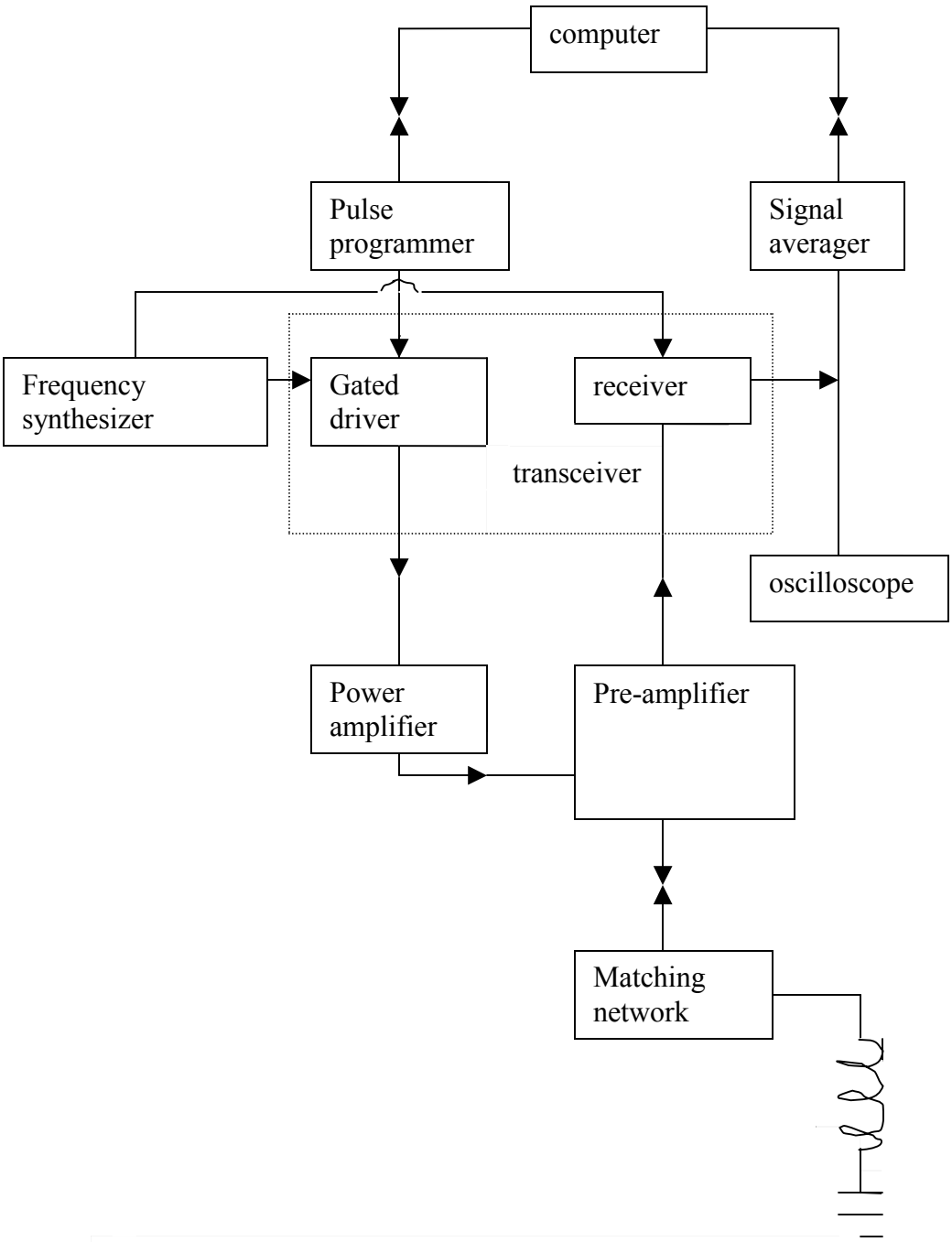

Figure 3.8: Block diagram for Novex™ NMR spectrometer

2.1.2 Probe

The probe is the most important and specialized part of the NMR spectrometer, which needs to be exchanged when switching between different NMR experiments, for example, from solid-state NMR experiments to liquid-state NMR experiments or for different frequency ranges. It has several functions such as locating the sample in the region of fringe field or homogeneous magnetic field and including radiofrequency electronic circuits for irradiating the sample with radiofrequency waves. In some cases, the probe has devices for stabilization of the temperature of the sample, and also rapidly rotating the sample in order to increase the resolution in the solid state.

The matching network for transmitter and receiver in the probe is shown in Figure 3.9. It consists of a matching capacitor C_M that couples the transmitter power into the probe circuit with maximum efficiency, a tuning capacitor C_T that is wired in parallel with the rf-coil of rectangular cross section enclosing the sample. Both C_M and C_T are high-voltage variable capacitance (0.8-10 pf) capacitors obtained from Polyflon Company.

The homemade coil has a rectangular cross section for a better filling factor (than cylindrical coil) corresponding to the flat samples was used. We have used two different sizes of rectangular coils for our set of measurements. The fringe field probe coil (coil with n = 8 turns, 1.9cm x 0.7 cm) used for the gradient calibration and the high pressure bomb coil (coil with n = 5 turns, 0.6 cm x 0.5 cm) used for our investigation.

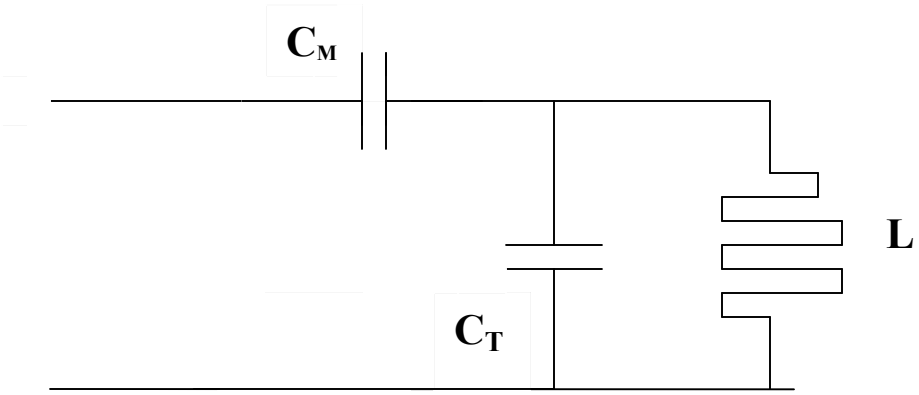

Figure 3.9: The L-C matching in NMR probe.

2.2 High Pressure Bomb in the Fringe-Field

2.2.1 Description of High Pressure Apparatus (Probe + Bomb + Attachment)

The experimental set up consists of three parts: the hydraulic pressure pump, the bomb made with CuBe alloy and two electrical feed-through connections holding the coil. The bomb was housed within the bore of the magnet and a home-built computer-controlled motorized stage moves the probe in precise steps to center the coil at precise particular values of field gradient strength ($g = dH_z/dz$), $g = 0.26$ T/cm for ^{1}H and $g = 0.24$ T/cm for ^{19}F. More details are given in the next chapter.

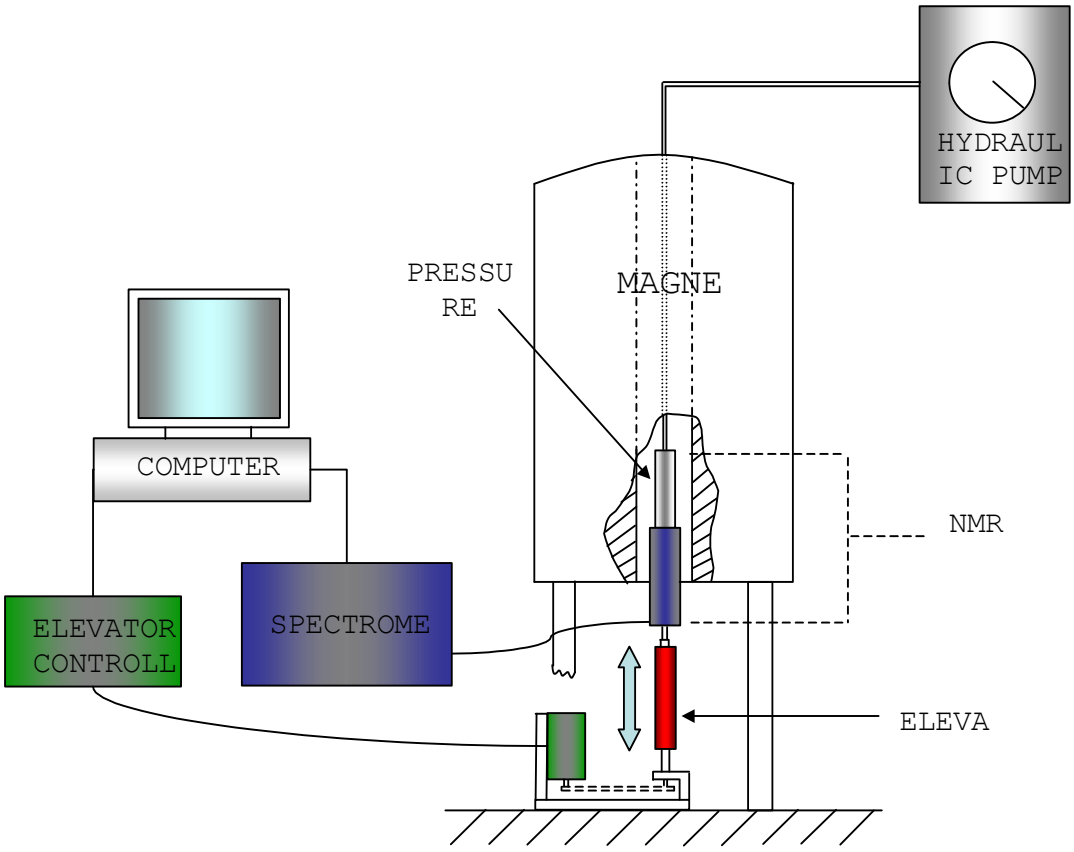

Fig. 3.10: Experimental setup. The magnetic and gradient are varied by changing the vertical position of the pressure cell.

2.2.2 Samples for NMR High Pressure Measurements

Our first application of high-pressure diffusion measurements was in NAFION, a sulfonated fluoropolymer used as the electrolyte in Polymer Electrolyte Membrane (PEM) fuel cells. Next, a high pressure NMR study of ^{1}H and ^{19}F self-diffusion in Diglyme/LiTf solution has been performed. For NMR measurements, the samples were hermetically sealed in thin polyethylene bags, which were shown to produce a negligible proton NMR background signal compared to the signal from the NAFION, Diglyme/LiTf, SPTES or Phosphoric Acid. This was necessary in order to isolate the sample from the pressure transmitting fluid. Results and discussion for four samples (Nafion, Diglyme/LiTf, SPTES, H_3PO_4 acid) are given in the next chapter.

PART 4:

EXPERIMENTAL RESULTS

Chapter 1:

High Pressure NMR Study of Water Self-Diffusion in NAFION-117 Membrane

J. Phys. Chem. B 2004, 108, 4260-4262

1.1 Introduction

There are a number of powerful NMR spectroscopic techniques that yield information for both structural and dynamic properties of materials. Additionally, diffusion and flow can be measured with good precision using NMR methods. When NMR is applied to the study of electrolytes, the gathered self-diffusion coefficients can be of great importance in characterizing ionic conduction and molecular motion. In this study, self-diffusion coefficients are measured and then used to evaluate mass transport in NAFION, a model material useful for hydrogen fuel cell applications. In general, the study of ion and molecular transport in polymers can be greatly assisted by employing pressure as the

thermodynamic variable. Although many investigations of NMR self-diffusion and electrical conductivity have been carried out in proton conducting membranes [55,56], and some electrical conductivity and NMR spin-lattice relaxation time (T_1) studies as a function of applied pressure have been published [57,58], to our knowledge, no work has been reported on the effect of high pressure on self-diffusion in a membrane. The NMR signal is dominated by water in the kinds of membranes used in fuel cells; nevertheless, it has been shown that water mobility is strongly correlated with electrical conductivity in these materials. Molecular motions and ionic diffusion are associated with volume fluctuations that can be probed directly by employing pressure as the thermodynamic variable. It is of interest to compare these new results (pressure dependent diffusion measurements) with previous work reported for variable pressure electric conductivity and NMR T_1 measurements for NAFION membranes at different water contents. Activation volumes for four different water concentrations in NAFION-117 are reported in the present work. Self-diffusion measurements are customarily made by the pulsed gradient spin-echo method [50], but in this work the static gradient associated with the fringe field of the NMR magnet was used. Two advantages of the static gradient are that its magnitude is typically much larger than obtainable with NMR probe gradient coils, and the relative ease of incorporating a pressure cell into the experiment (Figure 3.10).

1.2 Experimental Details

All studies were carried out on NAFION-117 supplied by E. I. du Pont de Nemours. Samples were made from 13 rectangular strips of film comprising a stack with dimensions 0.6 cm × 0.5 cm × 1.8 mm. Samples were first dried in a vacuum oven at 50 °C for several days and then saturated in distilled water for a few hours. After this preparation, the sample weight increased due to water uptake such that 100% × (weight of absorbed water) /(dry weight of NAFION) = 22%. Variation of the water uptake in samples was achieved by exposing the saturated sample (22 wt %) to the atmosphere for a limited time until the required water percentage was reached. For NMR measurements, the samples were hermetically sealed in thin polyethylene bags, which were shown to produce a negligible proton NMR background signal compared to the signal from the NAFION. This was necessary to isolate the sample from the pressure transmitting fluid (hydrogen-free FLUORINERT electronic fluid, FC-77 manufactured by 3M Co.).

The naturally existing field gradient of a conventional 7.3 T superconducting magnet was used for the measurements. The central field and gradient strength were varied continuously, within the limits of the magnet, by moving the NMR probe head within the bore of the magnet. The position of the NMR coil (which contains the sample) determines both the resonant frequency and the magnetic field gradient. A home-built computer controlled motorized stage, capable of moving the probe in precise steps of 0.25 mm, was used to center the coil at a central field value of 1.7 T with a gradient strength ($g = dH_z/dz$) of 0.253 T/cm. The latter quantity was determined experimentally

using the standard self-diffusion coefficient of water [54]. Accurate variation of the pressure (0-2.5 kbar) was carried out using an ENERPAC 11-400 hydraulic system fitted to a sealed Cu-Be alloy high-pressure chamber (bomb) inside of which resides the NMR excitation coil and sample. Electronic leads between the coil and external matching and tuning capacitors was facilitated by a hermetic feedthrough.

A home-built broadband NMR spectrometer operating at 72 MHz (the central field value corresponding to the position of the sample in the fringe-field) and utilizing a phase cycled spin-echo pulse sequence ($\pi/2$-τ-π-τ-acquire) was used to detect the proton echo signal from the sample. Pulse widths ($\pi/2$) were typically of 2.5 μs duration. Although it is acknowledged that this pulse width constitutes somewhat less than the full spectral coverage of all of the protons in the sample, estimated to be about 2 MHz (based on the ~2 mm sample thickness and the ~0.025 T/mm gradient), this value was chosen on the basis of the maximum signal amplitude obtainable for a given pulse separation.

1.3 Results

Proton spin-echo intensities $M(\tau)$ were measured as a function of the pulse separation, τ, and self-diffusion coefficients D were extracted from the data using the equation [2.2.23]

$$M(r,2\tau) = M_o \exp(-2\tau / T_2) \exp[-D(\gamma \partial H / \partial z)^2 2\tau^3 / 3].$$

In this expression M_0 is the maximum magnetization (at τ = 0) and γ is the proton gyromagnetic ratio. To assist in the analysis, proton transverse relaxation times T_2 were measured independently and the data were fit to a linearized version of equation [2.2.23] with slope = $2(\gamma g)^2 D/3$ and intercept = $2/T_2$. In this way the diffusion coefficients as a function of pressure were gathered. Linearized results (i.e., data presented as a function of the square of the pulse separation, τ^2) and pressure at 22-wt % water content in NAFION are illustrated in Figure 4.1. The self-diffusion coefficients as a function of pressure for four different water contents in NAFION are plotted in Figure 4.2.

The data in Figure 4.2, can be further analyzed to yield the activation volume ΔV associated with the diffusing water molecules according to the equation [2.2.54]:

$$\Delta V = V = -RT\left(\frac{\delta(\ln D)}{\delta p}\right)_T .$$

The activation volumes for four different water contents in NAFION-117 are given in Table 4.1.

Table 4.1 Activation Volumes for Different Water Contents in NAFION-117

Wt % H_2O	Activation vol (cm^3/mol)
6.6	13.2 ± 1.0
11.4	4.8 ± 0.4
16.0	3.9 ± 0.3
22.0	2.7 ± 0.2

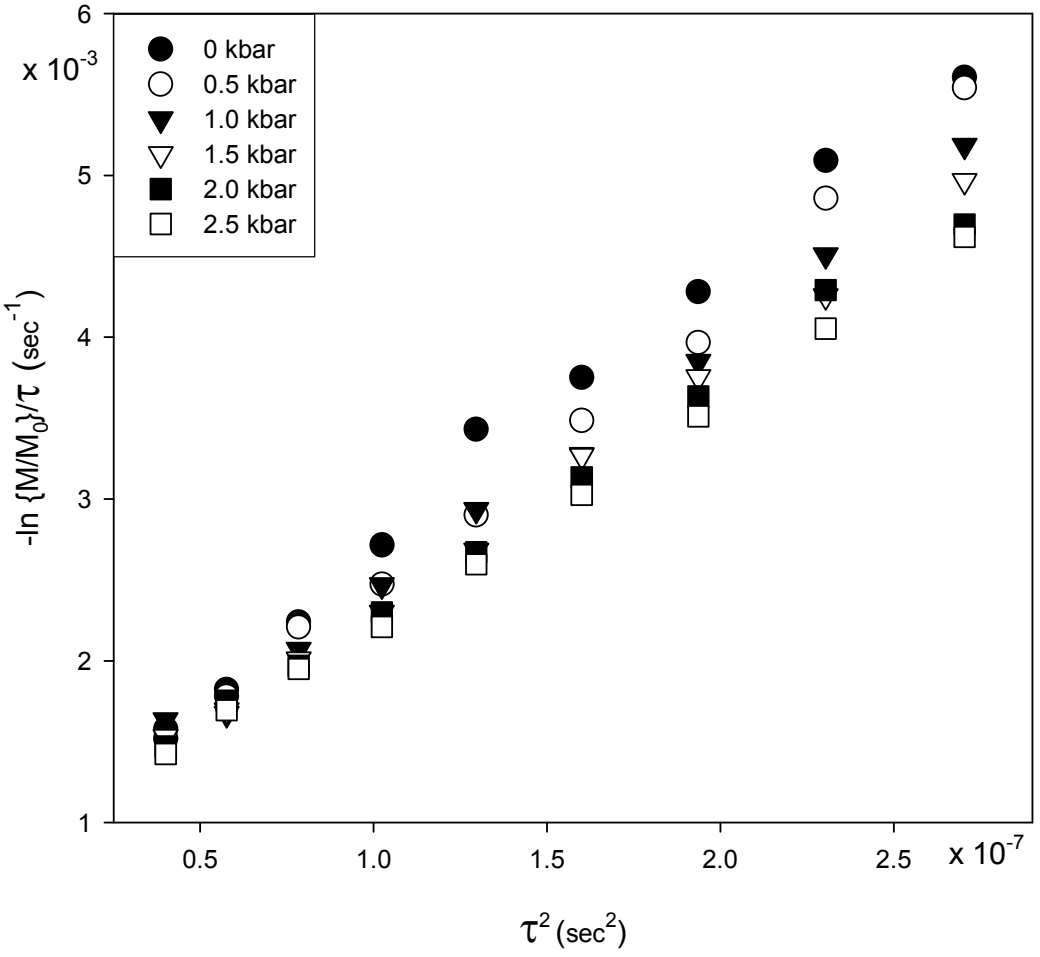

Figure 4.1: Semilog plot of nuclear magnetization, as a function of the square of the pulse separation (τ^2) and pressure at 22 wt % water content in NAFION at temperature 288 K.

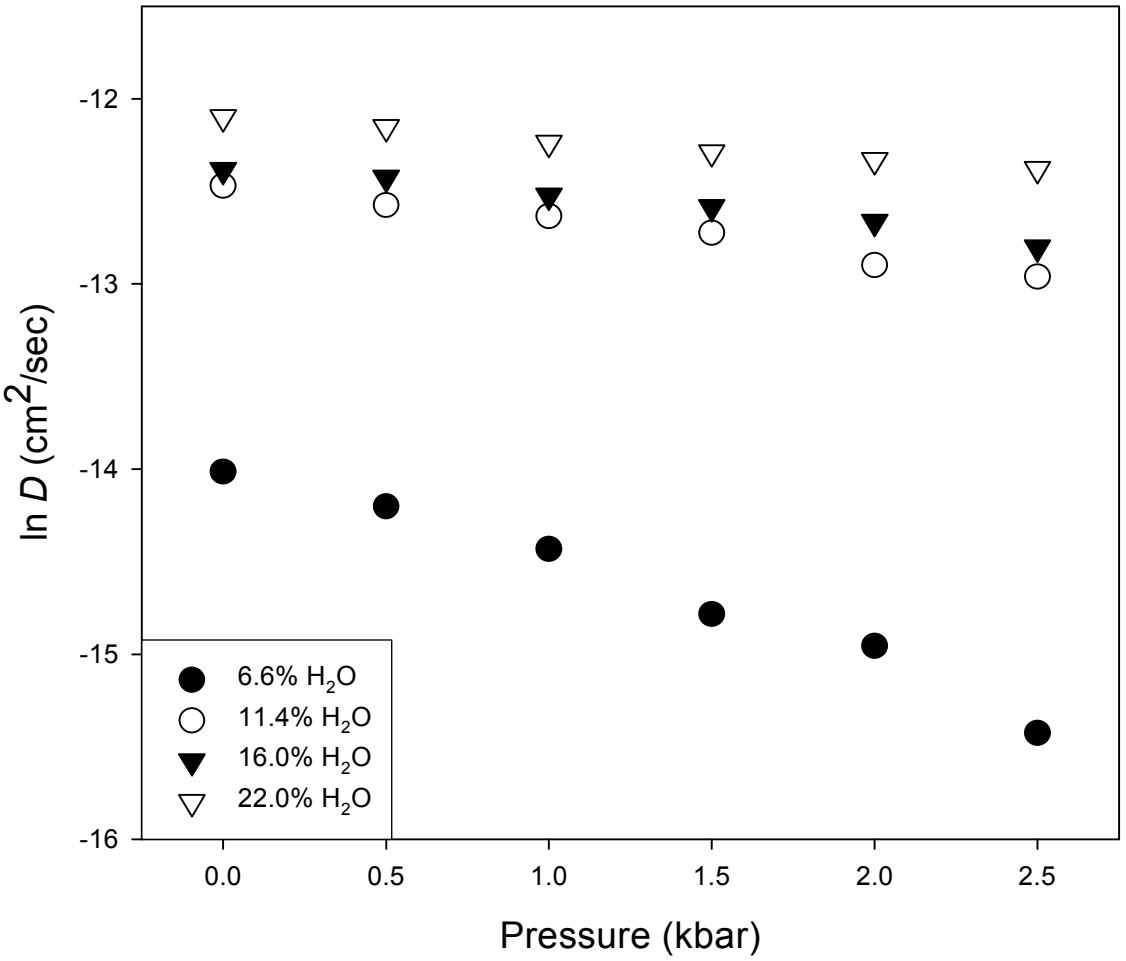

Figure 4.2: Semilog plot of the self-diffusion coefficient (*D*), as a function of pressure for different water contents in NAFION at temperature 288 K.

1.4 Discussion

The self-diffusion coefficient generally decreases with decreasing water content and also with increasing pressure as these yield greater restrictions for water molecular motions. In addition, the behavior of ΔV versus water content (wt %) exhibits two well-defined regions: a low water content region, where ΔV decreases rapidly with increasing water contents, and a high water content region, where ΔV decreases further by a very small amount with increasing water content. Others have previously observed this behavior in conductivity and T_1 results [19,40]. It is important to point out that T_1 is generally sensitive to fluctuations occurring on the time scale of the inverse of the NMR frequency and is thus responsive to short-range processes, whereas self-diffusion measurements probe typically longer (~1 μm) processes. Thus for example, molecular rotation, which is an effective relaxation means, could be expected to present a different activation volume than long-range translational motion. In the present case, both probes reveal a similar qualitative pressure dependence of the water molecular motion.

A relatively large ΔV of 13 cm^3/mol is observed for low water content. Similar values for ΔV have been obtained from electrical conductivity measurements of hydrated NAFION-117 films, and from ^1H and ^2H NMR spin-lattice relaxation measurements of comparably low water content films [57,60]. The observation that high activation volumes are often associated with solvent-free lithium polymer electrolytes suggests that ion transport in these cases is controlled by polymeric segmental motion [40,60]. Conductivity results for

very low water content NAFION yield an activation volume of about 50 cm^3/mol, consistent with values reported for lithium polymer electrolytes [61]. The highest activation volume presented here, though somewhat lower than the values usually associated with segmental motion are still consistent with the general view that NAFION with low water content can be viewed in terms of water molecule "clusters" and ions separated by polymer pendant chains. Conductivity takes place as protons move from cluster to cluster, as this motion is enhanced due to the segmental motion of the polymer.

At high water contents, ΔV is relatively small and does not vary much with increasing water content. In a previous paper [40], it was suggested that the electrical conductivity in this region is controlled more by bulk water than by the polymer. Zawodzinski et al. has also pointed out that the conductivity mechanism at high water content is expected to approach that of protons in bulk water due to the large number of pores within the polymer that are filled with water [55]. In fact, electrical conductivity of aqueous acid solutions tends to give small negative activation volumes, due to a compressibility factor (i.e., more ions per unit volume) that slightly outweighs the viscosity factor [19,62]. This is a complication that does not appear in the diffusion measurements, despite the correlation between water diffusivity and proton conductivity.

In our measurements the self-diffusion coefficient for the NAFION-117 sample with 22 wt % hydration decreased about 25% (from 5.56×10^{-6} cm^2/s to 4.20×10^{-6} cm^2/s) as the pressure increased from 0 to 2.5 kbar. Upon comparison with the results for pure water, as given by Benedek and Purcell, the self-diffusion coefficient was observed to decrease by roughly 10% as the pressure increased by the same amount [22]. This shows that even

though molecular motion at high water content is similar to that of bulk water, the polymer is still involved in the diffusion process. The advent of new polymer membranes that do not contain water for higher temperature fuel cell applications will require an understanding of alternative proton transport mechanisms, and it is expected that high-pressure NMR will become a very useful analytical tool in investigating these new materials.

1.5 Summary

High-pressure NMR measurements of the water self-diffusion coefficient in NAFION were conducted in the nonuniform (fringe) region of a superconducting magnet. Activation volumes associated with water mobility have been obtained at several different water contents. The largest activation volume (13 cm^3/mol) is found at the lowest water content (6.6%). As the water content increases, ΔV at first decreases rapidly and only gradually thereafter. This indicates that the transport mechanism in low water content films is significantly different than that at high water content, and possibly involves some contribution from segmental motions of the polymer. At higher water content, the change in ΔV is comparatively small, suggesting that the transport mechanism in high water content membranes is dominated by bulk water. These new results, which are in good agreement with the previous studies of spin-lattice relaxation

and electrical conductivity, illustrate how the pressure dependence of self-diffusion coefficients can be a useful tool in characterizing molecular motion in fuel cell membranes.

Chapter 2:

NMR Studies of Mass Transport in Lithium Conducting Polymer Electrolytes

From

Spring 2004, Proceedings Volumes

The Electrochemical Society, Inc.

The Society for Solid-State and Electrochemical Science and Technology

2.1 Introduction

The advent of sufficiently conductive solvent-free polymer electrolytes is still eagerly awaited by the lithium battery community. Despite over two decades of intense research and development, the highest ambient temperature conductivity, a significant fraction of which is carried by the anions, is still around 10^{-5} S/cm. The vast majority of effort has

been on polyethylene oxide (PEO) or other polyethers or polyether blends complexed with lithium salts [87]. The generally accepted view of the ion transport mechanism is that the motion of the ions is rate-limited by polymer segmental motions, hence, the significant efforts of many groups to synthesize amorphous, low-glass transition temperature analogues of PEO [87].

There have been recent reports [88,89] citing evidence of an alternative transport mechanism occurring along the helical PEO axis in the ordered or crystalline phase, along the lines originally suggested by Armand in a paper that was one of the earliest stimuli of the development of polymer electrolytes [90]. However unless the ordered regions extend over macroscopic distances, the ion transport will be dominated by the segmental motion-assisted mechanism characteristic of the amorphous phase. One way to achieve such long-range order is apply uniaxial stress, and it has been demonstrated that stretched PEO:LiI films exhibit significant conductivity enhancement along the stretch direction, despite having a higher percentage crystalline content than corresponding unstretched film [90].

Nuclear magnetic resonance (NMR) methods have played a significant role in our developing understanding of ion and polymer dynamics in lithium polymer electrolytes, from the seminal work of Berthier and coworkers, published over two decades ago [63] which first demonstrated that cation transport is associated with the amorphous phase, to more recent work referenced above, which suggested that crystalline conductivity can dominate if the helical structural units are aligned [89].

In this presentation, we describe recent investigations of polymer electrolyte systems, in which the mobility of both cations and anions is probed by NMR self-diffusion

measurements, using standard pulsed field gradient methods [50] and static gradient measurements as a function of applied hydrostatic pressure. The classes of material covered in this chapter is low molecular weight liquid diglyme ($CH_3 (OCH_2CH_2)_2OCH_3$) / lithium triflate ($LiCF_3SO_3$) complexes, which serve as a useful model system to study ionic association effects without the complicating factors of chain entanglement and crystallization in much higher molecular weight poly(ethyleneoxide).

Mass transport phenomena in this solution were studied by NMR methods and under suitable conditions, it is possible to characterize the motion of solvent molecules, cations, and anions.

2.2 Experimental Details

The solutions of seven different ratios of Diglyme:LiTf were received from Prof. Roger Frech of the University of Oklahoma. These measurements were conducted for four different ratios of diglyme to salt. Due to very hygroscopic nature of the solutions, they were stored in a dry box.

For NMR measurements the solutions were packed in 0.6 cm x 0.5 cm x 0.18 mm hermetically sealed thin polyethylene bags, which were shown to produce a negligible proton NMR background signal compared to the signal from the solution. This was necessary in order to isolate the sample from the pressure transmitting fluid. The naturally existing field gradient of a conventional 7.3 T superconducting magnet was used for the measurements. The central field and gradient strength were varied

continuously, within the limits of the magnet, by moving the NMR probe head within the bore of the magnet. The position of the NMR coil (which contains the sample) determines both the resonant frequency and the magnetic field gradient. A home-built counter controlled motorized stage, capable of moving the probe in precise steps of 0.25 mm, was used to center the coil at a field gradient strength ($g = dH_z/dz$) of 0.263 T/cm for ^1H nuclei and of 0.24 T/cm for ^{19}F nuclei. These values were determined experimentally using the standard self-diffusion coefficient of water [54]. Accurate variation of the pressure (0 to 2.5 kbar) was carried out using an ENERPAC 11-400 hydraulic system fitted to a sealed Cu-Be alloy high-pressure chamber (bomb) inside of which resides the NMR excitation coil and sample. Electronic leads between the coil and external matching and tuning capacitors was facilitated by a hermetic feed through.

A homebuilt broadband NMR spectrometer operating at 70.03 MHz (the central field value corresponding to the position of the sample in the fringe-field) and utilizing a phase cycled spin-echo pulse sequence ($\pi/2 - \tau - \pi - \tau$ - acquire) was used to detect the proton and fluorine echo signal from the sample. Pulse widths ($\pi/2$) were typically of 2.6 μs duration.

2.3 Results

Proton and fluorine spin echo intensities $M(\tau)$ were measured as a function of the pulse separation, τ, and self-diffusion coefficients D were extracted from the data using equation [2.2.23]:

$$M(r,2\tau) = M_o \exp(-2\tau / T_2) \exp[-D(\gamma \partial H / \partial z)^2 2\tau^3 / 3].$$

In this expression M_0 is the maximum magnetization (at $\tau = 0$) and γ is the gyromagnetic ratio of the nuclei. To assist in the analysis, proton and fluorine transverse relaxation times T_2 were measured independently and the data were fit to a linearized version of equation [2.2.23], with slope = $2(\gamma g)^2 D/3$ and intercept = $2/T_2$. In this way the diffusion coefficients were gathered with respect to applied pressure. Linearized results as a function of the square of the pulse separation, τ^2 and pressure at 10:1 ratio of diglyme:salt concentration is illustrated in Figure 4.4.

Figure 4.6 displays self-diffusion coefficients of all three mobile nuclei, ^{1}H, ^{7}Li, and ^{19}F in variable salt-concentration diglyme/LiTf, measured at ambient pressure using the pulsed field gradient method. Not surprisingly, all mobile species show the same trend in the viscous liquid medium, that their motion slows as the salt concentration increases. In fact, at the highest salt concentrations, all species move essentially at the same rate, indicating a highly associated complex.

The self-diffusion coefficients of proton as a function of pressure for four different salt contents in diglyme are plotted in Figure 4.5. The data in Figure 4.5 can be further analyzed to yield the activation volume Δν associated with the proton diffusion according to equation [2.2.54]:

$$\Delta V = V = -RT\left(\frac{\delta(\ln D)}{\delta p}\right)_T$$

The activation volumes for four different salt concentrations in diglyme are given in table 4.2.

The self-diffusion coefficients of fluorine were measured in same way as a function of pressure for the 10:1 diglyme:salt concentration and is plotted in Figure 4.5. The extracted activation volume for this salt concentration is 20.9 ± 1.5.

2.4 Discussion

The self-diffusion coefficient of protons decreases with increasing salt concentration and also with increasing pressure as this reflects greater restrictions for solvent molecular motions. This behavior is generally due to the increase of viscosity of the solution, as increase with salt concentration, thereby reduce diffusion.

In addition, the activation volume of proton ΔV increases with increasing salt concentration. A relatively large ΔV of 26.6 cm^3/mol is observed for 6:1 diglyme:salt concentration. The observation of high activation volume suggests the existence of strong correlations between solvent molecules and ions or ion pairs. That is, motion of any species involves significant reorganization of nearby species, resulting in a large ΔV.

The measured activation volume of ^{19}F for the 10:1 diglyme:salt concentration was 20.9 cm^3/mol., nearly the same as that obtained for the proton at same concentration (21.3 cm^3/mol). Again this result suggests that at high salt concentration the proton and fluorine diffusion are correlated.

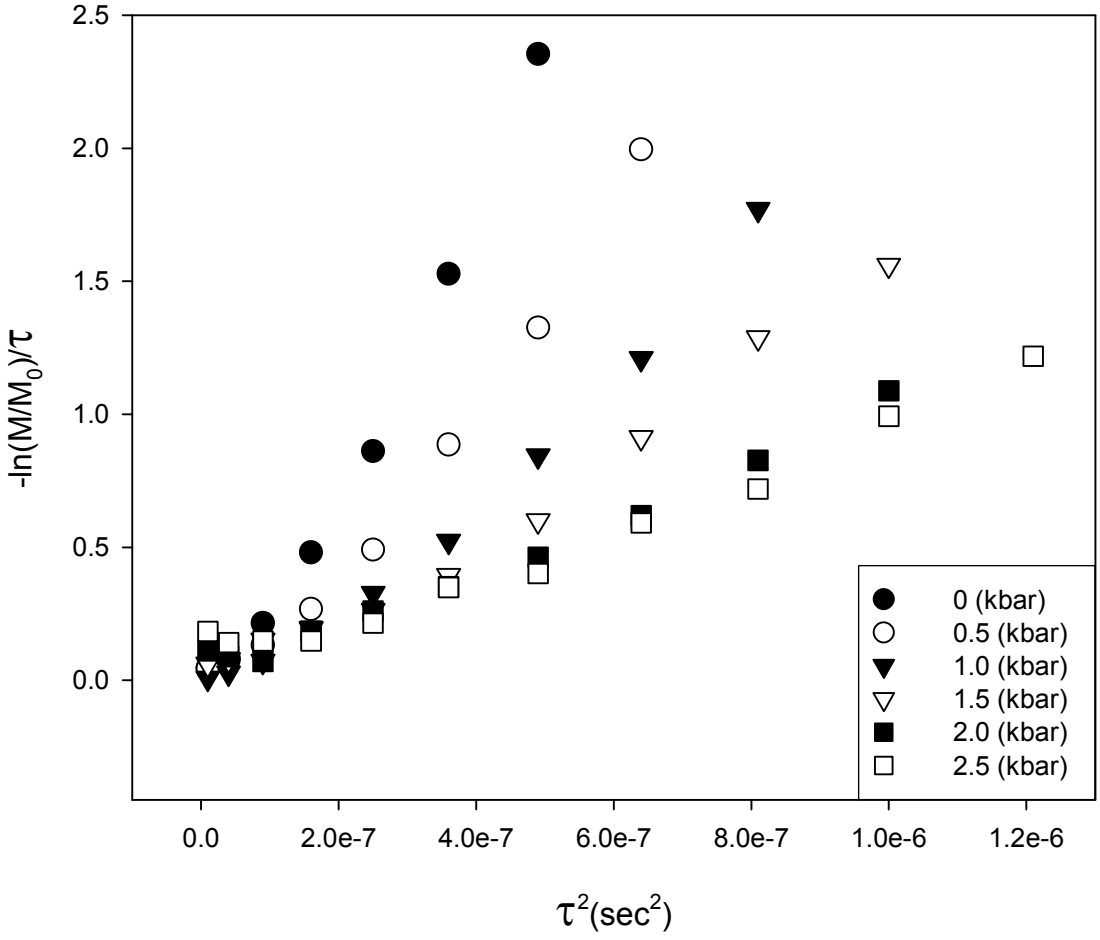

Figure 4.3: The Semi log plot of ^{1}H nuclear magnetization, as a function of square of the pulse separation and pressure at 10:1 diglyme:salt concentration at temperature 293K.

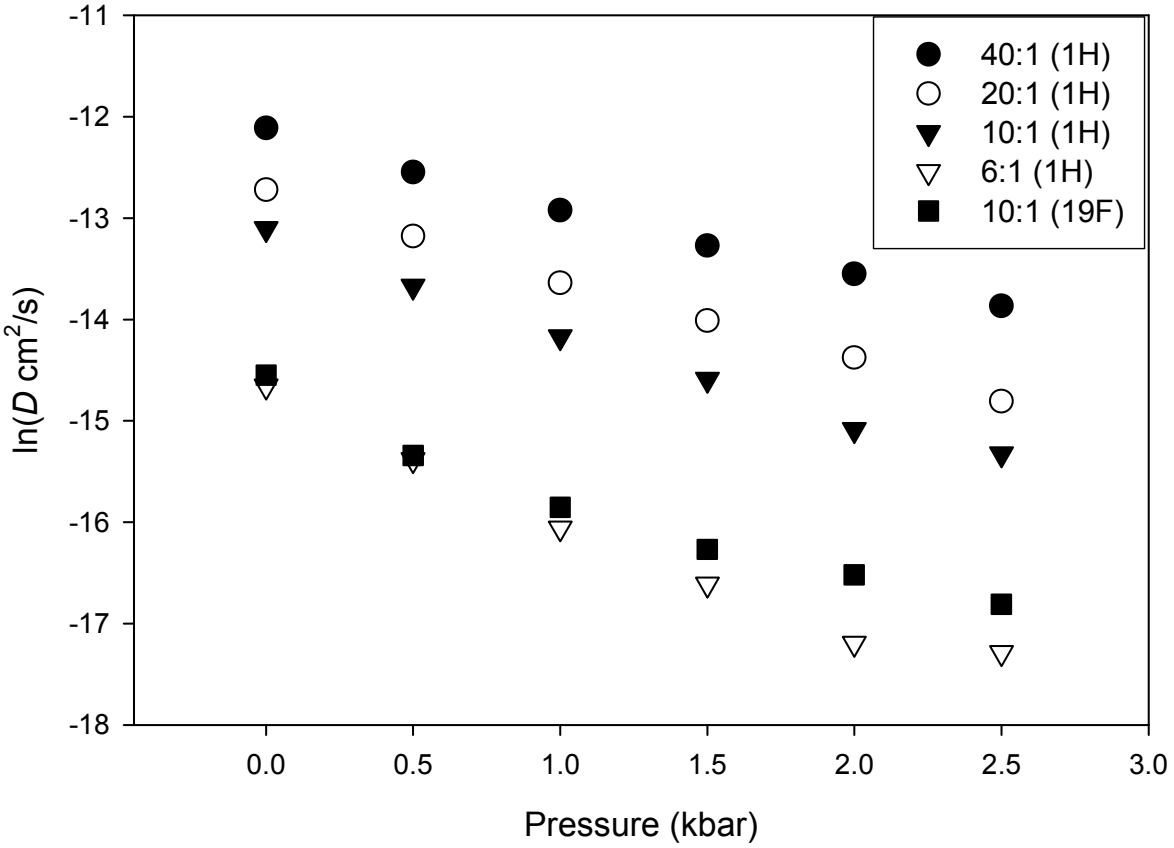

Figure 4.4: Variable pressure diffusion for different salt concentrations in diglyme/LiTf system. Data obtained by static gradient diffusion method.

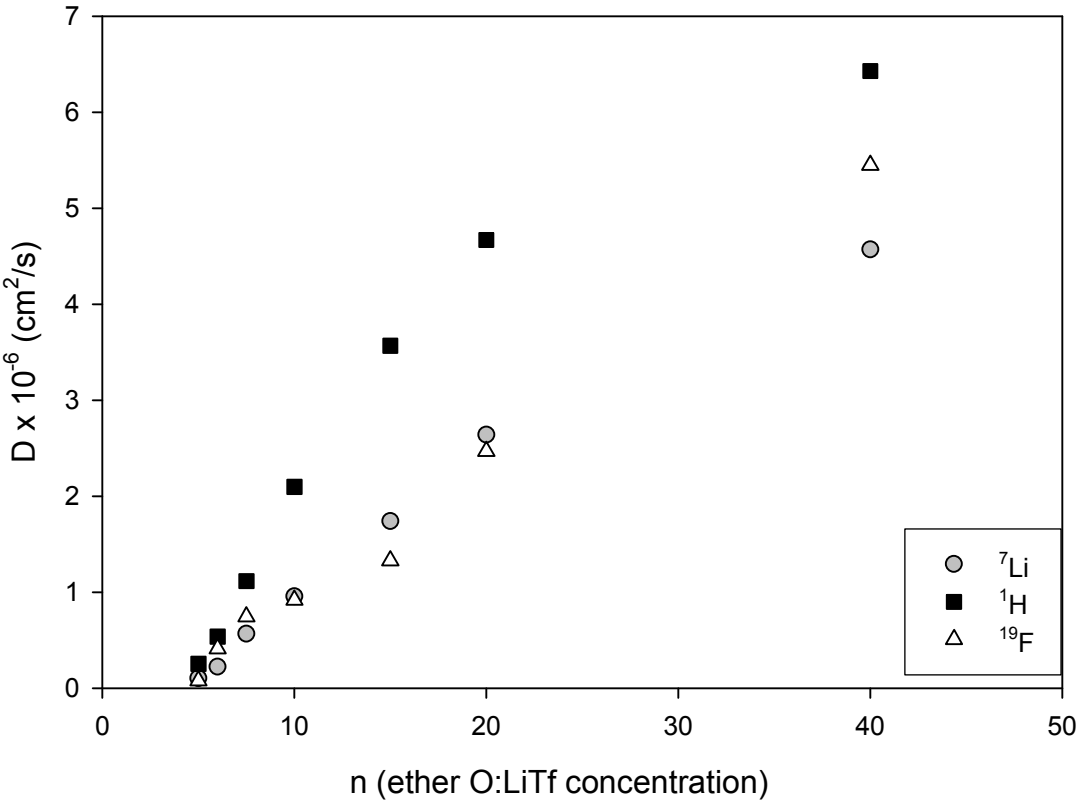

Figure 4.5: Self-diffusion coefficients for solvent, cation, and anion, respectively from ^{1}H, ^{7}Li, and ^{19}F pulsed field gradient NMR measurements in dyglyme/LiTf.

Table 4.2 The activation volumes for four different salts concentrations in diglyme (^{1}H).

Diglyme:Salt	Activation volume (cm^3/mol)
6:1	26.6 ± 2.0
10:1	21.9 ± 1.6
20:1	20.3 ± 1.5
40:1	16.8 ± 1.2

Chapter 3:

NMR investigation of water and methanol transport in sulfonated polyarylenethioethersulfones for fuel cell applications

Accepted For Publication, May 2005: J. Power Sources

3.1 Introduction

The development of high performance polymer electrolyte membrane fuel cells (PEMFC) is critically dependent upon the transport properties of the polymer electrolyte membrane available [64]. At present, Nafion, which is a perfluorosulfornated membrane with a hydrophobic fluorocarbon backbone and hydrophilic sulfornic pendent side chain, is the

only commercially available and successfully used membrane in PEMFC applications. However, since the performance of these membranes highly depends on their hydration levels, use of Nafion is limited to a temperature regime below 80^{o} C [65]. Significantly, higher temperatures (~ 120^{o} C) are considered optimum for operation of the PEMFC [66]. Other disadvantages include the high cost of Nafion and its high permeability to methanol, which is used as a fuel in direct oxidation fuel cells (DOFC) [67, 68].

Over the last decade, several new proton conducting polymer electrolyte membranes have been investigated [18,23,66]. High performance sulfonated polyarylenether, polyaryleneether sulfone, and polyaryleneether polymers have been described in the literature due to their exceptional thermal stability, good mechanical properties, and proton conductivity [55,70,73]. Direct oxidation fuel cell processes involve the transfer of fuel to the anode where it undergoes oxidation with the help of a catalyst. Advantages of DOFC include low-cost, reduced weight and volume compared with indirect fuel cells in which the fuel is reformed into hydrogen before use. The widely used fuel for DOFC is methanol. Methanol is of low cost and has easy storage capabilities. Nonetheless, it has a low boiling point (~ 65^{o} C) and permeates proton conduction membranes in fuel cells rather easily. This fuel permeability directly correlates with crossover, which refers to the transport of the intact fuel molecules to the cathode compartment, where the fuel molecules react with oxygen to produce water, carbon dioxide and heat. The result is the consumption of fuel without the production of electricity, thus reducing the overall efficiency of the fuel cell. Methanol crossover is especially high in Nafion.

The advent of sufficiently low cost, solid polymer electrolytes with high ionic conductivity, high temperature operation capability (i.e. high temperature water

retention), and low methanol permeability is still eagerly awaited by the direct methanol fuel cell (DMFC) community.

New membranes must also have physical, chemical and thermal stability and be relatively insensitive to metal-ion impurities [71], thus making it possible to use low cost catalysts and hardware materials.

One potential solution is the synthesis of new high performance polymer electrolyte membrane materials using a wholly aromatic polymer backbone along with a high sulfonic acid content that enhances water retention and can consequently allow elevated temperature operation. Moreover, endcapping of these new highly sulfonated polymers takes advantage of a bulky aromatic end group to eliminate water solubility of these polymers without adversely affecting their proton conductivity. These materials offer the possibility of fuel cell operation at temperatures >120^{o} C [73].

In this investigation, important parameters such as proton self-diffusion coefficient D, proton selectivity ratio (D_{OH}/D_{CH3}), and integrated proton intensities (CH_3/OH) were measured as a function of temperature for highly sulfonated polyarylenethioethersulfone (SPTES) polymer membrane with particular emphasis on water and methanol transport.

These measurements have been performed by using nuclear magnetic resonance pulse gradient spin-echo (NMR-PGSE) [72]. The PGSE method is a powerful technique, which allows measuring distinct diffusion coefficients in cases where the different nuclear (proton) environments can be resolved in the NMR spectrum, for example those of water and methanol [68].

Furthermore, self-diffusion coefficients were measured for four different water concentrations in SPTES sample as a function of pressure in addition to the above

measurements. Greater understanding of the mechanism of ion and molecular transport in polymers can be greatly assisted by employing pressure as the thermodynamic variable. Previous NMR and electrical conductivity investigations have been carried out in PEM materials as a function of applied pressure [19,57]. Variable pressure measurements can probe molecular motion and ionic diffusion processes associated with volume fluctuations. It is of interest to compare our new results taken from SPTES samples in this investigation with previous work reported for variable pressure self-diffusion and electrical conductivity for Nafion membrane at different water contents [19,40,57,74].

3.2 Experimental Details

Synthesis of the SPTES polymers has been described in detail elsewhere[73], and was provided by Dr. Robert Mantz of the Air Force Research Laboratory at Wright-Patterson Air Force Base. The SPTES membranes were cut into thin (~ 4 mm X 10 mm) rectangular strips, dried in a vacuum oven at 50^{o} C for 24 hours and then saturated in 2M methanol / deionized water for two days. Nafion-117 membranes were purchased from Dupont, boiled in 5% H_2O_2 solution and then 5% H_2SO_4 solution, rinsed on deionized water, and then dried over P_2O_5. Total solution uptake was determined by using a microbalance and recorded as 100% x (weight of saturated film-weight of dry film)/(weight of dry film).

For NMR measurements, samples were packed into 5 (OD) x 20 mm NMR tubes and flame-sealed under ambient atmosphere. The temperature range investigated were 20^{o} C to 140^{o} C, with equilibration times of 20 - 25 minutes between each temperature change.

NMR measurements were performed on a Chemagnetics CMX-300 spectrometer with ^{1}H operating at 301.02 MHz. Spectral information, and self-diffusion coefficients (D) were obtained. Spectral information were obtained by transforming the resulting free-induction decay (FID) of single $\pi/2$ (13□s) pulse sequence. Self-diffusion coefficients were obtained by the NMR Pulse Gradient Spin-Echo technique (NMR-PGSE). This technique involves the use of the Hahn spin-echo pulse sequence ($\pi/2$ - τ - π) and allows the determination of the rate of translational motion of diffusing species. For a diffusing system in the presence of a magnetic field the application of square-shaped magnetic gradients of magnitude g and duration δ results in attenuation of the echo amplitude A. This attenuation may be represented by $A(g) = \exp[-\gamma^2 g^2 D \delta^2(\Delta-(\delta/3))]$, where γ, D and Δ represents the nuclei's gyromagnetic constant, self-diffusion coefficient, and gradient delay. Applied gradient strengths ranged from 0.2 – 2.2 T/m, $\delta$and Δ ranged from 0.5 – 2.0 and 8-15 ms respectively. The resulting echo profile vs. gradient strengths is fitted to the above equation and D is extracted. Uncertainties in self-diffusion coefficient measurements are ~5%.

For the high pressure NMR measurements samples were first dried in a vacuum oven at 50º C for 24 hours and then saturated in water for another two days. After this preparation, the sample weight increased due to water uptake such that: 100% x (weight of absorbed water)/ (dry weight of PEM). Variation of the water uptake in samples was

achieved by exposing the saturated sample to the atmosphere for a limited time until the required water percentage was reached.

Stack samples were made from five rectangular strips of film with dimensions 0.6 cm x 0.5 cm x 1.5 mm. For NMR measurements, the samples were hermetically sealed in thin polyethylene bags, which were shown to produce a negligible proton NMR background signal compared to the signal from the sample. This was necessary in order to isolate the sample from the pressure transmitting fluid (hydrogen-free FLUORINERT electronic fluid, FC-77 manufactured by 3M Company).

The naturally existing field gradient of a conventional 7.3 T superconducting magnet was used for the measurements. The central field and gradient strength were varied continuously, within the limits of the magnet, by moving the NMR probe head within the bore of the magnet. The position of the NMR coil (which contains the sample) determines both the resonant frequency and the magnetic field gradient. A home-built counter controlled motorized stage, capable of moving the probe in precise steps of 0.25 mm, was used to center the coil at a field gradient strength ($g = dH_z/dz$) of 0.26 T/cm. This value was determined experimentally using the standard self-diffusion coefficient of water [54]. Accurate variation of the pressure (0 to 2.5 kbar) was carried out using an ENERPAC 11-400 hydraulic system fitted to a sealed Cu-Be alloy high-pressure chamber (bomb) inside of which resides the NMR excitation coil and sample. Electronic leads between the coil and external matching and tuning capacitors was facilitated by a hermetic feedthrough.

A homebuilt broadband NMR spectrometer operating at 69.35 MHz (the central field value corresponding to the position of the sample in the fringe-field) and utilizing a phase

cycled spin-echo pulse sequence ($\pi/2$ - τ - π - τ - *acquire*) was used to detect the proton echo signal from the sample. Pulse widths ($\pi/2$) were typically of 2.5 μs duration. This value was chosen on the basis of the maximum signal amplitude obtainable for a given pulse separation.

3.3 Results

A typical proton spectrum of an SPTES sample equilibrated in 2M methanol is shown in Figure 4.6. The sample chosen is denoted SP50 which is an endcapped 50/50 blend of sulfonated polyarylenethioethersulfone sulfite / polyarylenethioethersulfone sulfite. The two distinct proton environments namely that of water (OH) and (CH_3) are clearly resolved, even in the membrane, allowing one to determine the equilibrium methanol concentration in the film and to measure self-diffusion coefficients separately for each component. Self-diffusion measurements were made as a function of temperature for SPTES and / Nafion-117 samples, both equilibrated in 2M MeOH aqueous solutions. Diffusive decay of the main peak (OH) of the spectrum represents the water self-diffusion because the water OH groups far outnumber the methanol OH groups for the present MeOH concentration.

The ratio of the integrated intensities of the CH_3 to OH proton NMR peaks is approximately proportional to the methanol concentration in the membrane (at low methanol concentration), and thus can provide a direct measure of selective methanol uptake (i.e. partitioning), if the equilibrium concentration in the membrane is not equal to

that of the solution. The CH_3/OH percentage NMR intensity ratio is plotted in figure 4.9. The integrated CH_3/OH intensity ratio in a 2 M solution was determined to be about 6% in agreement with the calculated value. This is close to the values measured for Nafion below about 80^o C. From these results it is clear that the SPTES membrane takes up considerably less methanol from the 2M starting solution than Nafion, especially at low temperature.

The direct comparison of self-diffusion coefficients as a function of temperature between SPTES and Nafion is shown in Figure 4.7. The water diffusion coefficients in both membranes are quite comparable up to 80^o C, as are previously reported conductivity measurements[73]. However above 80^o C, the water diffusion coefficient in Nafion is reduced whereas it is increased in SPTES all the way up to the highest measurement temperature, 140^o C. This result provides indirect but nevertheless compelling evidence that water is well retained in SPTES at temperatures up to 140^o C. The drop in water diffusion in Nafion above 80^o C has been previously attributed to membrane dehydration [76]. Results of the diffusion coefficient of CH_3 in both samples are also included in Figure 4.7. Methanol diffusion is clearly lower in SPTES than in Nafion, but, in order to obtain more meaningful results with respect to operation in a DMFC, we define the membrane selectivity as the ratio of D (OH)/D (CH_3). The rationale for this definition is that D (OH) is correlated with proton conductivity and D (CH_3) is correlated with methanol permeability and hence crossover. It is thus desirable to have a proton conduction membrane with high selectivity. Variable temperature selectivity results for the two membranes are plotted in Figure 4.8. Selectivity ratio of SPTES is about a factor of two

higher than that of Nafion, although both membranes exhibit a decrease in selectivity with increasing temperature.

For high-pressure NMR measurements we used SPTES60 (SPTES 60/40) and SPTES50 (SPTES50/50) membranes for three different water contents. Proton spin echo intensities M (τ) were measured as a function of the pulse separation, τ, and self-diffusion coefficients D were extracted from the data using equation [2.2.23]:

$$M(r,2\tau) = M_o \exp(-2\tau / T_2) \exp[-D(\gamma \partial H / \partial z)^2 2\tau^3 / 3].$$

In this expression M_0 is the maximum magnetization (at τ = 0) and γ is the proton gyromagnetic ratio. To assist in the analysis, proton transverse relaxation times T_2 were measured independently and the data were fit to a linearized version of equation [2.2.23] with slope = $2(\gamma g)^2 D$ /3 and intercept = $2/T_2$. In this way the diffusion coefficients were gathered with respect to applied pressure. The self-diffusion coefficients were extracted from the above graphs as a function of pressure for four different water contents in SPTES 60 are plotted in Figure 4.10.

The data in Figure 4.10 can be further analyzed to yield the activation volume ΔV associated with the diffusing water molecules according to equation [2.2.54]:

$$\Delta V = V = -RT\left(\frac{\delta(\ln D)}{\delta p}\right)_T$$

The activation volumes for four different water contents in SPTES 60 are listed on the same plot. The self-diffusion coefficient generally decreases with decreasing water content and also with increasing pressure as this reflects greater restrictions for water molecular motions. In addition, the membranes with higher water contents shows ΔV increasing by a small amount with decreasing water content, and as the water content

lessens, ΔV increases by a reasonable amount. The same authors and others have previously observed this behavior in diffusion and conductivity measurements on Nafion [19,40,57].

A relatively large ΔV of 8.40 cm^3/mol is observed for moderately low water content in SPTES60 membrane. Similar behavior has been observed from diffusion and electrical conductivity measurements of hydrated NAFION-117 films with low water content [19,40,57,60,74]. The observation that high activation volumes are often associated with solvent-free polymer electrolytes suggests that ion transport in these cases is controlled by polymeric segmental motion. The highest activation volume we have seen here is lower than the values usually associated with segmental motion. The reason for that is probably the amount of water content (20%) in SPTES membrane is not low enough to have a reasonable effect by segmental motion. But we can still see that it's beginning to increase exponentially as water content decreases.

At high water contents, ΔV is relatively small in both membranes and does not vary much with increasing water content. In a previous paper [74], it was suggested that the diffusion in this region is controlled by bulk water more than by the polymer. Zawodzinski et al. has also pointed out that the conductivity mechanism at high water content is expected to approach that of bulk water due to the large number of pores within the polymer that are filled with water [55].

3.4 Conclusion

Water and methanol mobility in Nafion and SPTES membranes equilibrated in 2M MeOH were studied by PGSE NMR diffusion techniques. The new membranes exhibit significantly higher water diffusion than Nafion, especially for temperatures above 80^{o}C. Diffusivity remains high even beyond 140^{o}C, providing evidence of water being well-retained at higher temperature. We have also defined a selectivity criterion D(OH)/D(CH_3) and SPTES exhibits a higher value than Nafion.

High-pressure NMR measurements of the water self-diffusion coefficient in SPTES60 and SPTES50 were conducted in the non-uniform region (fringe) of a superconducting magnet. Activation volumes associated with water mobility have been obtained at several different water contents. The relatively largest activation volume (8.40 cm^3/mol) is found at the moderately lower water content (20%) of SPTES60 membrane. As the water content increases, ΔV decreases rapidly and only gradually thereafter. This indicates that segmental motions of the polymer govern the transport mechanism in low-water content films. At higher water content, the change in ΔV is comparatively small, suggesting that the transport mechanism in high-water content membranes is dominated by bulk water. These results, which are in good agreement with the previous studies of spin-lattice relaxation, diffusion and electrical conductivity of Nafion, illustrate how the pressure dependence of self-diffusion coefficients can be a useful tool in characterizing molecular motion for new fuel cell membranes.

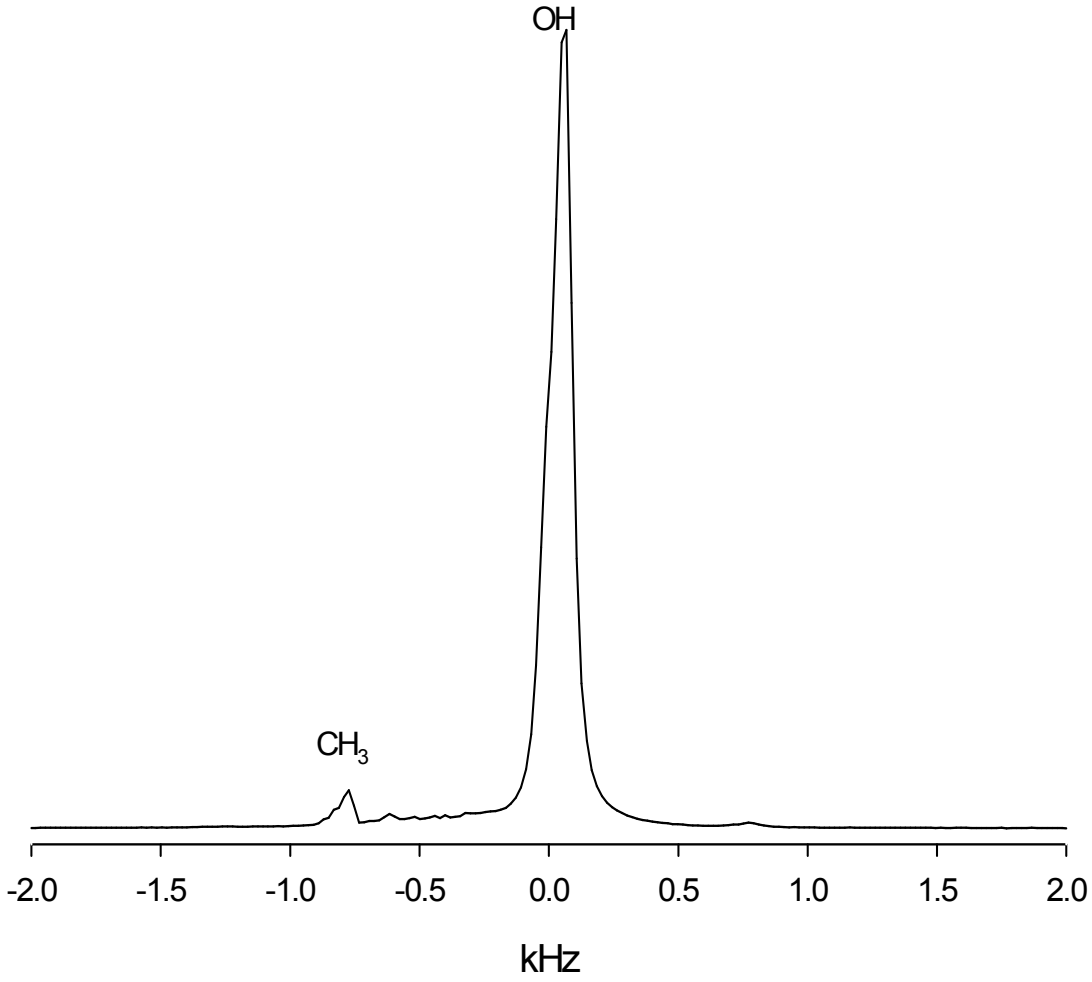

Figure 4.6: ^{1}H NMR spectrum of SPTES equilibrated in 2M MeOH at 313K

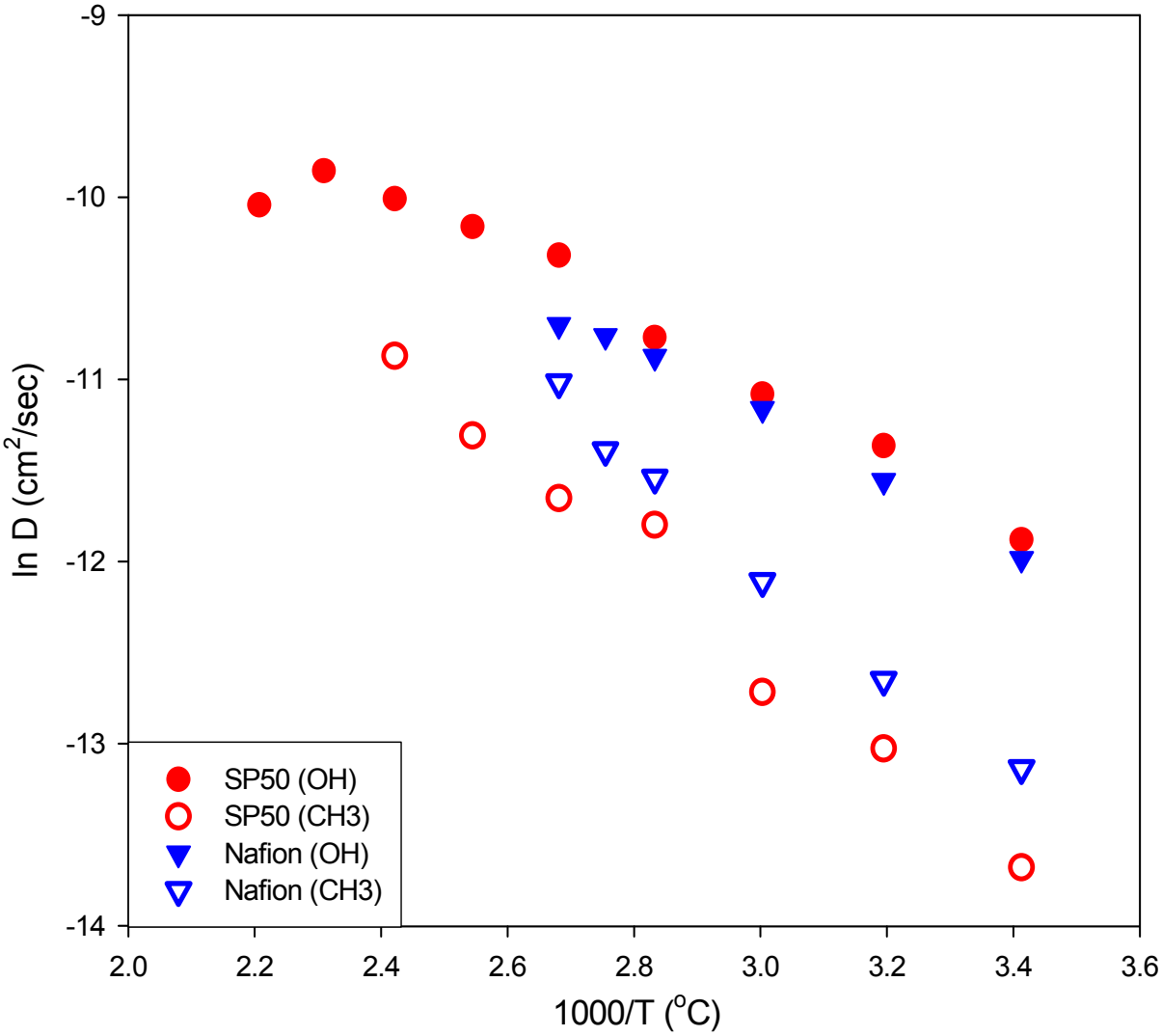

Figure 4.7: ^{1}H self-diffusion coefficients of 2M MeOH saturated SPTES and Nafion membranes

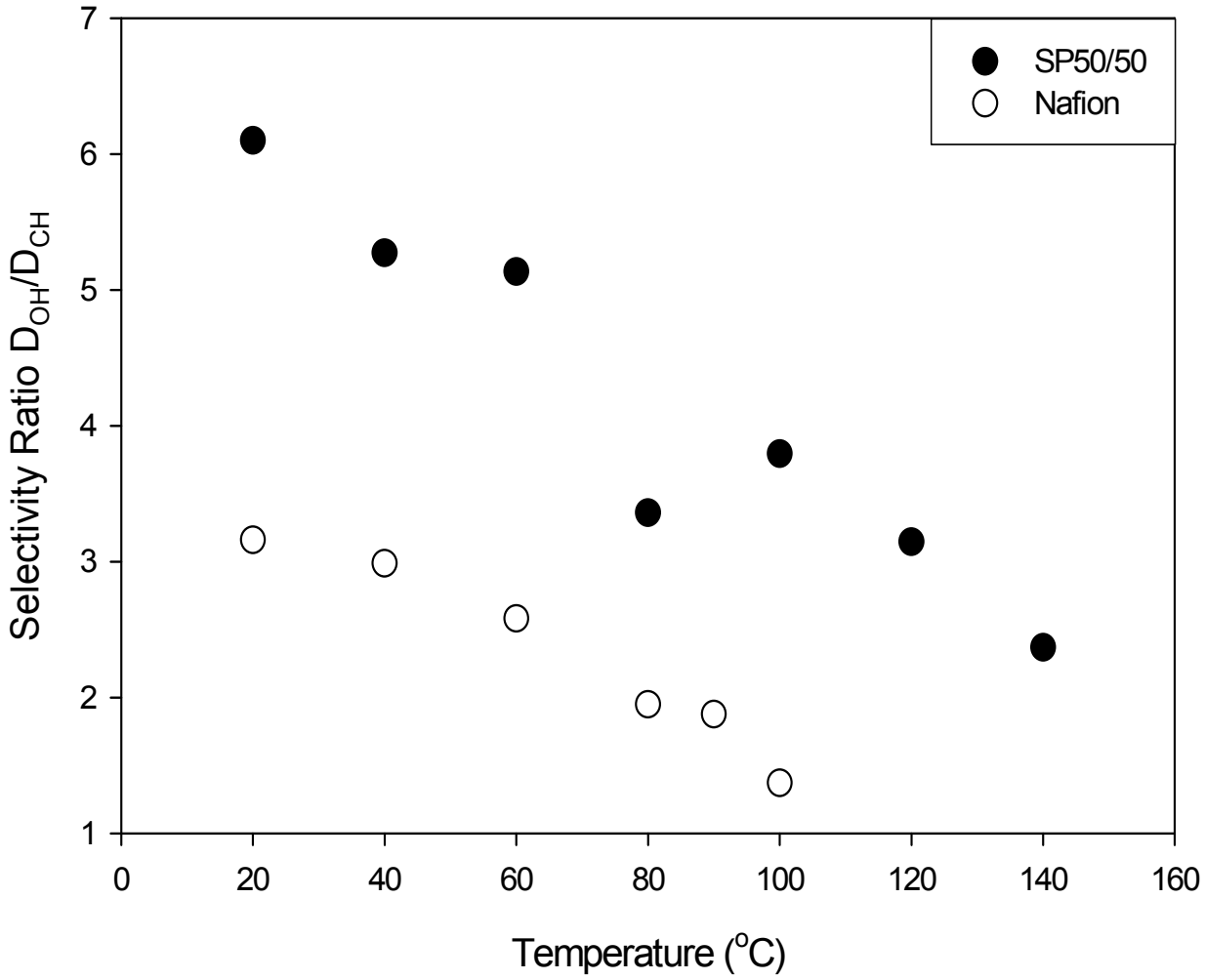

Figure 4.8: ^{1}H selectivity ratio of 2M MeOH saturated SPTE and Nafion membranes.

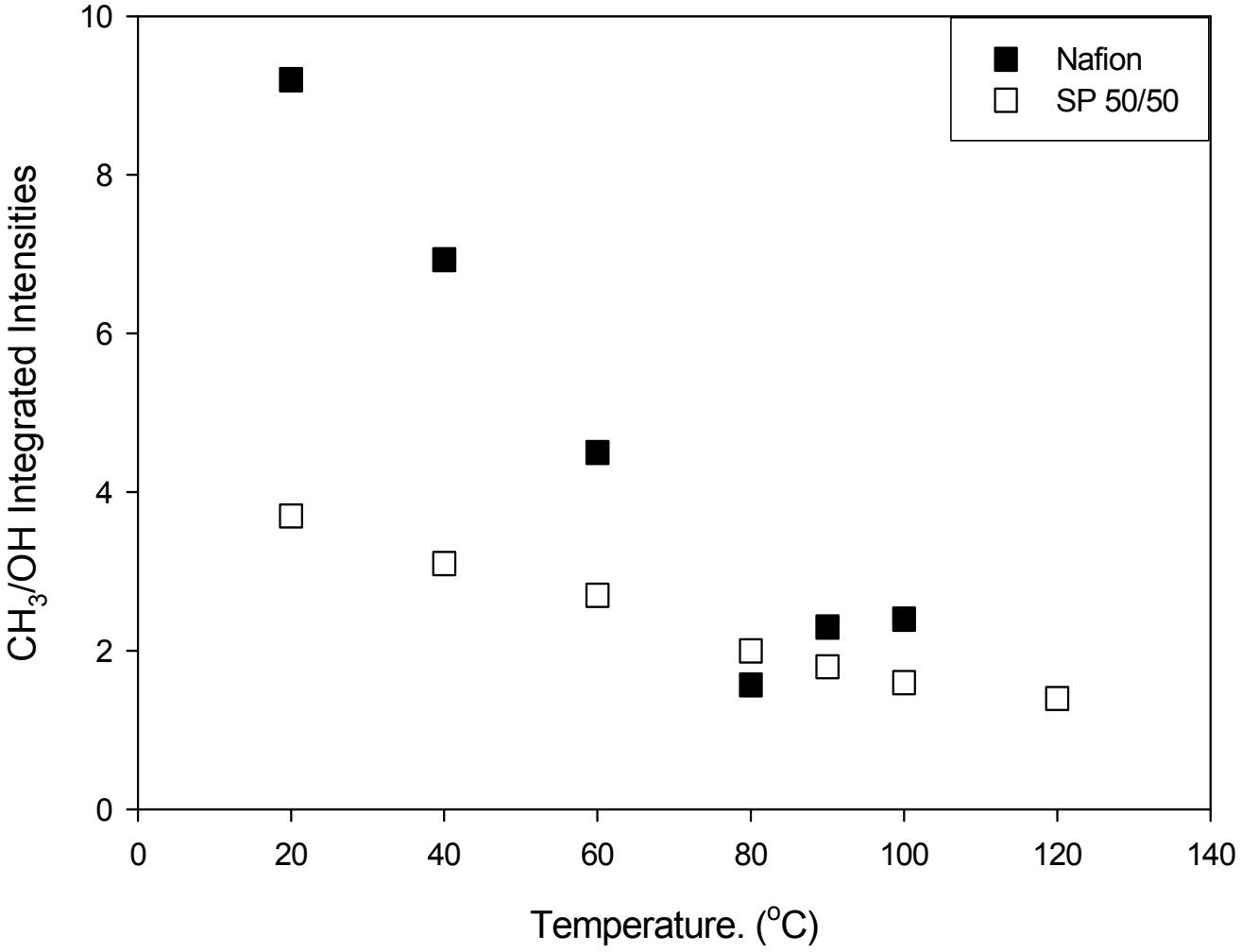

Figure 4.9: Integrated proton NMR intensity as percentage of methanol to water peaks in SPTES and Nafion membranes equilibrated in 2M MeOH.

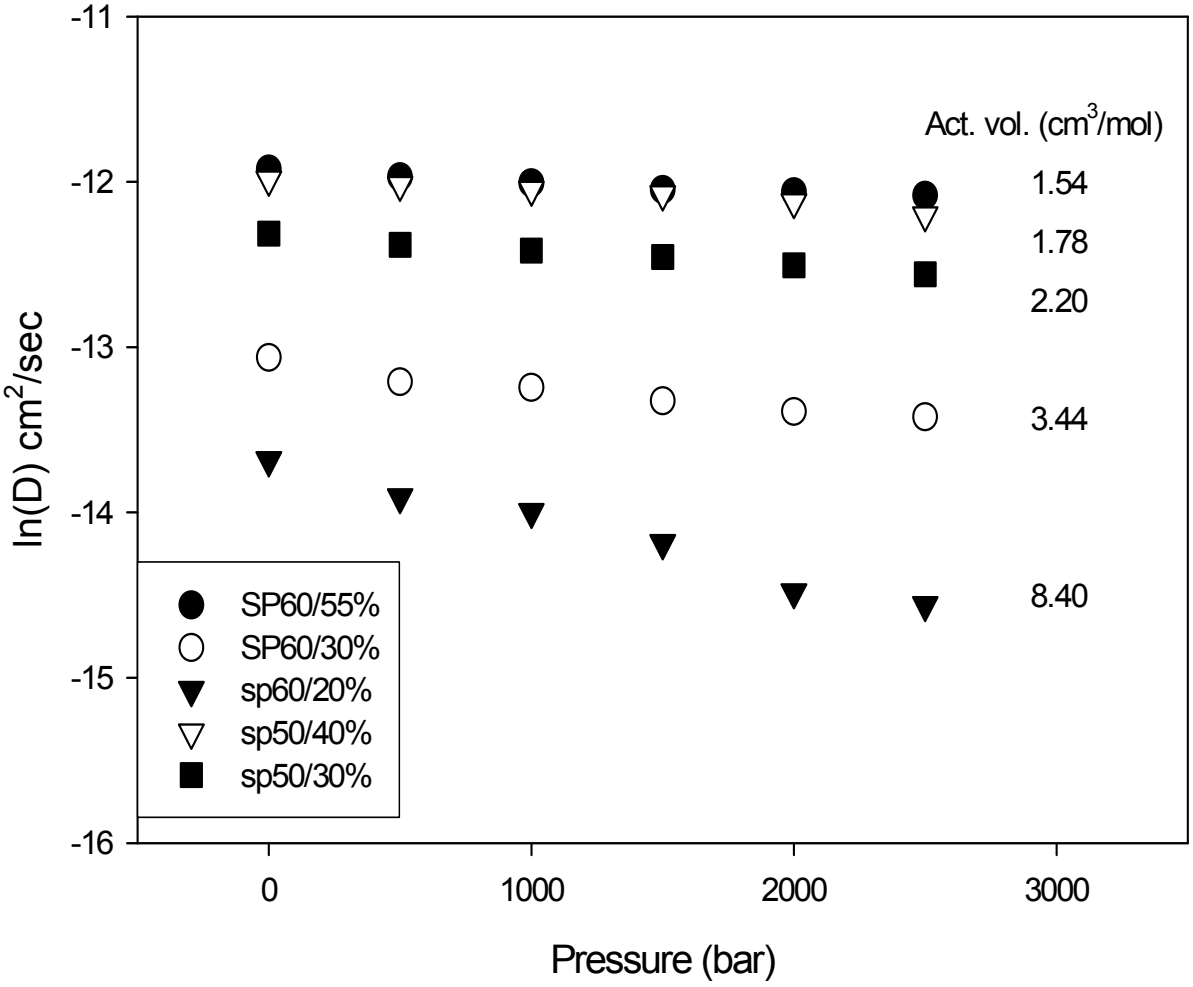

Figure 4.10: ^{1}H Diffusion coefficients of SPTES50 and SPTES60 Membranes as a function of pressure for different water concentrations.

Chapter 4:

High Pressure Diffusion Studies Of Phosphoric Acid in Water: A ^{1}H and ^{31}P Static Field Gradient Spin-Echo Nuclear Magnetic Resonance Study

4.1 Introduction

Phosphoric acid also called Orthophosphoric (O-Phosphoric) acid is a three element compound made up of phosphorus, oxygen, and hydrogen (H_3PO_4). Phosphoric acid is a clear, colorless, viscous liquid, which is miscible with water in any ratio. Among the commercially available concentrations of Phosphoric acid, 85% (by weight, corresponding to 1:1 ratio of H_3PO_4 and H_2O) is the most common and our analysis will be mainly focused on it. Apart from its intrinsic theoretical interests as a model system

for investigating mass and charge transport in disordered systems, phosphoric acid has many applications such as in the chemical industry, metal surface treatment, paint and food industries[77]. Recently, phosphoric acids also became very attractive with their use as proton conductors in electrochemical devices such as fuel cells [78,79]. For example phosphoric acid fuel cells, as the name implies, use liquid phosphoric acid as electrolyte. These fuel cells operate at around 150^{o} C to 200^{o} C, above the boiling point of water. At a phosphoric acid fuel cell's operating temperatures; the expelled water can be converted to steam for space and water heating. In this combined heat and power application, overall efficiencies can approach 80%. In addition, J. J. Fontanella and al [81] recently have studied the phosphoric acid doped polybenzimidazole (PBI). The PBI contained about 600-mol % of 85 % phosphoric acid. They find that the acid doped PBI behaves like a true polymer electrolyte where ion transport is mediated by segmental motions of the polymer. Thus, it is important to know the ion transport mechanism in these materials so that proton conducting polymeric membranes can be optimized for efficient fuel-cell performance. In this regard we studied experimentally, the self-diffusion coefficient, D, which is an important parameter to characterize the translational mobility of a molecular or ionic species in homogeneous media. The measurement of the diffusion coefficient performed by NMR as a function of pressure has yielded additional information about the ion transport process, and vital parameters such as the activation volume are obtained. In this investigation, we use FFG spin echo method to measure ^{1}H and ^{31}P diffusion coefficients and activation volumes for various concentrations of H_3PO_4 in water.

For the same resonance frequency, proton and phosphorus nuclei have two different resonance positions (two different gyromagnetic ratios) inside the magnet's bore.

It is important to report that the diffusion coefficient is related to the conductivity through the Nernst-Einstein relation, which can be written as:

$$\sigma = {q^2 nD}/{\kappa_B T} \qquad [4.4.1]$$

where n is the number density of the charge carriers, q is the charge on the ion, and κ_B is the Boltzmann constant.

The diffusion can provide information on the shape of the diffusing molecule, as Benedek and Purcell[22] had pointed out. High pressure is known also to cause relatively large changes in viscosity. From the Stokes-Einstein equation:

$$D = {\kappa_B T}/{f}, \qquad [4.4.2]$$

where f is the friction coefficient, it follows that pressure should also affect D. For the simple case of a spherical particle with an effective hydrodynamic radius r in a solution of viscosity η, the friction coefficient is:

$$f = 4\pi\eta r . \qquad [4.4.3]$$

In this study of high-pressure diffusion coefficients describing macroscopic motions, we used FFG technique because the pressure cell is easily incorporated in this system.

We investigated pressure-dependent ^{1}H (I=1/2) and ^{31}P (I=1/2) diffusion properties of 6 %, 55 %, 85 % and 100 % H_3PO_4 solution.

4.2 Experimental Details

4.2.1 Materials

Eighty-five percent and 100 % phosphoric acid obtained from Sigma-Aldrich and used as received. Appropriate amounts of water were added to the 85 % H_3PO_4 to generate the 55 % and 6 % solutions. For NMR measurements the solutions were packed in to 0.6 cm x 0.5 cm x 0.18 mm hermetically sealed thin polyethylene bags, which were shown to produce a negligible proton NMR background signal compared to the signal from the solution.

4.2.2 Nuclear Magnetic Resonance

The naturally existing field gradient of a conventional 7.3 T superconducting magnet was used for the measurements. The central field and gradient strength were varied continuously, within the limits of the magnet, by moving the NMR probe head within the bore of the magnet. The position of the NMR coil (which contains the sample) determines both the resonant frequency and the magnetic field gradient. A home-built computer controlled motorized stage, capable of moving the probe in precise steps of 0.25 mm, was used to center the coil at a central field value of 1.7 T with a gradient strength ($g = dH_z/dz$) of 0.253 T/cm. The latter quantity was determined experimentally using the standard self-diffusion coefficient of water [54]. Accurate variation of the pressure (0-2.5 kbar) was carried out using an ENERPAC 11-400 hydraulic system fitted to a sealed Cu-Be alloy high-pressure chamber (bomb) inside of which resides the NMR

excitation coil and sample. Electronic leads between the coil and external matching and tuning capacitors was facilitated by a hermetic feedthrough.

A home-built broadband NMR spectrometer operating at 72 MHz (the central field value corresponding to the position of the sample in the fringe-field) and utilizing a phase cycled spin-echo pulse sequence ($\pi/2$-τ-π-τ-acquire) was used to detect the proton echo signal from the sample. Pulse widths ($\pi/2$) were typically of 2.8 μs duration. Although it is acknowledged that this pulse width constitutes somewhat less than the full spectral coverage of all of the protons in the sample, estimated to be about 2 MHz (based on the ~2 mm sample thickness and the ~0.025 T/mm gradient), this value was chosen on the basis of the maximum signal amplitude obtainable for a given pulse separation. The phosphorus (^{31}P) echo signal was also detected in the same manner as previously, with the sample moved upward to a different position from the proton resonance position at the same resonance frequency. For the phosphorus signal, the coil was centered at a central field value of 2.3 T with a gradient strength ($g = dH_z/dz$) of 0.48 T/cm.

4.3 Results

Proton spin-echo intensities $M(\tau)$ were measured as a function of the pulse separation, τ, and self-diffusion coefficients D were extracted from the data using the equation [2.2.23]

$$M(r,2\tau) = M_o \exp(-2\tau / T_2) \exp[-D(\gamma \partial H / \partial z)^2 2\tau^3 / 3].$$

In this expression M_o is the maximum magnetization (at τ = 0) and γ is the proton gyromagnetic ratio. To assist in the analysis, proton and phosphorus transverse relaxation times T_2 were measured independently and the data were fit to a linearized version of equation [2.2.23] with slope = $2(\gamma g)^2 D/3$ and intercept = $2/T_2$. In this way the diffusion coefficients were gathered with respect to applied pressure.

Linearized results (i.e., data presented as a function of the square of the pulse separation, τ^2) and pressure of the 6 % and 85 % phosphoric acid for ^{1}H are illustrated respectively in Figure 4.11 and Figure 4.12. The ^{31}P linearized results and pressure of the 85 % and 100 % H_3PO_4 also are shown respectively in Figure 4.13 and Figure 4.14.

The self-diffusion coefficients as a function of pressure for four different phosphoric acid concentrations are plotted in Figure 4.15.

The data in Figure 4.15 can be further analyzed to yield the activation volume ΔV associated with the diffusing molecules according to the equation [2.2.54] [74],

$$\Delta V = V = -RT\left(\frac{\delta(\ln D)}{\delta p}\right)_T .$$

The activation volume for ion, or molecular motion is usually interpreted as the volume

change when a diffusing species transfers from a "normal" position to an activated position (sometimes referred to as the "saddle point") [81]. ^{1}H and ^{31}P activation volumes versus concentrations in H_3PO_4 are given in Figure 4.16.

4.4 Discussion

Figure 4.15 shows that the self-diffusion coefficient decreases with decreasing water content and also with increasing pressure as these yield greater restrictions for water molecular motions. This figure shows also how the pressure affects the ^{1}H diffusion mechanism respectively for four different H_3PO_4 concentrations and ^{31}P diffusion only at the two highest concentrations. For comparison purposes, we are using 85% H_3PO_4 concentration mainly because we are aware of the electrical conductivity results of the 85% phosphoric acid and of the acid doped polybenzimidazole containing about 600 mol % of 85% phosphoric acid as reported by J. J. Fontanella and al.[81]. S. H. Chung and al.[78] have reported the pulsed gradient spin echo (PGSE) NMR results of ^{1}H and ^{31}P with the pulsed field gradient measurements of the self-diffusion coefficients, and studied also the viscosity and the conductivity as a function of temperature for the 85% H_3PO_4.

4.4.1 85% phosphoric acid

From Figure 4.15 it is apparent that the phosphorus nucleus diffuses more slowly than the proton. At atmospheric pressure the value of D (D =12.7 x 10^{-7} cm^2 s^{-1}) for the proton is about 4.2 times higher than for the phosphorus nucleus (D = 2.90 x 10^{-7} cm^2 s^{-1}). The activation volume associated with the electrical conductivity at room temperature (T= 26^oC) for 85% phosphoric acid found by J.J. Fontanella and al. [81] (ΔV = 0.12 cm^3/ mol) is smaller than our value (ΔV = 4.20 cm^3/ mol) because in our investigation we are measuring all mobile protonic species while the conductivity measures only net charge migration.

In addition the conductivity results include a compressibility term, which gives an effectively higher ion concentration leading to a negative contribution to ΔV.

4.4.2 6%, 55% and 100% phosphoric acid

The first observation that can be made is that the proton diffusion coefficient for the 6% phosphoric acid at room pressure is very close to water proton diffusion coefficient. At 6 % H_3PO_4, the activation volume associated to the proton is small and increases with the increase of phosphoric acid. Figure 4.15 shows that for 100% H_3PO_4 the activation volume associated with the diffusing phosphorus nucleus is more than twice as high than that of proton. This is a substantial proof that the phosphate ion requires more room to diffuse than protons.

4.5 Conclusion

Self-diffusion coefficient studies of 6%, 55%, 85% and 100% phosphoric acid have been measured over a range of pressures from 0 to 2.5 kbars. The investigations have been carried out at room temperature, using ^{1}H (I=1/2) and ^{31}P (I=1/2) static field gradient Hahn spin-echo methods. At this ambient temperature, the diffusion decreases with increasing pressure for all four phosphoric acid concentrations. This behavior is expected for normal liquids and for ions in polymers where the viscosity increases with pressure. Furthermore, the data show that protons diffuse faster than the phosphorus carrying species. This conclusion was expected, based on their different size. Indeed, the diffusion generally depends on the size of the diffusing species. We also reported ^{1}H and ^{31}P activation volumes relevant to high pressure diffusion measurements. The activation volume value for ^{31}P is more than twice that of ^{1}H for the same H_3PO_4 concentration. This emphasized the fact that phosphate ions require more room to diffuse than protons. Understanding the proton transport mechanism in H_3PO_4 solutions can have important implications in phosphoric acid-based fuel cells.

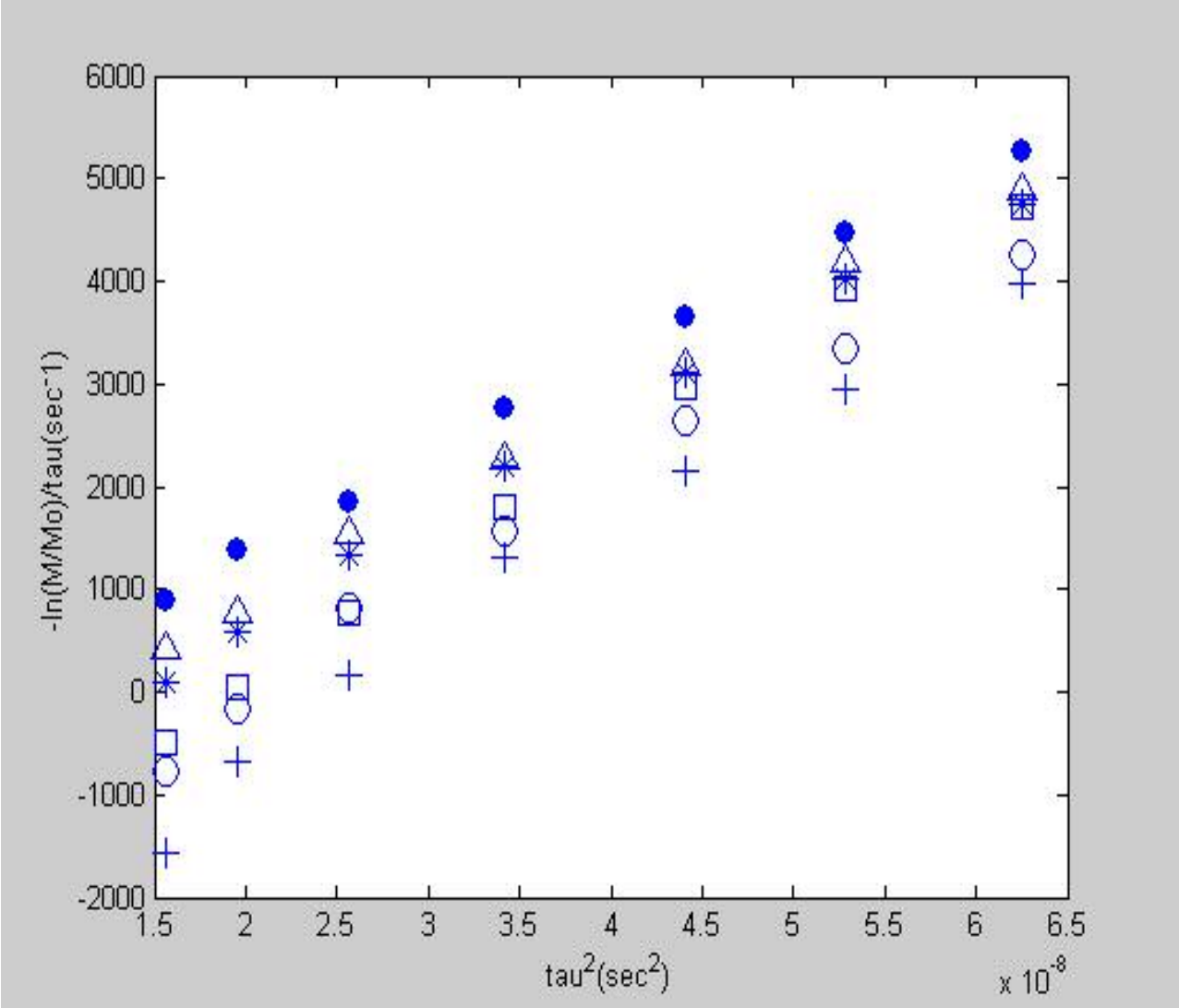

Figure 4.11: Semilog plot of nuclear magnetization, as a function of the square of the pulse separation and pressure for ^{1}H in 6 % H_3PO_4.

- P = 0

Δ P = 500 bars

* P = 1000 bars

□ P = 1500 bars

0 P = 2000 bars

\+ P = 2500 bars

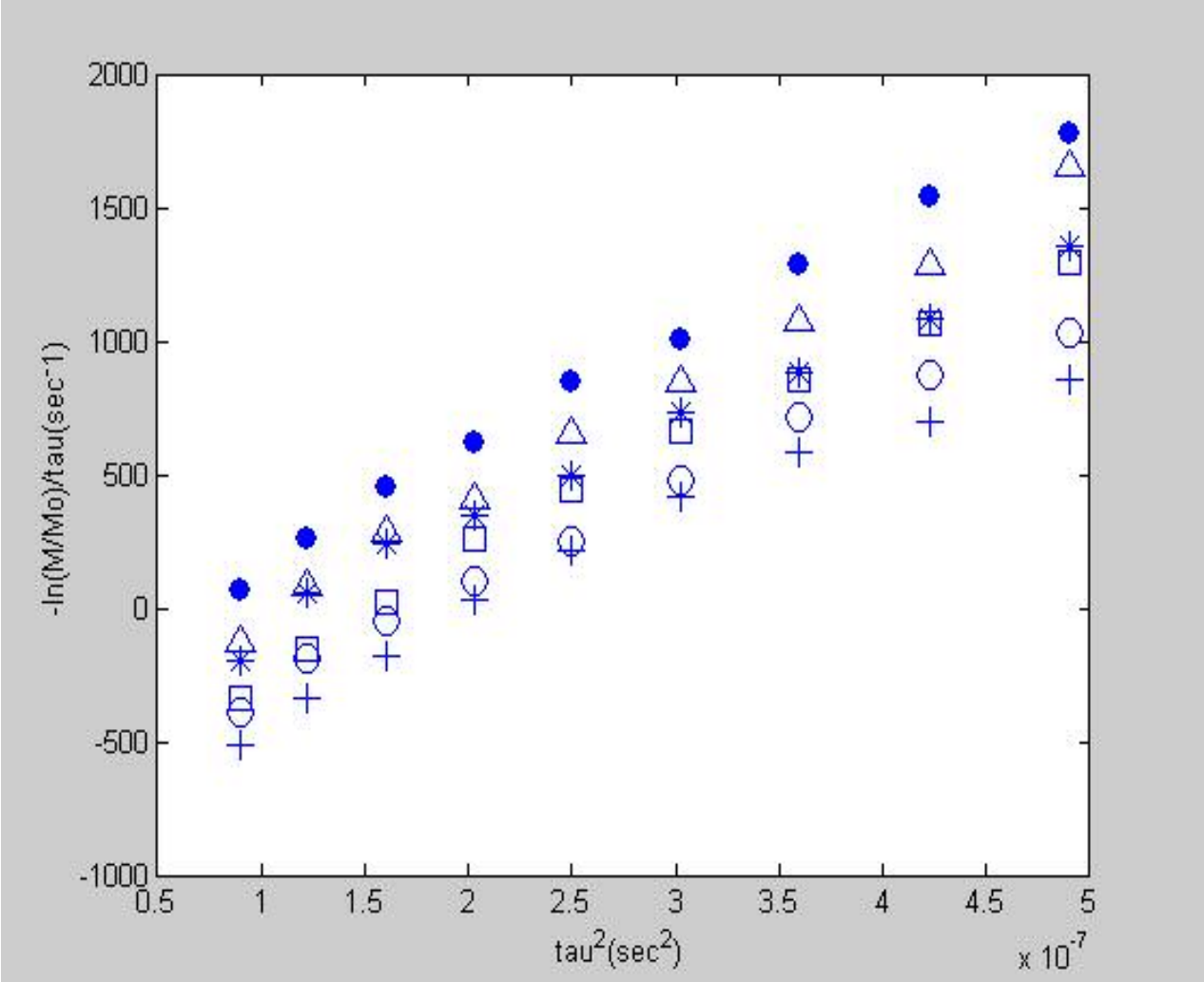

Figure 4.12: Semilog plot of nuclear magnetization, as a function of the square of the pulse separation and pressure for ^1H in 85 % H_3PO_4.

- • P = 0
- Δ P = 500 bars
- * P = 1000 bars
- □ P = 1500 bars
- 0 P = 2000 bars
- \+ P = 2500 bars

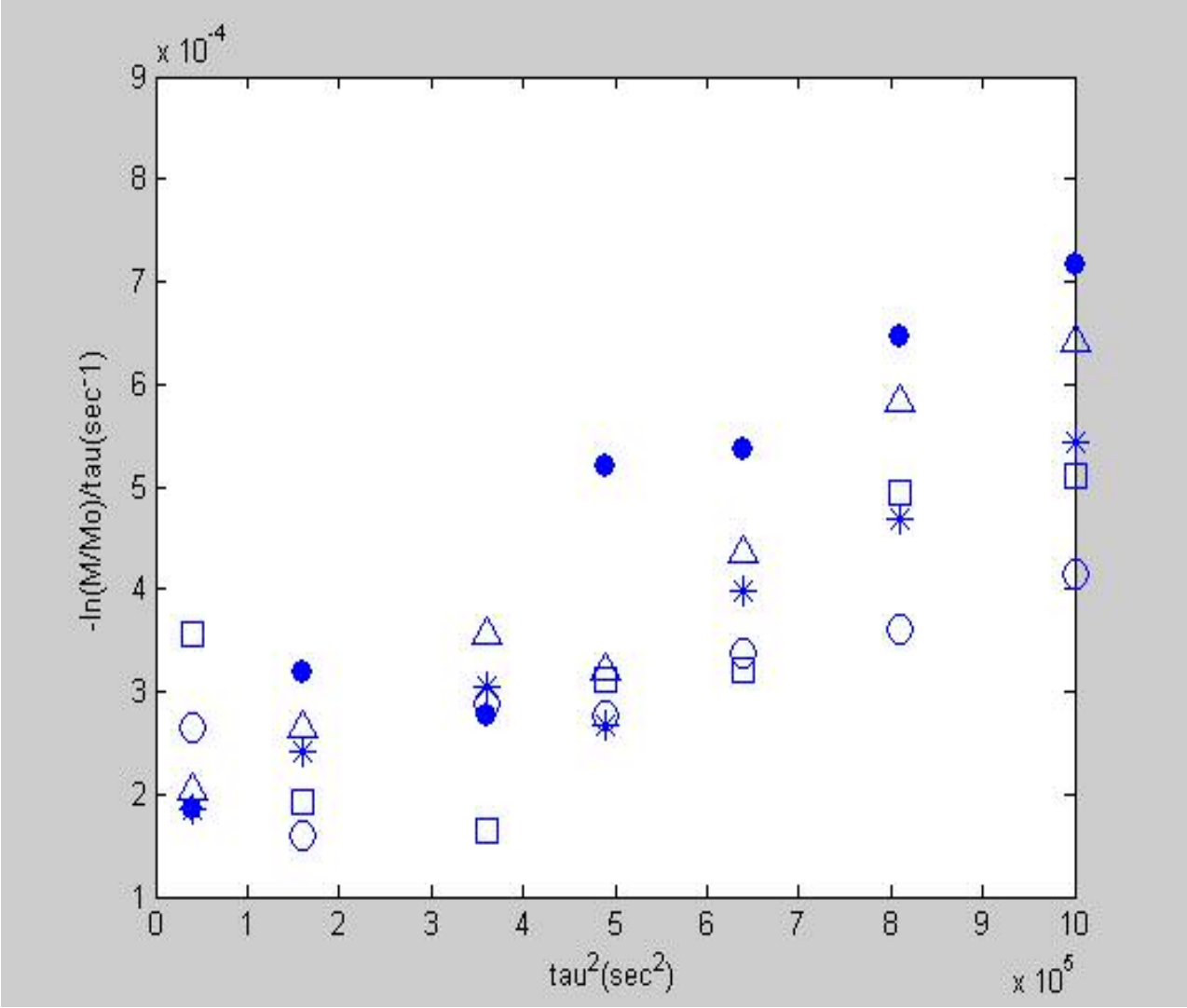

Figure 4.13: Semilog plot of nuclear magnetization, as a function of the square of the pulse separation and pressure for ^{31}P in 85 % H_3PO_4.

- • P = 0
- Δ P = 500 bars
- * P = 1000 bars
- □ P = 1500 bars
- 0 P = 2000 bars
- \+ P = 2500 bars

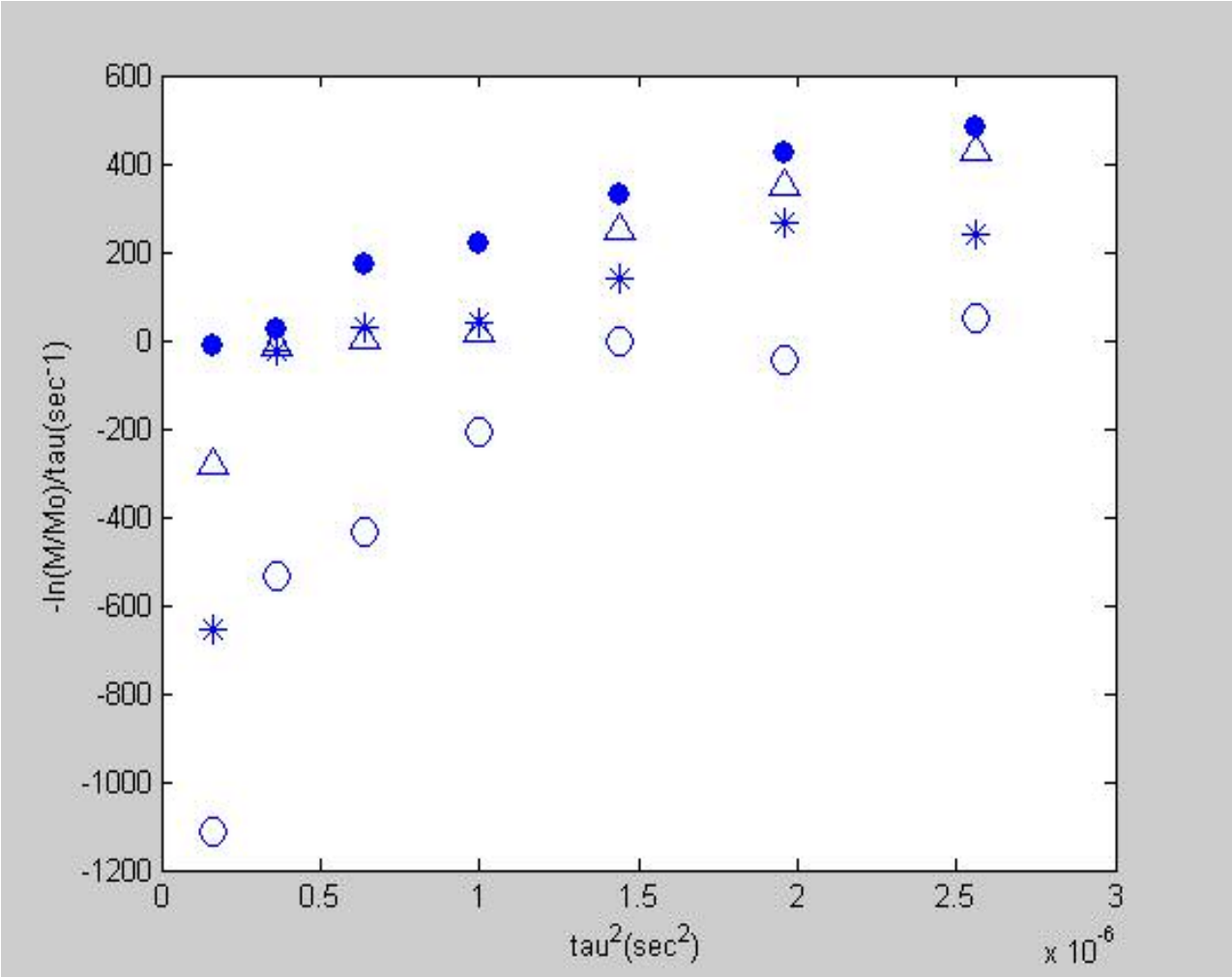

Figure 4.14: Semilog plot of nuclear magnetization, as a function of the square of the pulse separation and pressure for ^{31}P in 100 % H_3PO_4.

- • P = 0
- Δ P = 500 bars
- * P = 1000 bars
- □ P = 1500 bars
- 0 P = 2000 bars
- \+ P = 2500 bars

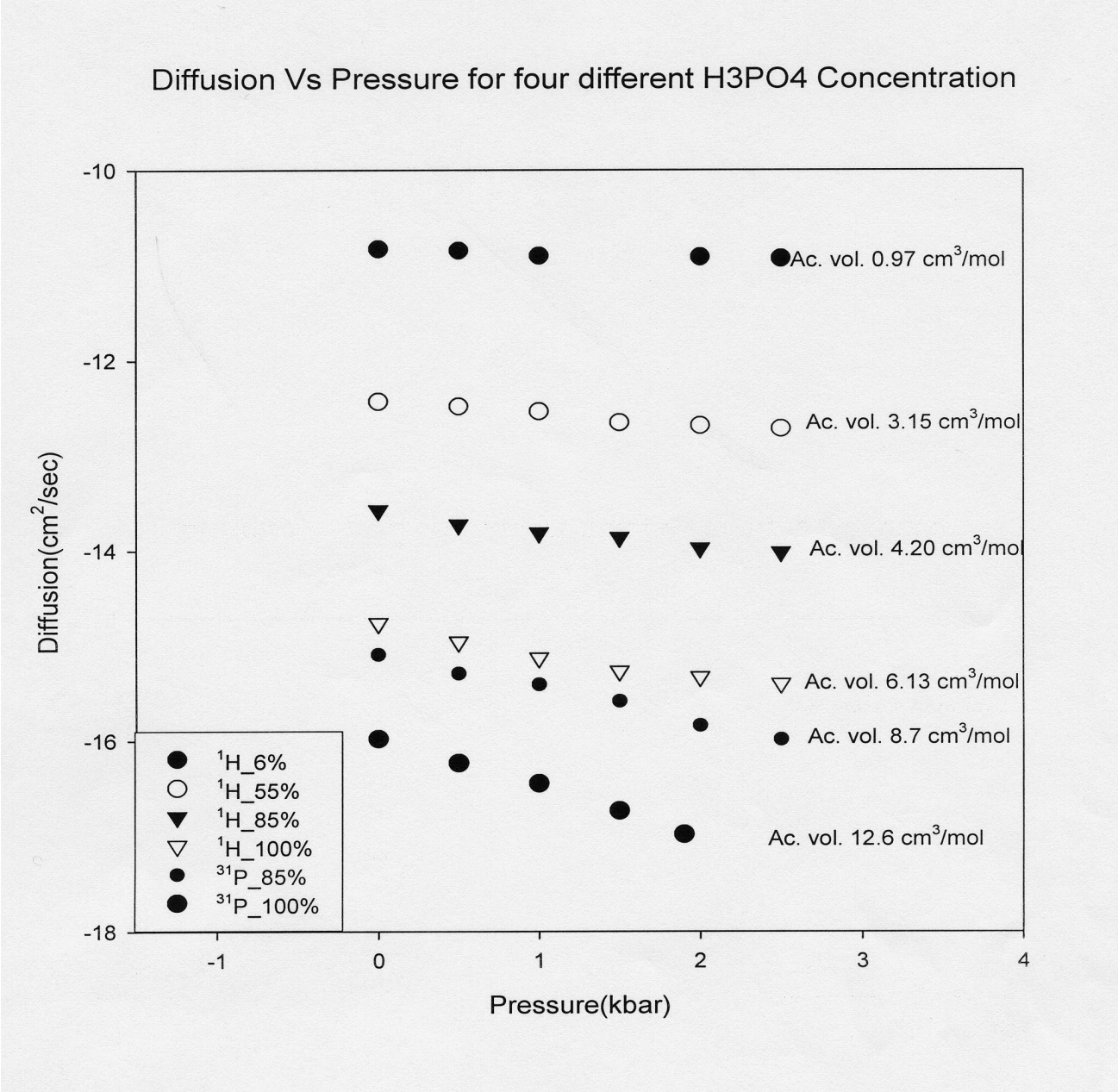

Figure 4.15: ^{1}H and ^{31}P Self-Diffusion Coefficients Versus Pressure for four different H_3PO_4 concentrations

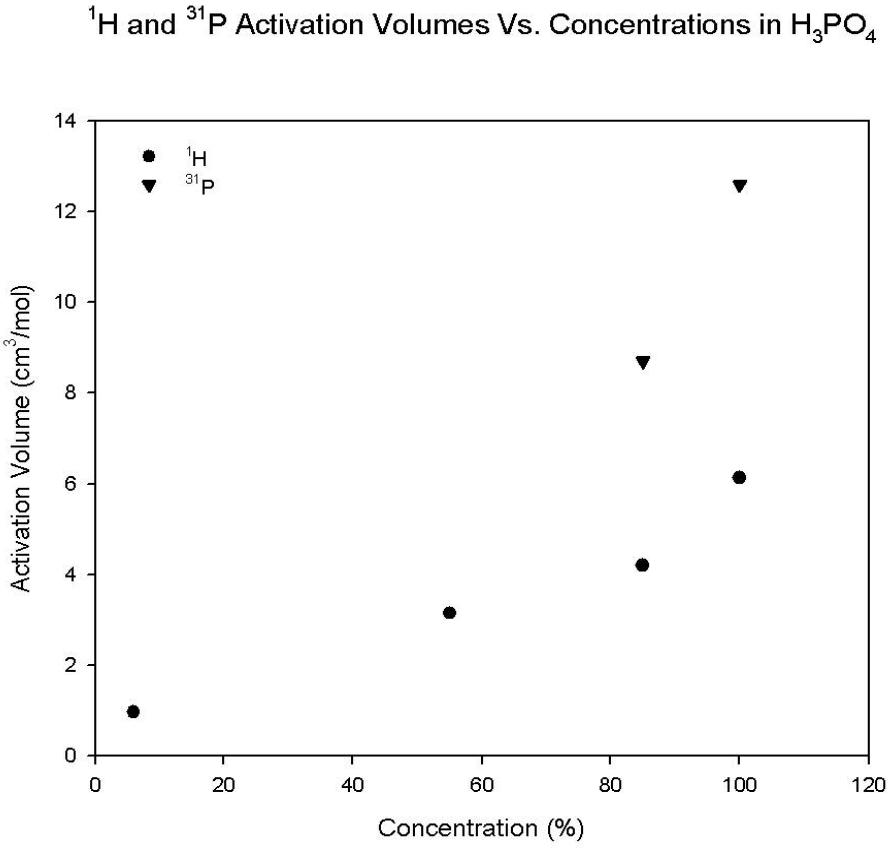

Figure 4.16: ^{1}H and ^{31}P Activation Volumes Versus Concentrations in H_3PO_4 concentrations

Chapter 5

GENERAL CONCLUSION

The goal of this research effort was to develop high-pressure NMR methods to investigate diffusion processes in polymers. Key to achieving this goal was to work at high field gradient. The static field or fringe field gradient (FFG) technique used is ideally suited for these studies, since it provides the high field gradient naturally with extreme stability.

The strength of the FFG method is its ability to measure very low diffusion coefficients but its primary disadvantage is that the effects of diffusion cannot be separated from spin-spin relaxation in a single experiment. This disadvantage is exaggerated for materials with very small spin-spin relaxation (T_2) values, in which the transverse relaxation observed for a very short time masks the entire spin diffusion. Thus, the FFG technique was not applicable to materials exhibiting fast T_2 values such as "dry BB_2", $P_{13}BF_6$, $P_{11}BF_4$. However, we were very fortunate that the majority of the materials investigated in this thesis presented long T_2 values, which enabled the successful application of the FFG technique.

We have used high-pressure as a thermodynamic parameter in an attempt to characterize the dynamics of ^{1}H, ^{11}F, ^{7}Li and ^{31}P in Nafion, SPTES, Phosphoric Acid and for

Diglyme/Salt solution. The high-pressure diffusion measurements provide additional information in the transport process and yield the vital parameter of the activation volume in the same manner as the variable temperature measurements yield the activation energy. In proton conducting membranes, the self-diffusion coefficient decreases with decreasing water content and also with increasing pressure as these yield greater restrictions for water molecular motions. All materials investigated in this thesis present the largest activation volume at the lowest water content. However, it is important to point out that the magnitude of the activation volume parameter is related to the method of investigation used and we noted that there is a net discrepancy between the NMR high pressure diffusion activation volume and the activation volume due to electrical conductivity measurements. For example, 85% phosphoric acid has the activation volume of 4.2 cm^3/mol when measured with high pressure NMR diffusion data, while 0.12 cm^3/ mol is calculated with the electrical conductivity.

We have demonstrated that nuclear magnetic resonance is capable to explore fuel cell electrolytes and improve the understanding of fuel cells technology. Fuel cells are the next generation of alternative energy, and currently, they are typically characterized by the electrolyte between the two electrodes.

We have used the high pressure in FFG NMR technique to obtain substantial results in agreement with our expectation for two fuel cell membrane types: Nafion-117, SPTES and different dilutions of phosphoric acid used as an electrolyte in phosphoric acid fuel cells. To our knowledge, this is the first time the high-pressure diffusion measurements in FFG NMR method has been performed in membranes or any non-liquid. As part of this

work, we have also investigated LiTf salt in diglyme solution, which is used as a lithium battery electrolyte.

In the near future, our group will expand these studies to include the variable temperature measurements in the high pressure NMR set-up, so both crucial thermodynamic variables can be controlled simultaneously.

Our group expects to continue to used this technique to study transport properties through the electrolytes/membranes for others polymer electrolyte components and membranes. We expect this to become a vital tool in the characterization of molecular motion in new fuel cell membranes and others types of fuel cells, batteries and glass-forming liquids controlled by slow diffusion.

References

[1] A. Abragam, Principles of Nuclear Magnetism, Oxford Science Publication, Oxford University Press, 1961.

[2] M. H. Cohen and F. Reif, Solid State Physics, Vol.5, 321, 1957.

3. I.I. Rabi, S. Millman, P. Kusch and J.R. Zacharias (1939), Phys. Rev., 55, 526.

4. Brian Cowan, Nuclear Magnetic Resonance and Relaxation, Cambridge University Press, 1997.

5. E.M. Purcell, H.C. Torrey and R.V. Pound (1946), Phys. Rev, 79, 37.

6. F. Bloch, W.W. Hansen and M. Packard (1946), Phys. Rev., 70, 474.

7. M.L. Martin, E.J. Martin, J.J. Delpuech, Practical NMR Spectroscopy.

8. Eiichi Fukushima, Stephen B.W. Roeder, Experimental pulse NMR, A nuts and Bolts Approach, Addison-Wesley, Massachusetts, 1981.

9. Horst Friebolin, Basic one- and two- Dimensional NMR Spectroscopy, third revised edition, Wiley-VCH Verlag GmbH, D-69469 Weinheim (Federal Republic Of Germany), 1998.

10. Slichter, C. P. Principles of Magnetic Resonance; Springer-Verlag: Berlin, 1990.

11. H.S. Gutowsky, D.W. McCall, C.P. Slichter: J. Chem. Phys. 21, 279 (1953).

12. E.L. Hahn, D.E. Maxwell: Phys. Rev. 88, 1070 (1952).

13. J. H. Van Vleck: Ned. Tijdschr. Natuurkd. 27, 1 (1961).

14. H.M. McConnell: J. Chem. Phys. 28, 430 (1958).

15. D.H. Archer: Thesis, Harvard University (1953).

16. P.W. Anderson: J. Phys. Soc. Jpn. 9, 316 (1954).

17. William S. Price, J.Magn.Reson., 1997, 299-336.

18. K.D. Kreuer, Journal of Membrane Science 185(2001) 29-39.

19. J.J. Fontanella, C.A. Edmondson and M.C. Wintersgill, Y.Wu and S.G. Greenbaum, Macromolecules 1996, 29, 4944-4951.

20. C.A. Edmondson and al, Solid State Ionics 135 (2000), 419-423

21. R.S. Chen, P. E. Stallworth, S. G. Greenbaum, J. J. Fontanella and M. C. Wintersgill, Electrochimica Acta, Vol.40, No.3, pp.309-313, 1995.

22. G.B. Benedek and E. M. Purcell, The Journal Of Chemical Physics, Volume 22, Number 12, December, 1954.

23. Yaobang Wu, Ph. D thesis, The City University Of New York, 1997.

24. Karl Kordesch and Gunter Simader, Fuel Cell and Their Applications, VCH Verlagsgesellschaft mbH, D-69451 Weinheim, Federal Republic of Germany, 1996.

25. A.J. Appleby and D.G. Lovering, Fuel Cells, 2nd Grove Symposium '91, ELSEVIER SEQUOIA S.A. 1992.

26. U.S. Department of Energy, Office of Fossil Energy, Fuel Cell A Handbook, May 1988, Chapter 6.

27. T. A. Zawodzinski Jr., M. Neeman, L.O. Sillerud, and S. Gottesfeld, Determination of water diffusion coefficients in Perfluorosulfonate Ionomeric Membranes, J. Phys. Chem. 1991, 95, 6040-6044.

28. T.A. Zawodzinski, Jr., J. Davey, J. Davey, J. Valerio, and S. Gottesfeld, The Water Content Dependence of Electro-Osmotic Drag in Proton-Conducting Polymer Electrolytes, Electrochimica Acta, Vol.40, No.3, 1995, 297-302.

29. Rensheng Chen, Ph. D thesis, The City University Of New York, 1994.

30. David Linden, Thomas B. Reddy, Handbook of batteries, third edition, McGraw-Hill Handbooks, 2002.

31. H.A. Every, Ph. D theses, Monash University, February 2001.

32. T.C. Farrar and E. D. Becker, Pulse and Fourier Transform NMR: Introduction to Theory and Methods, (Academic Press, Inc., New York, 1971).

33. N. Bloembergen, E.M. Purcell and R.V. Pound, Phys. Rev. 73, 679-712 (1948).

34. H.C. Torrey: Phys. Rev. 104, 563 (1956).

35. H.Y. Carr, E.M. Purcell: Phys. Rev. 94, 630 (1954).

36. J. R. Singer, J. Phys. E: Sci. Instrum., Vol. 11, 1978.

37. Peter Stilbs, progress in NMR Spectroscopy, vol. 19 pp. 1-45, 1987.

38. R. E. Gordon, J. H. Strange and J. B. W. Webber, J. Phys. E: Sci. Instrum., Vol. 11,

39. M. Plischke, B. Bergersen, Equilibrium Statistical Physics, 2nd edition, World Scientific, 1994.

40. J.J. Fontanella, M.C. Wintersgill, R.S. Chen, Y. Wu, and S.G. Greenbaum, Electroche. Acta, 40, 2321 (1995).

41. D. W. McCall, D. C. Douglass and E. W. Anderson, Bell Telephone Laboratories, Incorporated Murray Hill, New Jersey.

42. J. J. Fontanella, M.C. Wintersgill, J. S. Wainright, R. F. Savinell and M. Litt, Electrochimica Acta, Vol. 43, Nos 10-11, pp. 1289-1294, 1998.

43. R. Kimmich, W. Unrath, G. Schnur, and E. Rommel, Journal of Magnetic Resonance 91, 136-140(1991).

44. Laurance D. Hall and Timothy J. Norwood, Journal of Magnetic Resonance 88, 192-198(1990).

45. P.T. Callaghan, Aust. J. Phys., 1984, 37, 359-87.

46. Dan E. Demco, Anna Johansson, and Jorgen Tegenfedt, Journal of Magnetic Resonance series A 110, 183-193(1994).

47. Gerald Fleisher, Franz Fujara, Macromolecules 1992, 25, 4210-4212.

48. Fieser, L.F.; Haddadin, M.J.J. Am.Chem. Soc. 1964, 86, 2081; Can. J. Chem. 1965, 43, 1599.

49. Eric E. Sigmund, Ph.D thesis, Northwestern University, December 2002.

50. Stejskal, E. O.; Tanner, J. E. J. Chem. Phys. 1965, *42*, 288.

51. P. Jeglic, A. Lebar, T. Apih and J. Dolingek, Journal of Magnetic Resonance 150, 39-42, 2001.

52. B. Gross and R. Kosfeld. Messtechnik 7-8, 171, 1969.

53. Malcolm H. Levitt, Spin dynamics, Basics of Nuclear Magnetic Resonance, John Wiley and Sons, 2001.

54. Bruker, Almanac 2001, Table by Courtesy of Dr. M. Holz, Institute of Phys. Chem., University of Karlsruhe, FRG.

55. Zawodzinski, T. A., Jr.; Derouin, C.; Radzinski, S.; Sherman, R. J.; Smith, V. T.; Springer, T. E.; Gottesfeld, S. J. Electrochem. Soc.1993, 140, 1041.

56. Cahan, B.; Wainright, J.; J. Electrochem. Soc. 1993, 140, L185

57. McLin, M. C.; Wintersgill, M. C.; Fontanalla, J. J.; Chen, R. S.; Jayakody, J. P.; Greenbaum, S. G. Solid State Ionics 1993, 60, 137.

58. Fontanella, J. J.; Wintersgill, M. C.; Smith, M. K.; Semancik, J.; Andeen, C. G. *J.* Appl. Phys. 1986, 60, 2665.

59. Zawodzinski, T. A., Jr.; Neeman, M.; Sillerud, L. O.; Gottesfeld, S. J. Phys. Chem. 1991, *9*5, 6040.

60. Edmondson, C. A.; Stallworth, P. E.; Wintersgill, M. C.; Fontenalla, J. J.; Dai, Y.; Greenbaum, S. G. Electrochim. Acta 1998, *43*, 1295.

61. Bendler, J. T.; Fontanella, J. J.; Shlesinger, M. F.; Wintersgill, M. C. Electrochim. Acta 2001, 46, 1615.

62. Wintersgill, M. C.; Fontanella, J. J. Electrochim. Acta 1998, 43, 1533.

63. C. Berthier, W. Gorecki, M. Minier, M. B. Armand, J. M. Chabagno, and P. Rigaud, Solid State Ionics*,* 11, 91 (1983).

64. J. A. Kerres, Membrane Science, 2001, 185, 29.

65. P. Dimitrova, K. A. Fridrich, U. Stimming, B. Vogt, Solid State Ionics 160, 115.

66. C. Yang, P. Costamagna, S. Sirinivasan, J. Benziger, A. B. Bocarsly, J. Power Sources. 103 (1) (2001), 1-9.

67. R. M. Mooze, S. Gottesfeld, P. Zelenay, ECS Proceedings 98 (27) (1999) 365.

68. S. Suarez, S. H. Chung, S. Greenbaum, S. Bajue, E. Peled, and T. Duvdivani, Electrochem. Acta, 48, 2187 (2003).

69. T. A. Zawodzinski, Jr., T. E. Springer, J. Davey, R. Jestel, C. Lopez, J. Valerio and S. Gottesfeld, J. electrochem.Soc 140 (7), 1981 (1993).

70. S. Matsumura, N. Kihara, T. Takata, Macromolecules, 34, (2001), 2848.

71. E. Peled, T. Duvdevani, A. Melman, Electronical and Solid State Letters 3 (12), 525 (2000).

72. J. R. P. Jayakody, A. Khalifa, E.S. Mananga and S. G. Greenbaum. Accepted for Publication, J. Power Sources, May 2005.

73. T. D. Dang, Z. Bai, M. J. Dalton, E. Fossum, Polymer Preprints ACS National Meeting, Anaheim, 45(1) (2004), 22.

74. J. R. P. Jayakody, P.E. Stallworth, E.S. Mananga, J. F. Zapata, and S. G.Greenbaum. J. phys. Chem.(B).108, 4260 (2004).

75. E.S. Mananga, M. Phil. Thesis, The City University Of New York, 2004.

76. T. A. Zawodzinski, Jr., C. Derouin, S. Radzinski, R. J. Sherman, V. T. Smith, T. E. Springer, S. Gottesfeld, J. Electrochem. Soc 140, (1993) 1041.

77. A. D. F. Toy and E. N. Walsh, phosphorus Chemistry in Everyday Living (American Chemical Society, Washington, DC, 1987).

78. S. H. Chung, S Bajue, S. G. Greenbaum, Journal of Chemical Physics, Vol. 112, 19 (2000).

79. S. Chandra, in Proceedings of the II International Symposium on Solid State Devices, edited by B. V. Chowdari and S. Radakrishna, World Scientific Publication, Singapore (1988), p. 265.

80. M. A. Ratner, in Polymer Electrolyte Review I, edited by J. R. MacCallum and C. A. Vincent (Elsevier, New York, 1987), p. 173.

81. J. J. Fontanella, M. C. Wintersgill, J. S. Wainright, R. F. Savinell and M. Litt, Electrochimica Acta, Vol. 43, pp. 1289-1294, 1998.

82. H. J. V. Tyrrell and K. R. Harris, Diffusion in liquids: A Theoretical and Experimental Study (Butterworth, London, 1984).

83. Maple V. Release 4, Waterloo Maple, Inc., Waterloo, ON, Canada, 1996.

84. Y. Wang, Ph. D thesis, The City University Of New York, 1999.

85. E. L. Hahn, Physical Review, Vol. 80, No. 4, pp. 580-600, 1950.

86. I. J. Lowe and R. E. Norberg, Physical Review, Vol. 107, No. 1, pp. 46-62, 1957.

87. F. Gray and M. Armand, in: T. Osaka and M. Datta, (Eds.), Energy Storage Systems for Electronics, Gordon and Breach Science Publications, Amshterdam, 2000.

88. G. S. MacGlashan, Y. G. Andreev, and P. G. Bruce, Nature 398 (1999), 792.

89. D. Golodnitsky, E. Livshits, A. Ulus, Z. Barkay, I. Lapides, E. Peled, S. H. Chung, and S. Greenbaum, J. Phys. Chem. A 105 (2001), 10098.

90. M. B. Armand, J. M. Chabagno, and M. Duclot, in Fast Ion Transport in Solids, P. Vashishta, J. N. Mundy, and G. K. Shenoy, Editors, p. 131, North Holland, New York (1979).